

Copyright

by

Bryan V. Bindrich

2009

**The Effects of Alkali-Silica Reaction and Delayed-Ettringite Formation on the  
Structural Performance of the Dapped End Region of Prestressed Concrete  
Trapezoidal Box Beams**

**by**

**Bryan V. Bindrich, B.S.C.E.**

**Thesis**

Presented to the Faculty of the Graduate School of  
The University of Texas at Austin  
in Partial Fulfillment  
of the Requirements  
for the Degree of

**Master of Science in Engineering**

**The University of Texas at Austin**

**May 2009**

**The Effects of Alkali-Silica Reaction and Delayed-Ettringite Formation on the  
Structural Performance of the Dapped End Region of Prestressed Concrete  
Trapezoidal Box Beams**

**Approved by**

**Supervising Committee:**

---

**James O. Jirsa, Supervisor**

---

**Oguzhan Bayrak**

## **Dedication**

To my parents,  
For giving me the guidance to succeed



## **Acknowledgements**

Many individuals aided the completion of this thesis. First, I would like to thank Dr. James O. Jirsa and Dr. Oguzhan Bayrak. Dr. Jirsa, your guidance and confidence kept me going even when the outcome looked bleak. Dr. Bayrak, thank you for ensuring that I obtained the most out of my experience at The University of Texas at Austin.

Furthermore, I would like to thank all my peers for making my experience at The University of Texas at Austin unforgettable. I would like to especially thank the team of Catherine Hovell, Dave Dunkman, and Andrew Moore for their guidance and help as we worked in tight quarters with each other. Moreover, I could not have completed this project without the help of Nancy Larson and Tz-Wei Wang. Our light-hearted work ethic made work at the lab enjoyable. The long hours you put in to aid in the completion of this thesis will not be forgotten. Finally, I would like to add a special thanks to Alejandro Avendaño and David Birrcher. Your patience in answering my incessant questions did not go unappreciated.

The author greatly appreciates all the help and guidance from the Ferguson Structural Engineering Lab Staff. Andrew Valentine, Blake Stasney, and Dennis Phillip were always willing and able to provide us with help and laboratory savvy. Eric Schell and Mike Wason, I would not have been able to complete the tests without your guidance in instrumentation. I am appreciative of Barbara Howard and Jessica Hanten for ensuring the lab is run smoothly.

Lastly, but certainly not least, I would like to thank my family. You always seemed be there when I needed it most. Your love and support has allowed me to get where I am today. Thank you.

May 8, 2009

## **Abstract**

### **The Effects of Alkali-Silica Reaction and Delayed-Ettringite Formation on the Structural Performance of the Dapped End Region of Prestressed Concrete Trapezoidal Box Beams**

Bryan V. Bindrich, M.S.E.

The University of Texas at Austin, 2009

Supervisor: James O. Jirsa

Tests were conducted on the dapped end sections of two beams that had undergone significant concrete cracking due to alkali-silica reactions (ASR) and delayed-ettringite formation (DEF). The purpose of the tests was to determine the effects of the cracking on the structural performance of the dapped ends of the beams. The beams were full-scale prestressed trapezoidal box beams. The beams were rejected because of fabrication errors and remained in a casting yard for over 14 years during which time the cracking damage occurred. The beams were transported to the laboratory for testing. Loading was applied to the beams to produce high shear forces at the dapped ends. Shear strength in the dapped end regions is critical and the effects of ASR/DEF damage on such beams has not been studied.

The observed strength of the dapped ends was compared with calculated strength using the provisions of the PCI Design Handbook, ACI 318-08, and AASHTO LRFD

Specifications. The observed strengths were greater than the computed strengths.  
Additional testing is underway.

## Table of Contents

<b>CHAPTER 1 INTRODUCTION</b>	<b>1</b>
1.1 BACKGROUND .....	1
1.2 OBJECTIVES .....	2
1.3 SCOPE .....	2
<b>CHAPTER 2 LITERATURE REVIEW</b>	<b>3</b>
2.1 ALKALI-SILICA REACTION .....	3
2.2 DELAYED-ETTRINGITE FORMATION .....	3
2.3 DIAGNOSING ASR AND DEF .....	4
2.4 EFFECTS OF CONCRETE DETERIORATION ON STRENGTH PROPERTIES .....	6
2.4.1 Reinforced Concrete Beams .....	6
2.4.1.1 Flexural Strength.....	7
2.4.1.2 Shear Strength.....	7
2.4.1.3 Anchorage.....	8
2.4.2 Prestressed Concrete Beams .....	9
2.4.2.1 Flexural Strength.....	9
2.4.2.2 Shear Strength.....	9
2.5 HISTORY OF DAPPED END RESEARCH AND DESIGN .....	10
2.5.1 Dapped End Terminology .....	11
2.5.2 PCI Design Handbook .....	12
2.5.3 Strut-and-Tie Modeling .....	14
2.5.3.1 General Strut-and-Tie Terminology .....	14
2.5.3.2 Cook and Mitchell (1988).....	15
2.5.3.3 Barton, Anderson, Bouadi, Jirsa, & Breen (1991).....	16
2.5.3.4 Bergmeister, Breen, Jirsa, & Kreger (1993).....	17
2.5.3.5 Mader (1990) .....	18
2.5.4 Recent Dapped End Studies.....	21

2.6	SIZE OF TEST SPECIMENS .....	23
2.7	OVERVIEW .....	23
<b>CHAPTER 3 EXPERIMENTAL PROGRAM</b>		<b>25</b>
3.1	BACKGROUND .....	25
3.2	TEST SPECIMENS .....	25
3.2.1	Delivery of Specimens .....	25
3.2.2	Specimen Details .....	27
3.2.2.1	General Geometric Information .....	27
3.2.2.2	Dapped End Regions .....	29
3.2.2.3	RF-3R-9 .....	32
3.2.2.3.1	RF-3R-9(a) .....	32
3.2.2.3.2	RF-3R-9(c) .....	34
3.2.2.3.3	Overview of assessment .....	35
3.2.3	Deck Casting .....	36
3.3	SHEAR TEST .....	38
3.3.1	Shear Test Set-up .....	38
3.3.2	Shear Span .....	42
3.3.3	Instrumentation .....	44
3.3.3.1	RF-3R-9(a) .....	44
3.3.3.2	RF-3R-9(c) .....	46
3.4	OVERVIEW .....	48
<b>CHAPTER 4 TESTING AND RESULTS</b>		<b>49</b>
4.1	INTRODUCTION .....	49
4.2	TEST RESULTS .....	50
4.2.1	Test of Dapped End RF-3R-9(a) .....	50
4.2.1.1	Dapped End Behavior .....	52
4.2.1.2	Measured Data .....	56
4.2.1.2.1	Load- Deflection .....	56

4.2.1.2.2	Crack Opening.....	56
4.2.2	Shear Test Dapped End RF-3R-9(c).....	57
4.2.2.1	Dapped End Behavior.....	59
4.2.2.2	Measured Data.....	62
4.2.2.2.1	Load vs. Deflection.....	62
4.2.2.2.2	Crack Opening.....	63
4.2.2.2.3	Strand Slip.....	68
4.3	CYLINDER TESTS.....	69
4.4	SUMMARY.....	71
<b>CHAPTER 5 COMPARISON OF MEASURED FAILURE LOADS WITH CODE PROVISIONS</b>		<b>72</b>
5.1	INTRODUCTION.....	72
5.2	CALCULATED FAILURE LOADS.....	74
5.2.1	Strut-and-Tie Model.....	74
5.2.1.1	ACI 318-08 Building Code Strut-and-Tie Model Provisions	74
5.2.1.1.1	RF-3R-9(a).....	74
5.2.1.1.2	RF-3R-9(c).....	78
5.2.1.2	2007 AASHTO LRFD Bridge Design Specifications.....	80
5.2.2	PCI Handbook Design.....	82
5.3	COMPARISON WITH CALCULATED LOADS.....	82
5.4	PROPOSED DIRECT STRUT MODEL.....	84
5.4.1	Model.....	85

5.5	CUT SECTION ANALYSIS: BEAM RF-3R-9(c).....	86
5.6	OVERVIEW .....	89
	<b>CHAPTER 6 SUMMARY AND CONCLUSIONS</b>	<b>91</b>
6.1	SUMMARY.....	91
6.2	CONCLUSIONS.....	91
6.3	FURTHER INVESTIGATIONS .....	92
	<b>APPENDIX A BEAM WEIGHTS</b>	<b>93</b>
	<b>APPENDIX B CALCULATIONS FOR PRESTRESS LOSSES</b>	<b>94</b>
	<b>APPENDIX C CALCULATIONS FOR CODE PROVISIONS</b>	<b>96</b>
C.1	ACI CALCULATION: RF-3R-9(a) .....	96
C.2	ACI CALCULATION: RF-3R-9(c) .....	102
C.3	AASHTO CALCULATION: RF-3R-9(a).....	109
C.4	AASHTO CALCULATION: RF-3R-9(c).....	119
C.5	PCI CALCULATION.....	130
C.6	ADJUSTED ACI CALCULATION: RF-3R-9(a).....	132
C.7	DIRECT STRUT ACI CALCULATION: RF-3R-9(a).....	137
C.8	DIRECT STRUT ACI CALCULATION: RF-3R-9(c).....	141
C.9	CUT ANALYSIS: RF-3R-9(c).....	146
	<b>REFERENCES</b>	<b>147</b>
	<b>VITA</b>	<b>150</b>

## **List of Tables**

Table 4-1 Crack widths of existing cracks before and after failure for beam RF-3R-9(a).....	55
Table 4-2 Crack widths of existing cracks before and after testing for beam RF-3R-9(c). ....	61
Table 4-3 Concrete cylinder core strengths from beam RF-3R-9(a).....	70
Table 4-4 Concrete cylinder core strengths from beam RF-3R-9(c). ....	70
Table 5-1 Tie capacities for beam RF-3R-9(a). ....	78
Table 5-2 Tie capacities for beam RF-3R-9(c). ....	80
Table 5-3 Calculated load carrying capacities of dapped ends compared with experimental capacities. ....	83
Table 5-4 Calculated load carrying capacities of dapped ends compared with experimental capacities with adjustments to beam RF-3R-9(a).....	84
Table 5-5 Comparison of adjusted final capacity calculations including cut analysis. ....	89
Table A-1 Measurements for beam weight of RF-3R-9(a).....	93
Table A-2 Measurements for beam weight of RF-3R-9(c).....	93



## List of Figures

Figure 2-1 Concrete deterioration present before testing, beam RF-3R-9(c). .....	5
Figure 2-2 Dapped end general terminology with <i>PCI Design Handbook</i> labeling (drawn from Precast/Prestressed Concrete Institute, 2004). .....	12
Figure 2-3 <i>PCI Design Handbook</i> potential failure cracks in a dapped end section (drawn from Precast/Prestressed Concrete Institute, 2004). .....	13
Figure 2-4 Strut-and-tie model for a dapped end that highlights terminology. ....	15
Figure 2-5 Typical strut-and-tie model proposed by Cook and Mitchell (Cook & Mitchell, 1988). .....	16
Figure 2-6 Typical orthogonal strut-and-tie model used in design (Barton, Anderson, Bouadi, Jirsa, & Breen, 1991).....	17
Figure 2-7 Adjusted orthogonal strut-and-tie model (Barton, Anderson, Bouadi, Jirsa, & Breen, 1991).....	17
Figure 2-8 Dapped end strut-and-tie model proposed by Bergmeister (Bergmeister, Breen, Jirsa, & Kreger, 1993). ....	18
Figure 2-9 Orthogonal strut-and-tie model used by Mader (Mader, 1990).....	19
Figure 2-10 Orthogonal strut-and-tie designed dapped end at failure (Mader, 1990).....	20
Figure 2-11 Strut-and-tie model for prestressed dapped ends proposed by Mader (Mader, 1990). .....	21
Figure 2-12 Typical reinforcement layout in Lin study (Lin, Hwang, Lu, & Tsai, 2003). ....	22
Figure 2-13 Detail of inclined headed reinforcement (Herzinger & Elbadry, 2007). ....	23
Figure 3-1 Moving the beams into FSEL. ....	26
Figure 3-2 Rented crane unloading beam at PRC.....	26
Figure 3-3 Labeling of beams upon arrival to FSEL.....	27
Figure 3-4 Typical beam cross section.....	28
Figure 3-5 Typical beam cross section with deck. ....	28
Figure 3-6 Dapped end reinforcement detail for 54" prestressed trapezoidal box beam.....	30
Figure 3-7 Dapped end reinforcing bars for 54" prestressed trapezoidal box beam.....	31
Figure 3-8 Moderately damaged end region of RF-3R-9(a). ....	33
Figure 3-9 Moderately damaged end region of RF-3R-9(c).....	35
Figure 3-10 Formwork installed ready for pour. ....	37
Figure 3-11 Casting of beam RF-3R-9(c). ....	38
Figure 3-12 Longitudinal cut through test set-up looking west. ....	39
Figure 3-13 Transverse cut through test set-up looking north. ....	39
Figure 3-14 Beam in test set-up looking north.....	40
Figure 3-15 Typical steel plate with 7-inch diameter, 3/8 inch deep counter-bored hole. ....	41
Figure 3-16 Dapped end supports (left). One of the two supports for the non-dapped end (right).....	41
Figure 3-17 Grouted support for bowed dapped end bearing for RF-3R-9(c). ....	42

Figure 3-18 Load plate and bearing pad locations. ....	43
Figure 3-19 Linear potentiometer installed at support.....	44
Figure 3-20 Set-up to measure crack opening at the reentrant corner. ....	45
Figure 3-21 Threaded rod epoxied into predrilled hole in trapezoidal box beam. ....	46
Figure 3-22 Crack measuring/shear distortion instrumentation installed at reentrant corner and in web. ....	47
Figure 3-23 Dimensions of shear distortion instrumentation. ....	47
Figure 3-24 Linear potentiometers installed to measure strand slip. ....	48
Figure 4-1 Free body diagram showing loads reported in Chapter 4.....	50
Figure 4-2 Pre-test cracking and crack widths due to ASR and DEF on the west side of the tested shear span of beam RF-3R-9(a). ....	51
Figure 4-3 Pre-test cracking and crack widths due to ASR and DEF on the east side of the tested shear span of beam RF-3R-9(a). ....	52
Figure 4-4 Cracking in beam on the east (left) and west (right) sides of the beam at a load of 1,000 kips.....	53
Figure 4-5 Cracking in beam on the east (left) and west (right) sides of the beam prior to failure. ....	54
Figure 4-6 Cracking on the west side of beam RF-3R-9(a) after failure. ....	54
Figure 4-7 Cracking on the east side of beam RF-3R-9(a) after failure. ....	55
Figure 4-8 Load-deflection plot for beam RF-3R-9(a) at load point relative to supports. ....	56
Figure 4-9 Measurements of crack opening at reentrant corner on west side. ....	57
Figure 4-10 Pre-test cracking and crack widths due to ASR and DEF on the west side of the tested shear span of beam RF-3R-9(c). ....	58
Figure 4-11 Pre-test cracking and crack widths due to ASR and DEF on the east side of the tested shear span of beam RF-3R-9(c). ....	58
Figure 4-12 Cracking in beam RF-3R-9(c) on the east (left) and west (right) sides prior to failure. ....	60
Figure 4-13 Cracking on the west side of beam RF-3R-9(c) after failure. ....	60
Figure 4-14 Cracking on the east side of beam RF-3R-9(c) after failure. ....	61
Figure 4-15 Load-deflection plot for beam RF-3R-9(c) adjusted for rigid body movement.....	63
Figure 4-16 Crack opening measurements at reentrant corner for west (left) and east (right) sides of beam RF-3R-9(c). ....	64
Figure 4-17 Strain measurements from shear distortion apparatus at the web on the west side of beam RF-3R-9(c). ....	65
Figure 4-18 Picture highlighting the new shear crack passing through the vertical measuring leg. ....	65
Figure 4-19 Strain measurements from the shear distortion apparatus at the web on the east side of beam RF-3R-9(c). ....	67

Figure 4-20 Picture highlighting shear cracks passing through the horizontal and vertical legs of the shear distortion apparatus.....	67
Figure 4-21 Measured strand slip under loading. ....	68
Figure 4-22 Location of cores taken from beam RF-3R-9(a). ....	69
Figure 4-23 Location of cores taken from beam RF-3R-9(c).....	71
Figure 5-1 Free body diagrams showing total failure load of beam. ....	73
Figure 5-2 Typical strut and tie model for a dapped end section. ....	75
Figure 5-3 Non-prestressed reinforcement (red) with strut-and-tie model overlay for beam RF-3R-9(a). ....	75
Figure 5-4 Proposed ACI strut-and-tie model for beam RF-3R-9(a).....	76
Figure 5-5 Extended nodal region at node 3. ....	77
Figure 5-6 ACI strut-and-tie model proposed for beam RF-3R-9(c). ....	79
Figure 5-7 Non-prestressed reinforcement (red) with strut-and-tie model overlay for beam RF-3R-9(c). ....	79
Figure 5-8 Proposed AASTHO strut-and-tie model for beam RF-3R-9(a).....	81
Figure 5-9 Proposed AASTHO strut-and-tie model for beam RF-3R-9(c). ....	81
Figure 5-10 Adjusted strut-and-tie model for RF-3R-9(a). ....	84
Figure 5-11 Proposed direct strut models for beam RF-3R-9(a)[left] and beam RF-3R-9(c)[right]. .....	85
Figure 5-12 Cut section of beam RF-3R-9(c).....	87
Figure 5-13 Cut section analyzed by summation of moments about compression resultant. ....	88

# CHAPTER 1

## Introduction

### 1.1 BACKGROUND

In 1995, a number of trapezoidal box beams were fabricated for the Texas Department of Transportation (TxDOT) for the US59 corridor between IH 610 and BW 8 in Houston, Texas. Many of the in-service beams display concrete cracking due to alkali-silica reaction (ASR) and delayed-ettringite formation (DEF). Five beams, intended for use in the US59 corridor, were rejected by TxDOT because of fabrication errors and were stored in a Houston casting yard. Four beams, cast in July 1995, were severely cracked due to ASR/DEF reactions in the concrete. A fifth beam, cast in November 1995, showed no signs of distress. The beams were rejected due to various deficiencies including: void floatation/rotation, lack of consolidation, poor concrete setting, and incorrect end skew. The five beams represent the possible future condition of the in-service beams as cracking continues from exposure to water that facilitates ASR/DEF. The in-service beams are protected by a deck that limits the amount of water in contact with the concrete, resulting in delayed cracking.

An extensive literature review revealed that flexural strength was not affected by ASR/DEF-related cracking. However, the effect of the cracking on shear strength is inconclusive. The beams of this study exhibit cracking concentrated in the end region where a solid 3 ft 6 in long end block and a dapped end are located. Shear strength in these regions is critical and decreases in the capacity of the end block or the dapped end resulting from ASR/DEF cracking could necessitate costly repairs to ensure that the load carrying capacity of the beams remains adequate. Therefore, a study on the effect of ASR/DEF cracking on the shear capacity of the four severely damaged beams relative to the undamaged beam will provide valuable data for assessing the condition of the beams.

## **1.2 OBJECTIVES**

In order to determine the structural effects of ASR/DEF cracking, TxDOT funded testing to investigate the structural performance of the beams. Testing was conducted in the Phil M. Ferguson Structural Engineering Laboratory (FSEL) at The University of Texas at Austin. The main objectives of the study include:

- i) determining the impact of the concrete cracking due to ASR/DEF on the shear capacity of the beams at the dapped ends for shear span-to-depth ratios between 1 and 2
- ii) and determining the impact of the concrete cracking due to ASR/DEF on the shear capacity of the beams within the hollow trapezoidal box section for variable shear span-to-depth ratios.

## **1.3 SCOPE**

Two specimens with dapped ends that were moderately cracked due to ASR/DEF have been tested. Strut-and-tie modeling and PCI Design Handbook methods have been used to estimate the uncracked capacities. Contained herein are the current findings on the structural performance of the ASR/DEF damaged dapped ends in comparison to the calculated capacities.

## **CHAPTER 2**

### **Literature Review**

#### **2.1 ALKALI-SILICA REACTION**

Alkali-silica reaction (ASR) is a potentially harmful chemical reaction that occurs between the alkali from cement and silica from aggregates. The process begins with highly alkaline pore water moving through the concrete and reacting with silica found in certain reactive aggregate types. The reaction produces a gel that expands as it absorbs moisture from the pores and produces pressure on the surrounding concrete. When the expansive pressure exceeds the tensile strength of the concrete, cracking can result. The presence of gel does not ensure damage; some gels have little expansion capabilities. Highly expansive gel, however, can produce the potentially harmful map cracking indicative of the existence of ASR. In elements protected from moisture exposure, such as bridge girders with a protective deck, cracking may be delayed for several years until the harmful gel absorbs enough moisture to facilitate cracking (Farny & Kerkhoff, 2007).

#### **2.2 DELAYED-ETTRINGITE FORMATION**

Few cases of delayed-ettringite formation (DEF) isolate DEF as the sole cause of concrete deterioration. However, cases such as the San Antonio Y (Thomas, Folliard, Drimalas, & Ramlochan, 2008) and Swedish railroad ties (Sahu & Thaulow, 2004) have proven that DEF can act alone. In most cases, deleterious DEF cracking occurs within pre-existing cracks (Thomas, Folliard, Drimalas, & Ramlochan, 2008). The process of DEF is triggered when concrete reaches temperatures in excess of 158°F in the curing phase. DEF is unlikely without the elevated temperature which causes sulfates and aluminates to be trapped by calcium sulfate hydrate (C-S-H). These trapped sulfates and aluminates are released from the C-S-H over time and react with monosulfate in the concrete to form ettringite. With sufficient available moisture, the ettringite formation can result in expansive forces as the ettringite pushes against the concrete. When these

expansive stresses exceed the tensile strength of the concrete, map cracking of the concrete can result (Folliard, et al., 2006). Originally, DEF was assumed to only occur within steam-cured members; however, in continuing research, DEF has been observed in non-steamed cured specimens (Diamond, 1996). The effect of this type of cracking on the structural performance of the concrete has yet to be fully resolved.

### **2.3 DIAGNOSING ASR AND DEF**

External symptoms of ASR or DEF are very similar. It is difficult to distinguish between ASR and DEF concrete deterioration by external visual inspection alone. Usually, visual inspection is accompanied by internal inspection using petrographic examination. However, it is possible to determine from visual inspection, with relative certainty, if ASR or DEF is the likely cause of the concrete deterioration. Visual symptoms of ASR and DEF are not exclusive to these deleterious mechanisms, but include: expansion, cracking, efflorescence, pop-outs, and discoloration (Farny & Kerckhoff, 2007).

Expansion is difficult to detect without prior instrumentation embedded within the structure. However, the type of cracking resulting from expansion can provide an indication if ASR or DEF is present. Map cracking is often indicative of the presence of ASR or DEF. Generally, the map cracking occurs in unstressed regions. In stressed regions some of the cracking is oriented parallel to the major stress distribution and restraining steel (Kapitan, 2006). Both map cracking and cracking aligned with compressive stress trajectories are visible in the large end block of the beams investigated in this study. Figure 2-1 represents typical cracking present in the end regions of the trapezoidal box beams. Map cracking is evident near the reentrant corner. Large amounts of orthogonal reinforcement are present to restrain vertical and horizontal expansions. ASR and DEF cracking tends to align with reinforcement or principal stress directions. Cracks in stressed regions begin developing at the bottom corner of the beam, and propagate to mid-depth where the horizontal crack continues through the box section. Cracks begin at about a 45-degree angle where stress is minimal, then bend over

becoming horizontal as large compressive forces develop within the section from the prestressing strands.

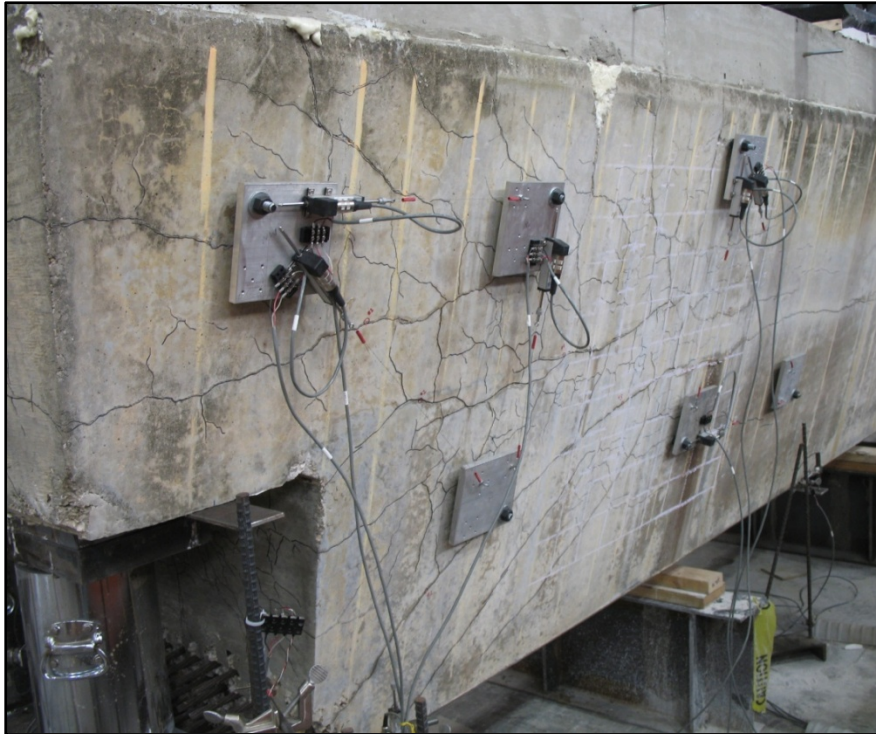


**Figure 2-1 Concrete deterioration present before testing, beam RF-3R-9(c).**

For DEF cracking to occur, the concrete needs to reach temperatures in excess of 158°F to initiate DEF (Folliard, et al., 2006). Similar beams cast at different temperatures can experience significantly different degrees of cracking. The trapezoidal beams in this study cast in July 1995 under hot, humid conditions in Houston exhibit substantial cracking due to ASR/DEF. On the other hand, the trapezoidal box beam cast in November 1995 under cooler conditions shows no signs of ASR/DEF-related cracking. Most of the cracking observed is located in the large end block region which contains a substantial volume of concrete and likely reached excessive temperatures while curing in a high temperature environment.

As previously mentioned, environmental conditions strongly influence ASR and DEF cracking. Sufficient moisture must be present to facilitate cracking due to these



mechanisms (Kapitan, 2006). The beams in this study have remained in a construction yard in Houston, Texas and were exposed to high humidity and rainfall for over 13 years prior to relocation to Austin. Therefore, ample opportunity existed for moisture influx within the pores.

In addition to cracking, other symptoms such as discoloration, efflorescence, and pop-outs can be indicative of ASR or DEF presence. ASR often can be found exuding from the cracks formed by the expansion of the ASR gel. Samples of the gel can confirm or refute the presence of ASR. Additionally, expansions due to ASR or DEF can result in pop-outs of surface concrete (Kapitan, 2006).

It is important to note that while these symptoms can be indicative of the existence of ASR or DEF, physical testing of beam cores is necessary for confirmation. Folliard and Drimalas (2008) cored one of the four cracked beams of this study to determine if ASR and/or DEF were the source of the cracking. Assessment of the cores revealed ettringite filled gaps surrounding the aggregate suggesting that DEF was the main cause of the cracking in the cored beam. Additionally, signs of distress within some aggregates suggested that ASR also contributed to the cracking.

## **2.4 EFFECTS OF CONCRETE DETERIORATION ON STRENGTH PROPERTIES**

Previous studies have produced varying results on the effects of ASF/DEF-related concrete deterioration on the strength properties of reinforced and prestressed concrete members. The majority of studies on flexural strength indicate minimal influence of pre-existing concrete deterioration. Shear effects, on the other hand, produce variable results with some researchers reporting decreased strengths, while others report increased strengths.

### **2.4.1 Reinforced Concrete Beams**

The majority of research on ASR/DEF-related damage has been conducted using reinforced concrete beams. While prestressed concrete beams are the basis of this study,

ASR damaged reinforced concrete provides a foundation for understanding the effect of the damage. Furthermore, the trapezoidal box beams of this study are designed to resist primarily flexural and shear forces when in service. Therefore, research findings from the investigation of the effects of ASR and DEF cracking on the flexural and shear capacities of reinforced concrete are presented here.

#### ***2.4.1.1 Flexural Strength***

According to a report issued by The Institution of Structural Engineers, the effect of ASR on the flexural strength of reinforced concrete is negligible under moderate expansions less than 0.006 in./in. (Kapitan, 2006). This conclusion is supported by research conducted by Fan and Hanson (1998) and Monette et al. (2002). Monette et al. tested beams under both sustained and cyclic loading with insignificant differences between cracked and uncracked beams. Swamy and Al-Asali (1989) reported findings of a decrease in flexural capacity of singly-reinforced beams due to ASR expansions; however, the general consensus is that ASR/DEF induced cracking does not significantly affect the flexural strength of reinforced concrete beams.

#### ***2.4.1.2 Shear Strength***

The effect of ASR/DEF-related concrete deterioration on the shear strength of concrete elements is less defined than the flexural strength. There is a lack of consensus on the effects of cracking on shear strength. Studies conducted by Cope and Slade (1990) and Bach et al. (1993) claim that shear strength is not changed due to the presence of ASR cracking. In both studies, the effect of ASR on shear capacities in the absence of shear reinforcement was studied. In addition to no change in shear strength, Bach et al. concluded that ASR damaged beams exhibited larger deformations at failure and greater cracking pre-failure. Cope and Slade, on the other hand, reported one test in which the beam experienced a brittle failure along an ASR crack at a lower than expected load. These two different failure modes represent the variability that is associated with heavily cracked reinforced concrete beams without shear reinforcement.

In contrast, Ahmed et al. (1998) concluded that the shear strength of reinforced concrete beams increased as a result of ASR damage. Tests were conducted on specimens with and without stirrups. Shear strength increased between 7.4 and 11.9 percent and shear failure cracks were found to initiate from existing ASR cracks. Additionally, Ahmed et al. reported increased fatigue life because of the increased concrete shear strength from ASR expansion.

On the other hand, den Uijl and Kaptijn (2003) reported that ASR reduced shear strength of beam specimens cut from ASR-damaged flat slab bridges without shear reinforcement. Test beams exhibited diagonal tension failures. The lack of transverse reinforcement to provide restraint at the cracks resulted in decreased failure loads. Failure loads reached only 75% of that expected without ASR damage. den Uijl and Kaptijn hypothesized that there would be less reduction in shear strength if shear reinforcement was present.

Considering the large inherent variation in reinforced concrete beam shear strengths, the majority of the reported increases or decreases appear minimal. Nevertheless, previous research is inconclusive on the affect of ASR/DEF on shear strength of reinforced concrete and the topic requires further investigation.

#### ***2.4.1.3 Anchorage***

Small-scale tests conducted by Chana and Thompson (1992) on beams with poor initial anchorage showed a possible decrease in shear strength of 20 – 30% with both plain and ribbed reinforcement and no transverse reinforcement. The researchers claimed the 30% decrease was insignificant due to the poor anchorage provided initially. In another study, Bach et al. (1993) performed tests on beams designed to experience anchorage failures. Beam specimens heavily damaged due to ASR failed at loads 20 – 30% lower than undamaged specimens. Additionally, Bach et al. performed pullout tests on longitudinal reinforcement. Researchers reported decreases in pullout strengths of up to 30% in specimens without transverse reinforcement. When shear reinforcement was included, pullout tests revealed no difference in capacities due to ASR/DEF cracking.

## **2.4.2 Prestressed Concrete Beams**

Few studies are reported regarding the effect of ASR/DEF-related concrete deterioration on prestressed concrete beams. The reported effects on member strengths are discussed below.

### ***2.4.2.1 Flexural Strength***

Boenig et al. (2001) compiled a report on the effects of concrete deterioration due to ASR and DEF on the flexural and shear capacity of full-scale box beams that were transported to the laboratory from the field. Beams exhibited ranges of damage from no apparent damage to extensive damage across the full-length. However, in all tests the region of maximum moment exhibited only a minimal level of damage. Beams subjected to flexural loads failed due to concrete compression zone crushing at loads exceeding 4-7% of the expected capacity. From the results, flexural capacity was deemed unaffected by the minimal visual concrete deterioration in the failure regions. These results support findings from flexural tests conducted by Clayton et al. (1990) on prestressed concrete I-beams.

### ***2.4.2.2 Shear Strength***

In the studies by Clayton et al. (1990) and Boenig et al. (2001), the effects of ASR-related concrete deterioration on shear strength were also investigated. Clayton's study showed varying results from ASR damaged I-beams tested in shear. Clayton tested I-beams with and without shear reinforcement. Three damage conditions were considered: undamaged, initial ASR cracking, and extensive ASR cracking. The objective of the tests was to determine if the concrete expansion caused a two-phase action:

- (1) concrete material strength decreases at the onset of ASR cracking,
- (2) then continued expansions due to the ASR cause a subsequent improvement in the structural performance of the member.

Clayton's tests revealed beams without shear reinforcement experienced the same 20% decrease in strength at both initial ASR cracking and extensive ASR cracking. On the other hand, beams with shear reinforcement experienced strength loss after initial ASR cracking, then subsequent strength gain back to the undamaged shear capacity after extensive cracking. Clayton stated that beams would experience strength loss at initial ASR cracking with or without shear reinforcement, but beams with shear reinforcement would experience increased strength as ASR expansions continued due to the restraint from the vertical reinforcement. Cracking in prestressed beams with shear reinforcement occurred along the length of the beam, engaging the vertical reinforcement as expansion continued. Measurements of crack widths indicated that enough expansion occurred to yield the reinforcement. To prevent yielding of stirrups at extensive expansions, it was hypothesized that two times the provided reinforcement would be required (Clayton, Currie, & Moss, 1990).

Boenig et al. (2001) investigated the effect of ASR/DEF-related concrete deterioration on the shear capacity of prestressed box sections. The box beams were cast with large, 26 in. long end blocks where the majority of the ASR/DEF concrete deterioration was observed. The beams were tested at an  $a/d$  ratio of about 1.9, in the range where web-shear strength,  $V_{cw}$ , controls. Test results indicated a decrease in shear capacity of 14% for heavily deteriorated beams. In addition, strand slip in the anchorage zone noticeably increased in heavily cracked beams indicating that the bond between the strand and concrete had been affected. Although strand slip was present, the researchers concluded strand slip was not the controlling factor in the failures. Instead, all beams failed in web crushing. While the researchers reported a decrease in shear capacity of 14%, such a discrepancy falls within the expected range of scatter for shear data.

## **2.5 HISTORY OF DAPPED END RESEARCH AND DESIGN**

Dapped end beams allow reduced floor depths and more efficient utilization of space. Dapped ends are used within the bridge industry for drop-in girders that allow for increased bridge spans.

While dapped ends have a variety of uses, studies of their behavior are limited. The first studies were completed in the early 1970s and were mainly analytical studies evaluating the elastic stress distribution of forces in the dapped end region (Mattock & Chan, 1979). The first study to determine design of dapped end beams was completed in the late 1970s by Mattock and Chan. The results of this study are still the basis of the PCI Design Handbook dapped end design today, 30 years later. Since Mattock's initial study, subsequent studies have been conducted to improve design equations. Strut-and-tie modeling, shear friction, and diagonal bending are a few of the proposed design methods introduced over the years for these complicated disturbed regions. The PCI Design Handbook and strut-and-tie modeling are the main design methods utilized in this study because they are acceptable methods used to calculate dapped end capacities.

### **2.5.1 Dapped End Terminology**

Figure 2-2 shows typical dapped end elements and related terminology. The nib is the reduced depth portion of the section where the member is supported. Hanger reinforcement is the group of reinforcing bars near the reentrant corner. Vertical stirrups continue beyond the hanger reinforcement and are not shown in Figure 2-2. The main dapped end reinforcement is the horizontal bars at the bottom of the nib extending into the full depth section. Important dimensions used in design include:  $H$ , the full depth of the section;  $d$ , the depth of the flexural reinforcement; and  $d_{\text{nib}}$ , the depth of the main dapped end reinforcement. These terms will be used frequently herein and are important for understanding the design of dapped ends.

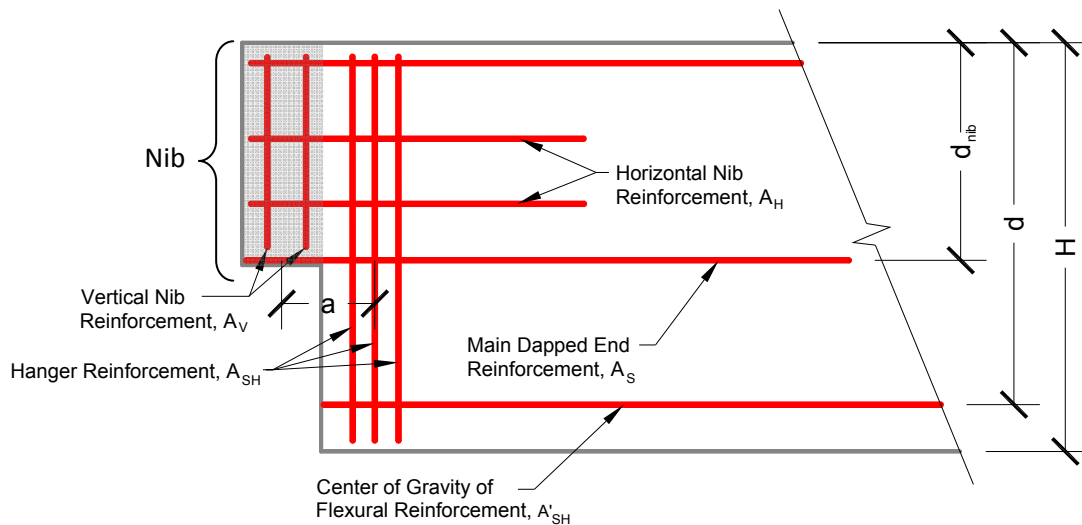


Figure 2-2 Dapped end general terminology with *PCI Design Handbook* labeling (drawn from Precast/Prestressed Concrete Institute, 2004).

## 2.5.2 PCI Design Handbook

The design of dapped ends according to the PCI Design Handbook is based upon two studies conducted by Mattock. The first, conducted in the late 1970s, comprises the main design equations within the Handbook. The latter improves the original design equations with additional findings.

Mattock and Chan (1979) completed a study that led to the existing design equations for dapped ends. Tests of eight dapped end beams provided data on the general behavior of dapped end sections. Design of the specimens were based on: corbel design for the nib, hanger reinforcement with yield strength equal to  $V_u/\phi$ , and resisting the moments created by two potential 45° failure cracks. Variables included the amount of main dapped end reinforcement, hanger reinforcement, and vertical and horizontal nib reinforcement. In addition, the amount of axial load introduced into the system varied between beams. Five conclusions arose from the Mattock and Chan study:

1. The nib region of the dapped end can be detailed using corbel design provisions with “a” being the distance from the center of the hanger reinforcement to the load point.

2. A sufficient amount of steel should be grouped near the face of the end of the full-depth section such that  $A_{sh}f_y$  is greater than or equal to  $V_u/\phi$ .
3. The dapped end shall be designed to resist the moment produced at the possible failure cracks labeled 3 and 5 in Figure 2-3. In addition, normal design should be conducted to ensure that the full-depth section can resist typical flexural and shear loadings.
4. The main dapped end reinforcement needs to contain positive anchorage at the face of the nib and must extend a sufficient distance past the diagonal crack from the bottom corner of the beam (crack 5, Figure 2-3) to ensure proper anchorage.
5. Horizontal reinforcement in the nib should be positively anchored to vertical bars at the face of the nib and should extend a distance  $1.7l_d$  beyond the reentrant corner.

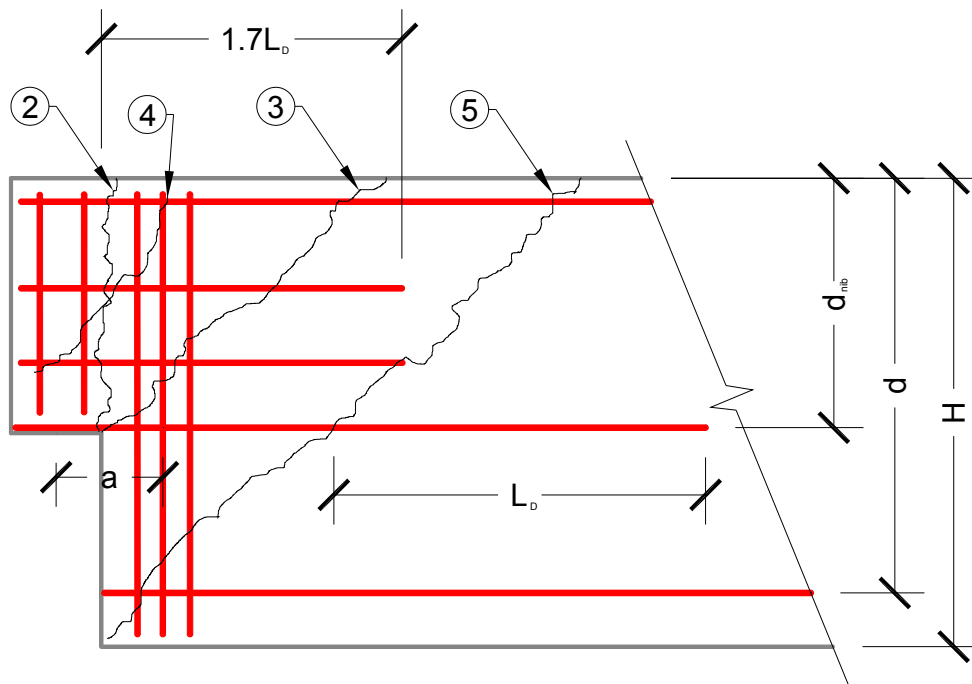


**Figure 2-3 PCI Design Handbook potential failure cracks in a dapped end section (drawn from Precast/Prestressed Concrete Institute, 2004).**



Upon completion of this study, the design recommendations provided by Mattock were incorporated into the PCI Design Handbook. An ensuing study conducted by Mattock expanded on the design provisions presented in 1979 completing the current design provisions in the Handbook (Mattock & Theryo, 1986).

### **2.5.3 Strut-and-Tie Modeling**

In recent codes, strut-and-tie modeling has been introduced as an effective design method to provide lower bound strengths of the disturbed regions of concrete members. In strut-and-tie models, struts and ties form a truss representing the flow of forces through a structure. Struts represent compression loads and ties represent tension loads. The truss should follow the flow of forces found in the elastic stress field diagram to produce the most effective model. The majority of the research utilizing strut-and-tie modeling for dapped ends occurred in the late 1980s and early 1990s. The geometry of a dapped end allows for effective use of strut-and-tie modeling for design.

#### ***2.5.3.1 General Strut-and-Tie Terminology***

Strut-and-tie models are composed of three elements: struts, ties, and nodes. Struts represent compression elements and are shown with dashed lines in the model. Concrete is generally the load-carrying element for struts. Ties represent tension elements and are shown with solid lines in the model. Reinforcing bars are generally the load-carrying elements for ties. Finally, nodes represent the intersection of the different elements. Ties are anchored within the nodal regions. Figure 2-4 shows a typical strut-and-tie model for a dapped end.

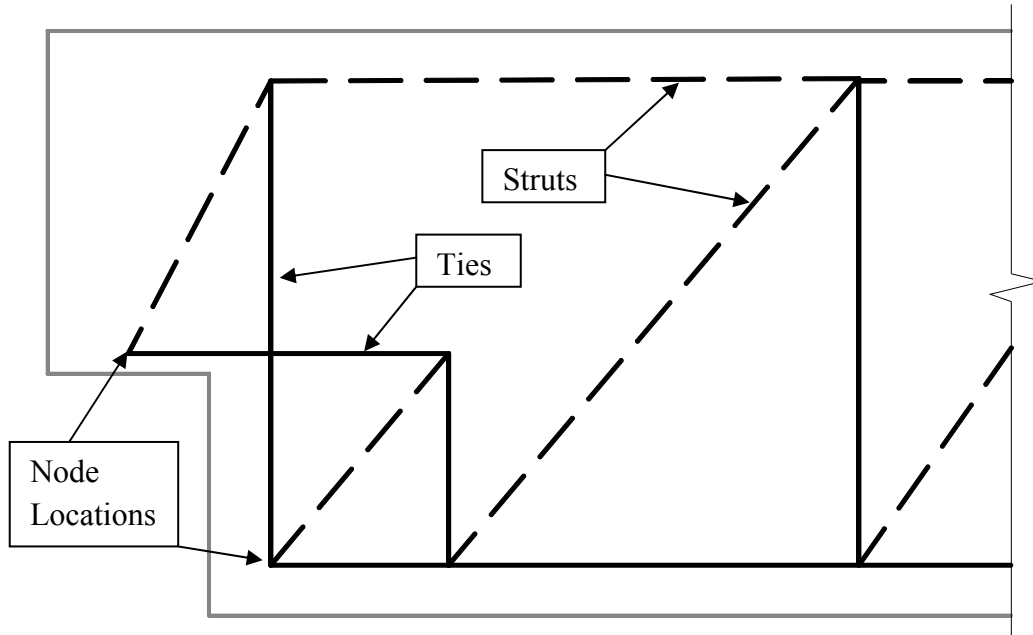


**Figure 2-4 Strut-and-tie model for a dapped end that highlights terminology.**

### **2.5.3.2 Cook and Mitchell (1988)**

Cook and Mitchell (1988) proposed a strut-and-tie model for dapped end design. The model was based on fanning compression fields created in concrete structures disturbed by point loads. The assumption of compression forces fanning out from the bottom corner of the beam provided the foundation for the strut-and-tie model. Figure 2-5 displays the strut-and-tie model. Two main ties, one horizontal and one vertical, are utilized to transfer the loads from the bottom corner of the beam to the support. Two struts intersect the horizontal tie forming a node to anchor the tie. However, the model is incompatible with an elastic model. The compression strut within the full-depth section connecting the horizontal tie to the vertical tie does not follow the flow of elastic forces and increases design forces in the vertical tie.

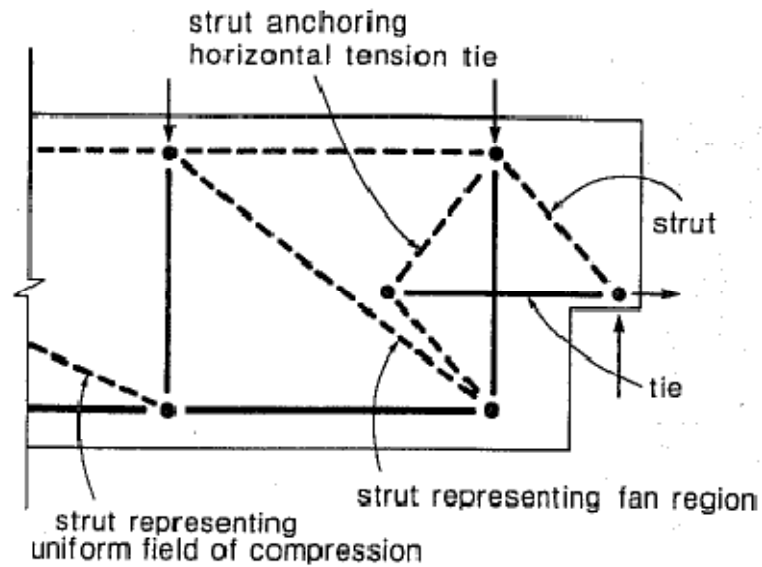


Figure 2-5 Typical strut-and-tie model proposed by Cook and Mitchell (Cook & Mitchell, 1988).

### 2.5.3.3 Barton, Anderson, Bouadi, Jirsa, & Breen (1991)

A study conducted by Barton et al. (1991) expanded understanding of dapped end strut-and-tie models by measuring strains in reinforcement to determine correlation with design stresses. Strut-and-tie models were compared against designs based on the PCI Design Handbook and Menon and Furlong (1977). The strut-and-tie models used for design are shown in Figure 2-6 and Figure 2-7. The designs are comparable to designs proposed by Cook and Mitchell except that Barton et al. form the node to anchor the main horizontal tie with a strut and vertical tie. The models represented the elastic stresses more closely than Cook and Mitchell while using only orthogonal reinforcement. The orthogonal models by Barton et al. provide efficient placement of reinforcement for construction. Upon testing the models, Barton et al. determined that the force expected in the second vertical tie was much smaller than calculated from the strut-and-tie model. Hence, the model in Figure 2-6 provides better representation of stress flow than Figure 2-7, which produces a larger secondary vertical tie.

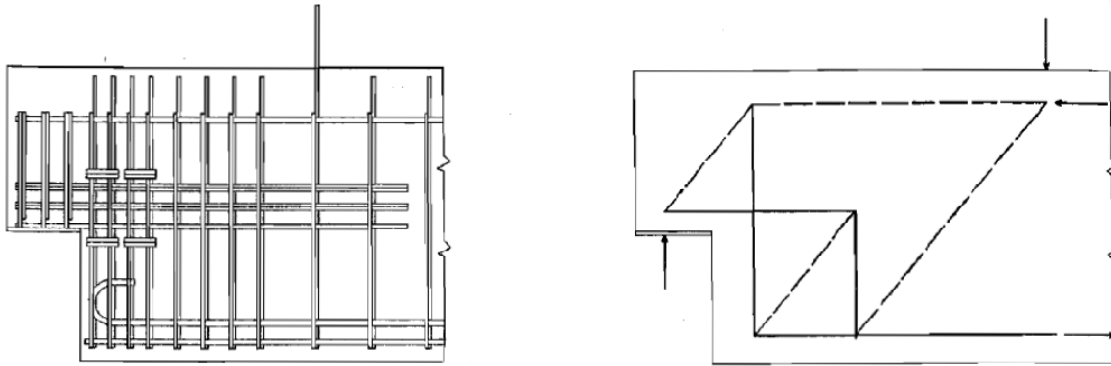


Figure 2-6 Typical orthogonal strut-and-tie model used in design (Barton, Anderson, Bouadi, Jirsa, & Breen, 1991).

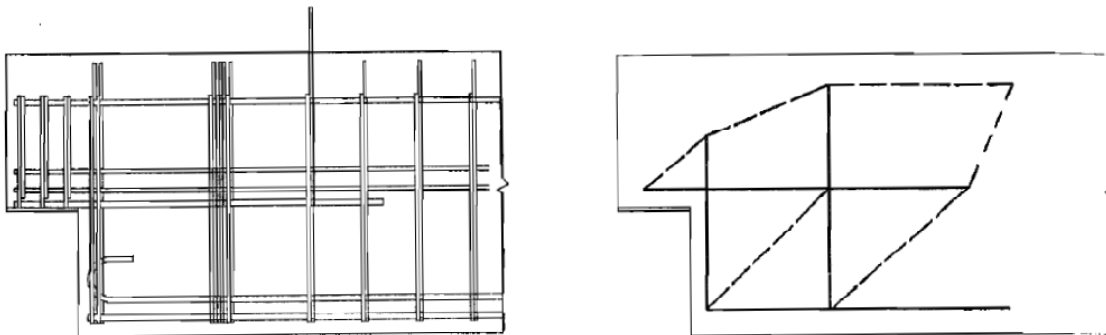


Figure 2-7 Adjusted orthogonal strut-and-tie model (Barton, Anderson, Bouadi, Jirsa, & Breen, 1991).

#### 2.5.3.4 Bergmeister, Breen, Jirsa, & Kreger (1993)

Expanding on the findings of Barton et al., Bergmeister et al. (1993) proposed a more detailed model to represent the forces in the dapped end (Figure 2-8). The arching of the struts and ties near the bearing area model the arching action the concrete utilizes to carry forces into the support. Strut C6 represents the fanning of the compressive stresses in the concrete while transferring from the load point to the bottom corner of the beam. The fanning of compressive forces represents the capability of the concrete to spread the force away from the load point in order to utilize a larger area thereby resulting in a decrease in compressive stresses in the concrete. The addition of strut C6 results in a decrease of the expected force in the secondary vertical tie, T6. The proposed strut-and-tie model can be utilized to estimate the capacity of a dapped end section.

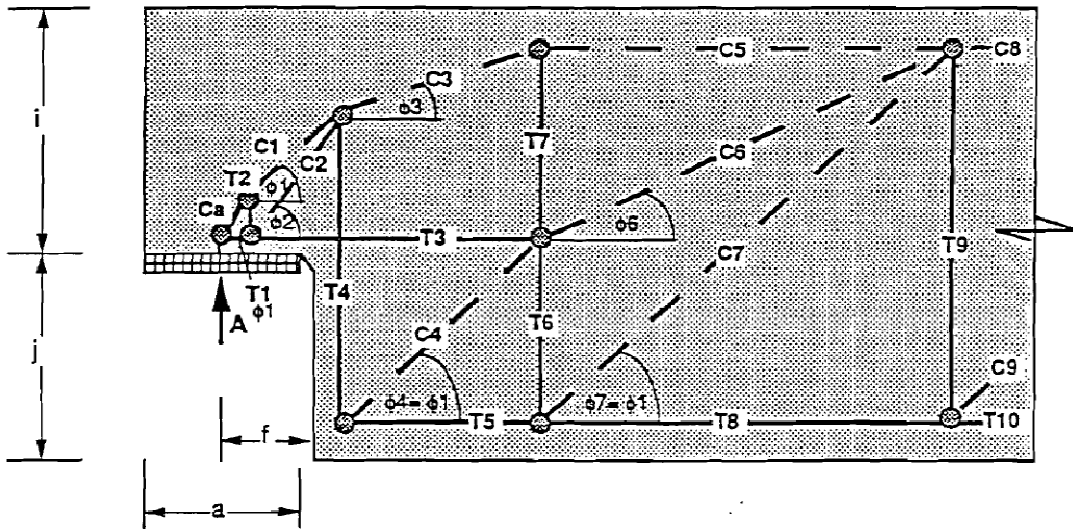


Figure 2-8 Dapped end strut-and-tie model proposed by Bergmeister (Bergmeister, Breen, Jirsa, & Kreger, 1993).

#### 2.5.3.5 Mader (1990)

Few dapped end studies include prestressing, and most of the prestressing studies utilize double-T sections. In a study conducted by Mader, the design of prestressed I-beam sections with dapped ends was examined. Mader tested four dapped ends designed according to the PCI Handbook, the Menon/Furlong method, an orthogonal strut-and-tie model (OST), and a combined strut-and-tie model utilizing inclined rebar at the reentrant corner. In the original design by strut-and-tie modeling, the section was idealized as reinforced concrete and did not include any prestressing forces. Figure 2-9 shows the orthogonal strut-and-tie model used for design. The amount of bottom reinforcement, tie 6, was the same for all beams and provided sufficient flexural capacity to produce a shear failure. The bottom reinforcing bars contained more than the required area to balance the necessary design tie force according to the strut-and-tie models. In addition to the bottom reinforcing steel, eighteen straight prestressing strands were placed in the bottom flange of the beam along with six draped prestressing strands. Each strand was stressed to 18 kips.

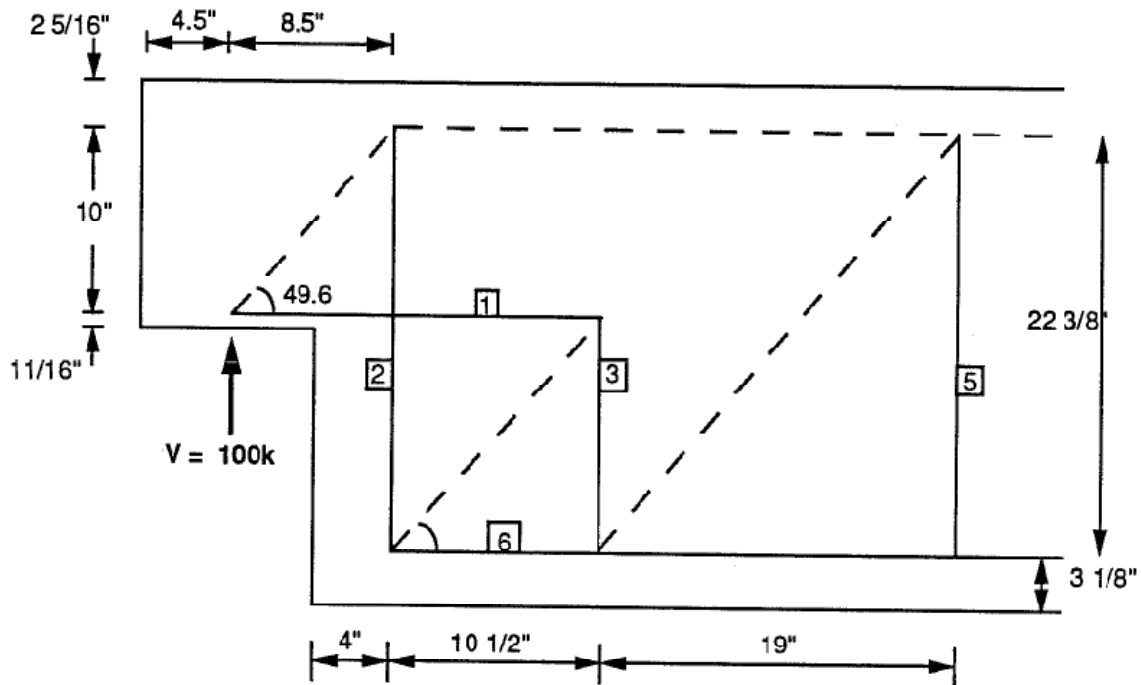
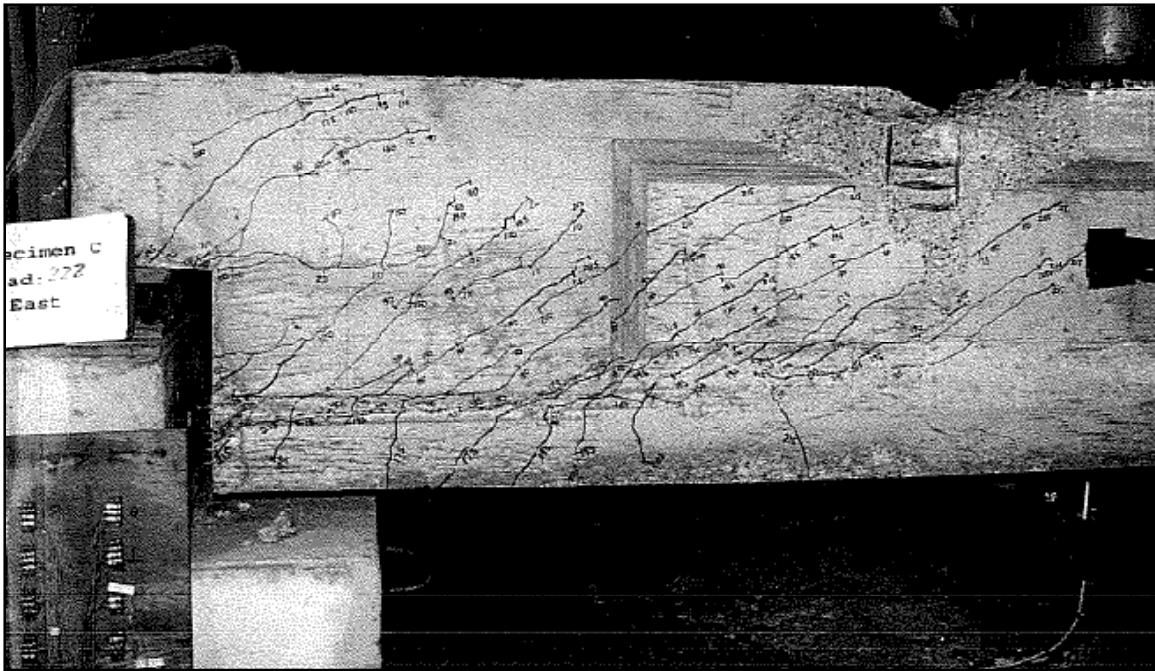


Figure 2-9 Orthogonal strut-and-tie model used by Mader (Mader, 1990).

Figure 2-10 shows the OST designed specimen at failure. Notice the large amount of cracking located at the bottom of the beam. The strains in the reinforcing bars in ties 1, 2, 3, and 6 were measured using strain gages in order to determine the action of the steel as the section began to crack; therefore, the researchers could determine if the ties and strands were acting as designed. Analyzing the data from the OST test, Mader found that the strains in the strands in the transfer length never increased. As expected, the strand cannot pick up any additional load within the transfer length. The strain measurements revealed that most of the reinforcing performed as expected. In the OST test, only the second vertical tie did not reach yield at failure. All tests showed failure before the vertical stirrups away from the dapped end reached yield. The main horizontal nib reinforcement and the vertical hanger reinforcement both yielded before beam failure. In addition to strains, strand slip was also measured and significant bond slip was observed in the OST specimen.



**Figure 2-10 Orthogonal strut-and-tie designed dapped end at failure (Mader, 1990).**

From the tests, Mader developed a strut-and-tie model for prestressed dapped end sections shown in Figure 2-11. The proposed model places point loads at the nodes within the prestressing strand transfer lengths. The point loads represent a portion of the prestressing force that has been transferred to the concrete. For the straight strands, due to geometric strengths, Mader applied half of the total prestressing force at each node. For the draped strands, three nodes collect the prestressing force with a third of the total draped strand prestressing force applied at each node. Vertical ties and inclined struts balance the vertical load introduced by the draped strands.

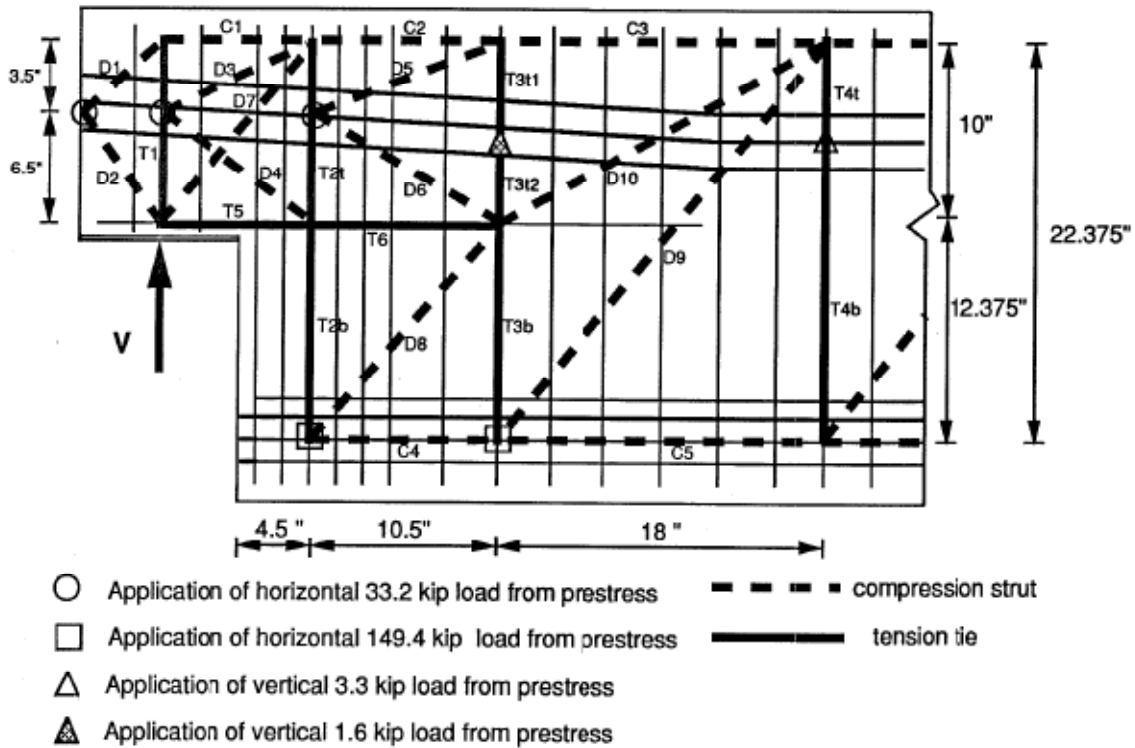


Figure 2-11 Strut-and-tie model for prestressed dapped ends proposed by Mader (Mader, 1990).

### 2.5.4 Recent Dapped End Studies

Recent studies aimed at evaluating and improving provided design equations for dapped end members include work by Lin et al. (2003), Wang et al.(2005), and Herzinger and Elbadry (2007). These studies have improved understanding of the behavior of dapped end sections.

Lin et al. (2003) tested 24 beams with the main variable being the location and amount of hanger reinforcement (Figure 2-12). Lin found that the shear strength of the beam increased as the effective shear span to depth ratio ( $a/d$ ) decreased, where  $a$  and  $d$  are defined in Figure 2-12. The study confirmed the importance of placing the hanger reinforcement as close to the reentrant corner as possible. In addition, Lin introduced a softened strut-and-tie model to estimate the shear capacity of the dapped end.



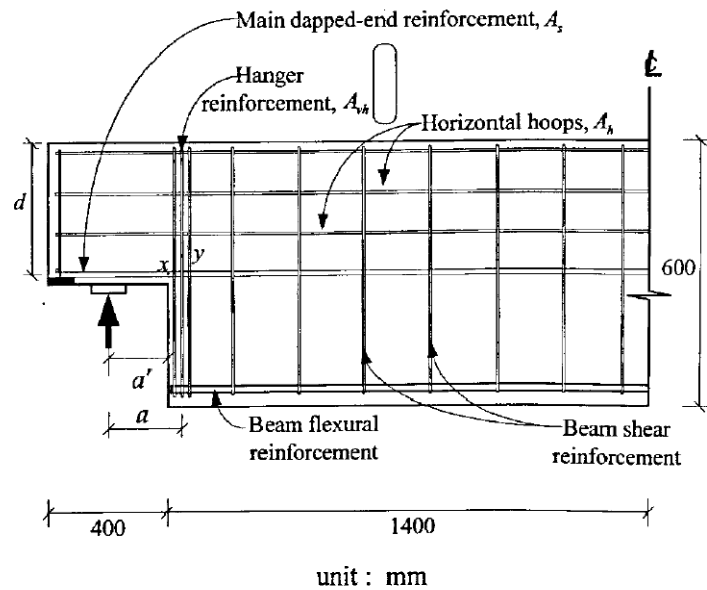


**Figure 2-12 Typical reinforcement layout in Lin study (Lin, Hwang, Lu, & Tsai, 2003).**

Wang, Guo, and Hoogenboom (2005) investigated multiple dapped end variables including orthogonal and inclined reinforcement, amounts of web reinforcement, form of web reinforcement (number of legs and orientation), and affect of the nib depth. Many of the variables had been previously studied, but an important conclusion from the Wang study related to the width of the hanger reinforcement that could be effectively utilized. The researchers instrumented the bars of the hanger reinforcement to determine distribution of strains. Strains indicated that reinforcing bars within  $\frac{1}{4}$  of the nib depth from the center of the hanger reinforcement experienced significant stresses. Wang concluded that the maximum effective width of the hanger reinforcement be half of the nib depth.

Most recent studies conducted by Herzinger and Elbadry (2007) have focused on incorporating headed reinforcing bars into dapped end sections. The headed reinforcing bars would allow for simpler details by reducing development lengths. Headed bars could lead to future use of inclined reinforcement due to the lack of congestion from the decreased development lengths as seen in Figure 2-13. Additionally, Herzinger and

Elbadry utilize shear friction and diagonal bending design methods for dapped end sections.

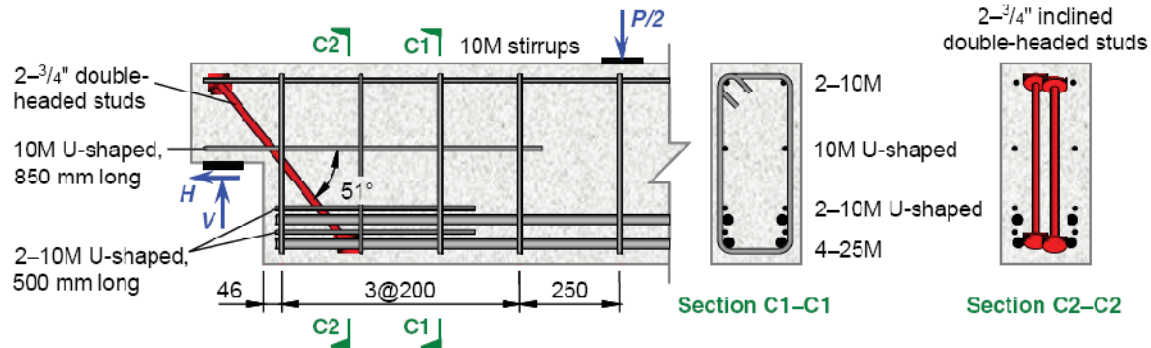


Figure 2-13 Detail of inclined headed reinforcement (Herzinger & Elbadry, 2007).

## 2.6 SIZE OF TEST SPECIMENS

It is important to note that most of the dapped end beams reported in the literature are of small-scale in relation to the trapezoidal box beams of this study. The maximum width of a beam from the previously discussed dapped end studies was 9 inches (Herzinger & Elbadry, 2007), and a maximum depth of about 24 inches (Lin, Hwang, Lu, & Tsai, 2003). The trapezoidal box beams considered in the research reported herein range from 36 inches to 59.75 inches in width and are 54 inches deep. No dapped end studies exist on beams of this size.

## 2.7 OVERVIEW

A review of the literature confirms that ASR/DEF cracking continues to be a problem of unknown dimensions in structures today. The effects of the concrete deterioration on strength have not been clearly defined. Flexural strengths appear unaffected by ASR/DEF-related concrete deterioration, but the effect on shear strength remains unresolved. Studies provide instances of increases and decreases in shear strength in both reinforced and prestressed concrete structures.

Additionally, ASR/DEF cracking in dapped end has not been extensively evaluated. Research of prestressed dapped ends is extremely limited and large-scale testing does not exist. Many different design methods exist for dapped end sections and

are continually being modified. The capacities of the dapped end sections of the trapezoidal box beams considered in this study are estimated using the PCI Design Handbook and strut-and-tie modeling.

## **CHAPTER 3**

### **Experimental Program**

#### **3.1 BACKGROUND**

Two dapped end specimens were tested. In this chapter, the experimental program for these two specimens is discussed including: specimen delivery, specimen details, test set-up, shear spans, and instrumentation.

#### **3.2 TEST SPECIMENS**

##### **3.2.1 Delivery of Specimens**

The original beams ranged in length from 102 ft to 113 ft, weighing between 65 and 71 ton. Due to laboratory constraints of a maximum lifting capacity of 25 ton, the beams were cut into thirds to meet lab capabilities and for ease of transportation. The precasting plant cut the beams and arranged shipping to J.J. Pickle Research Campus (PRC). Beam segments were stored either in the Phil M. Ferguson Structural Engineering Laboratory (FSEL) or on site at PRC. Transfer of beams from the truck to FSEL and to storage at PRC is shown in Figure 3-1 and Figure 3-2.



**Figure 3-1 Moving the beams into FSEL.**



**Figure 3-2 Rented crane unloading beam at PRC.**

### 3.2.2 Specimen Details

Specimens were fabricated with the intention of being installed in the US 59 corridor in Houston. Beams were rejected for various deficiencies including: void floatation/rotation, lack of consolidation, poor concrete setting, and incorrect end skew. Specimen labeling remained consistent with the original labeling. Since the beams were cut, additional labeling was required for the three separate pieces. Each of the three pieces were assigned a letter a, b, or c. The middle sections were all labeled b and the two end sections were labeled a or c. Figure 3-3 provides explanation of beam labels.

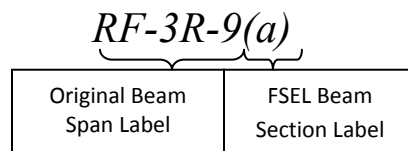


**Figure 3-3 Labeling of beams upon arrival to FSEL.**

#### 3.2.2.1 General Geometric Information

Beam cross-sections outside the end regions were consistent for all beams. Figure 3-4 represents a typical beam cross section. The actual cross section contains an optional 6-inch chamfer between the webs and bottom flange. Strand numbers vary from 58 to 64 with 22 to 24 unbonded strands per section. The unbonded strands are critical in the dapped end regions because a significant decrease in flexural capacity occurs due to these unbonded strands. For beam RF-3R-9, the flexural capacity of the 62-strand section with a deck as in Figure 3-5 was 10,744 kip-ft versus 6,623 kip-ft for the 38-strand section with a deck.

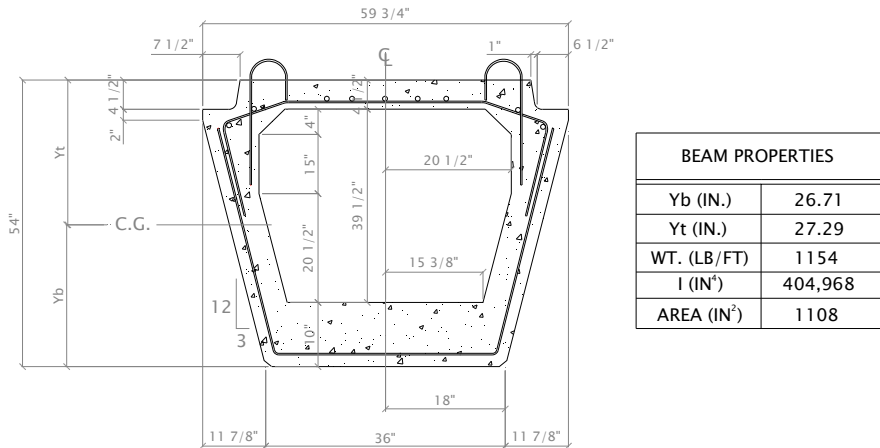


**Figure 3-4 Typical beam cross section.**

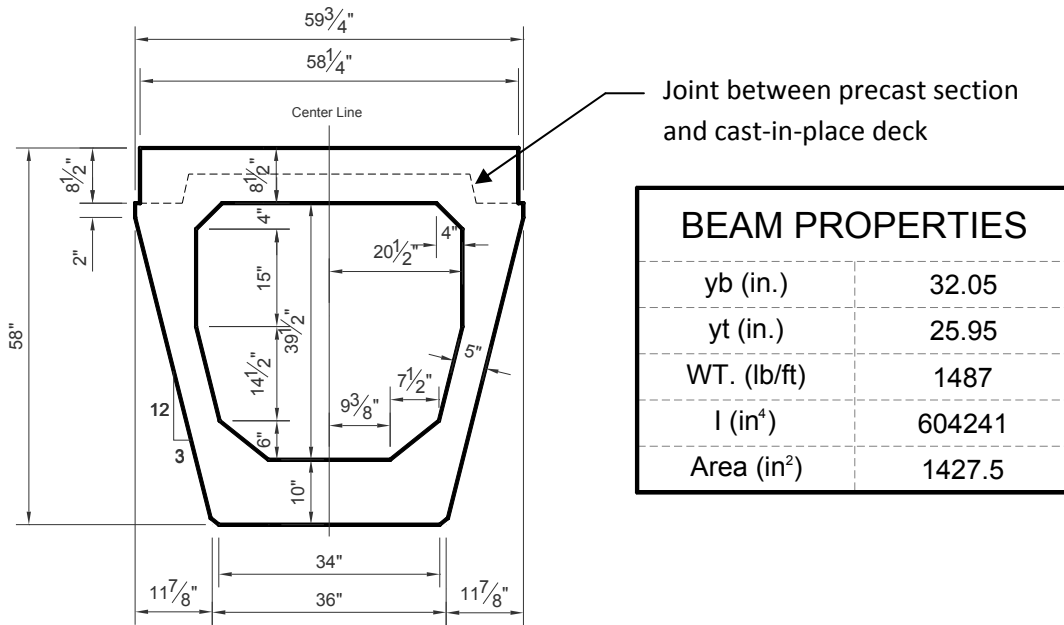


**Figure 3-5 Typical beam cross section with deck.**

Cross section properties at testing vary from those listed in Figure 3-4 mainly due to the addition of the deck slab. Figure 3-5 represents the dimensions and properties of a typical cross section with the deck slab in place. The moment of inertia and area increase significantly upon addition of the deck. Additionally, the centroid moves closer to the top of the beam. The deck causes the weight of the beam to increase above the crane

capacity resulting in the need to cut the beam before removal from the lab after testing. Beam properties from Figure 3-5 were used in subsequent calculations.

### ***3.2.2.2 Dapped End Regions***

The dapped end regions of the beam have a solid end block that extends 3 ft. 6 in. past the reentrant corner as seen in Figure 3-6. The typical reinforcement detail is shown in Figure 3-6 and Figure 3-7. The heavy vertical reinforcement located near the reentrant corner is characteristic of both strut-and-tie modeling and PCI Design Handbook design methods. However, with no distinct grouping of reinforcement away from the reentrant corner, it is unlikely design was according to strut-and-tie modeling. Typical orthogonal strut-and-tie models contain a distinct secondary vertical tie slightly into the beam away from the reentrant corner. The heavily reinforced reentrant corner, designed to prevent failure in this region, can be seen in Figure 3-6 and Figure 3-7. A bar anchors both the top and bottom of the main vertical hanger reinforcement near the nib. The main dapped end horizontal reinforcement is anchored at the back face of the nib via a plate welded to each of the 12 horizontal bars. These features are typical of dapped end design as anchorage can be challenging due to the congestion of reinforcement.



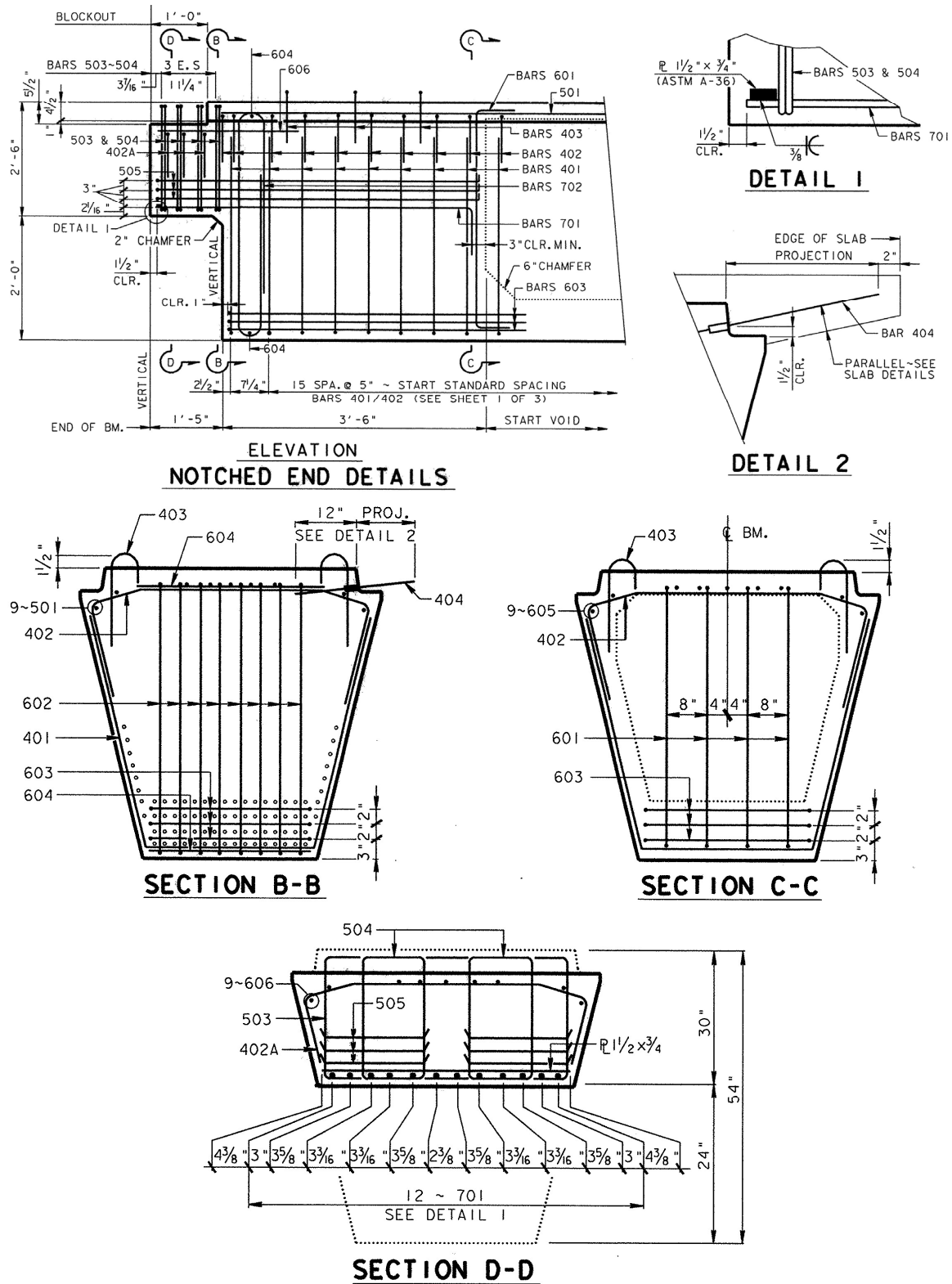


Figure 3-6 Dapped end reinforcement detail for 54" prestressed trapezoidal box beam.

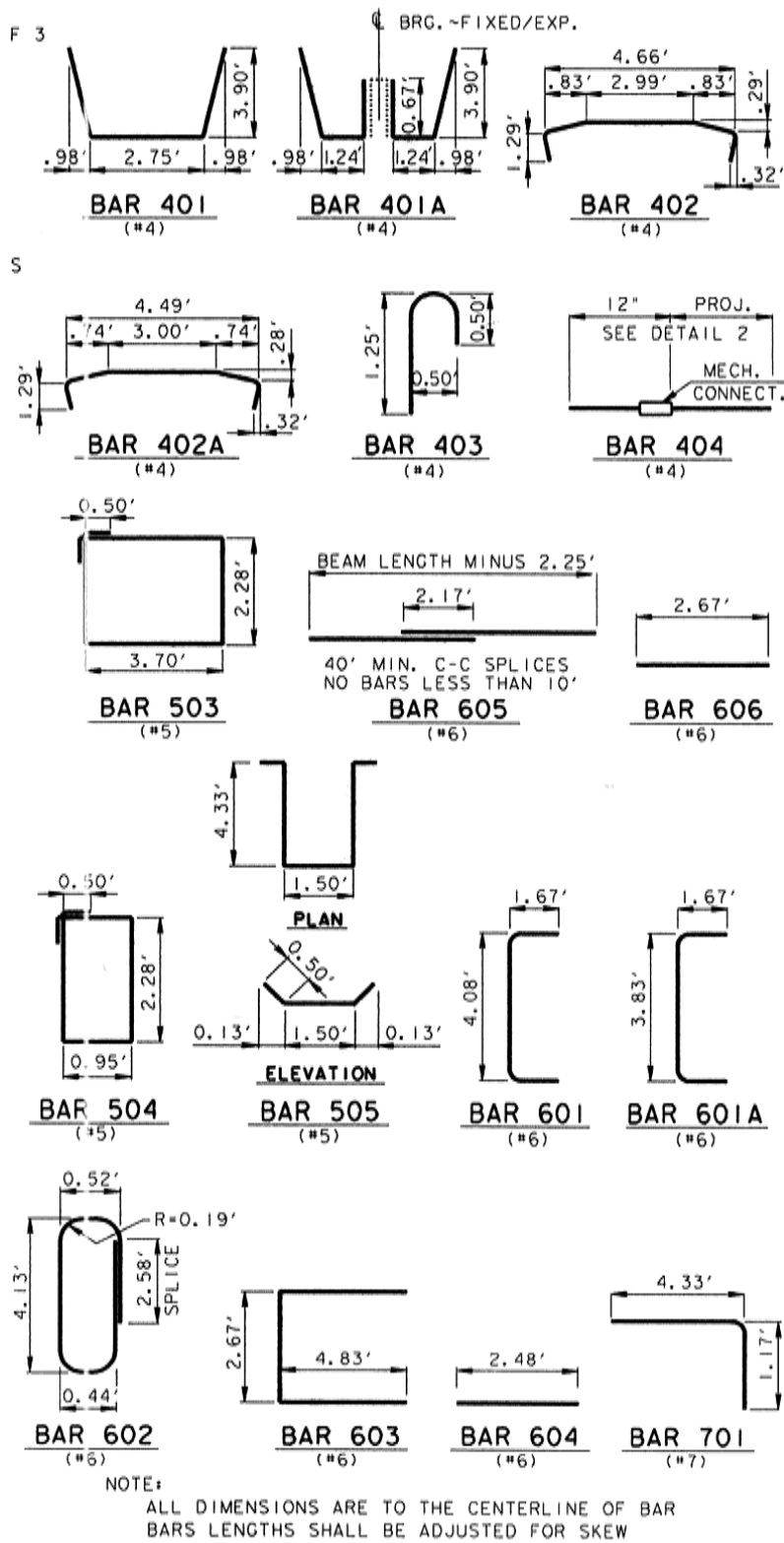


Figure 3-7 Dapped end reinforcing bars for 54" prestressed trapezoidal box beam.

Beams tested in this study include RF-3R-9(a) and RF-3R-9(c). A brief description of each beam is provided below.

### **3.2.2.3 RF-3R-9**

Beam RF-3R-9 was cast on July 6, 1995. The beam was rejected at casting due to void floatation. Concrete placement and consolidation appeared sufficient throughout the beam. The mix design number was 392-3-95R, which specified a concrete mix with a water-to-cement ratio of 0.40. No compressive strength data was provided at release or 28-days. RF-3R-9 had a length of 113 ft. 3 <sup>3</sup>/<sub>4</sub> in. and contained two dapped ends. Cut into three pieces, the ends had lengths of 35.9 ft. and the middle section had a length of 39.7 ft. RF-3R-9 contained 62 prestressing strands running the length of the beam with 24 unbonded strands, leaving only 38 bonded strands at either end. Strands were debonded in 3-ft. increments: 8 strands at 3 ft., 6 strands at 6 ft., 4 strands at 9 ft., 4 strands at 12 ft., and 2 strands at 15 ft. In order to provide sufficient moment capacity to reach failure of the dapped end, a deck was added to increase flexural capacity. The only deficiency was void floatation and considerable concrete cracking. A description of each segment from RF-3R-9 along with a damage assessment is provided in the following sections.

#### **3.2.2.3.1 RF-3R-9(a)**

RF-3R-9(a) measured 35.9 ft. in total length. Void floatation resulted in final web thicknesses at the cut end that varied from 4 <sup>1</sup>/<sub>2</sub> in. to 6 <sup>3</sup>/<sub>8</sub> in. Void location changes over the length of the beam, therefore, actual web thicknesses in the region of testing cannot be determined with complete certainty. However, NDT testing determined that the sum of the web thicknesses generally resulted in a total web thickness of 10 inches. Void floatation also resulted in a top flange thickness that varied from 3 <sup>1</sup>/<sub>2</sub> inches to 4 <sup>3</sup>/<sub>8</sub> inches. With the addition of a deck, the variation in the flange thickness becomes insignificant.

Examination of RF-3R-9(a) revealed moderate concrete deterioration. Map cracking was extensive in the end region, with crack widths ranging from hairline to 0.06 inches. The majority of the cracking was in the end block of the box section, with a horizontal crack continuing into the hollow section that appears to have formed at the joint between casting stages. Minimal cracking continued into the box portion of the beam. Figure 3-8 shows the extent of the cracking on the west side of the dapped end. Neither side appeared to experience significantly more cracking than the other. Cracks of large width were located across the top of the beam, with the widest crack across the top of the beam at the end of the end block as seen in Figure 3-8. High heat associated with a large volume of concrete cast during the summer most likely facilitated DEF in the end block region. Diagonal cracks radiated from the bottom corner of the beams towards mid-depth, similar to a shear crack, then continued horizontal near beam mid-depth. These cracks are noted for future evaluation of shear crack development.

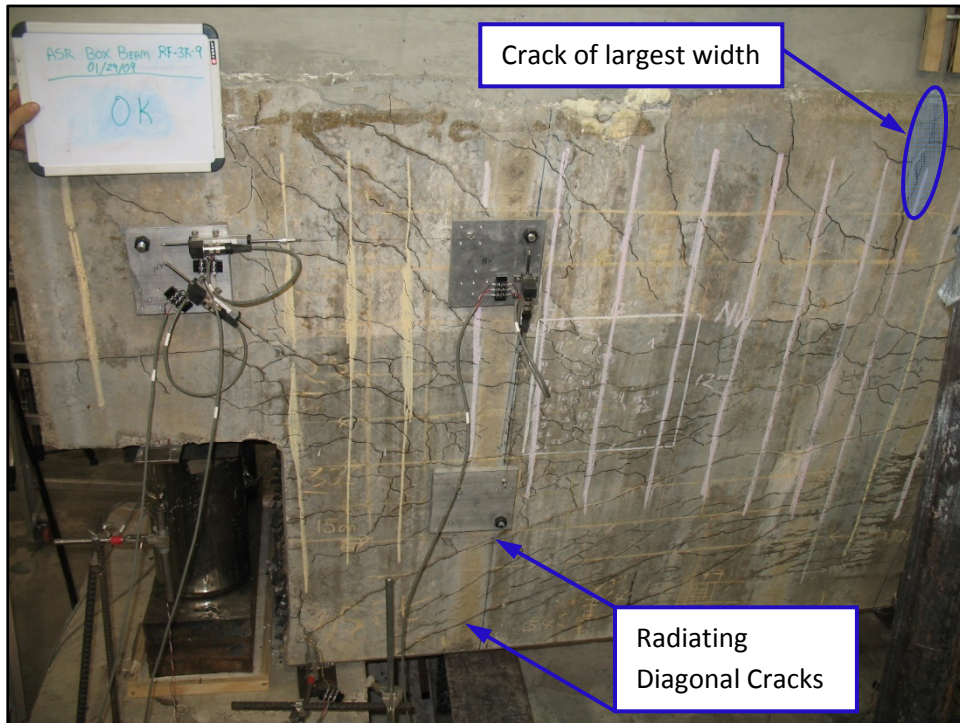
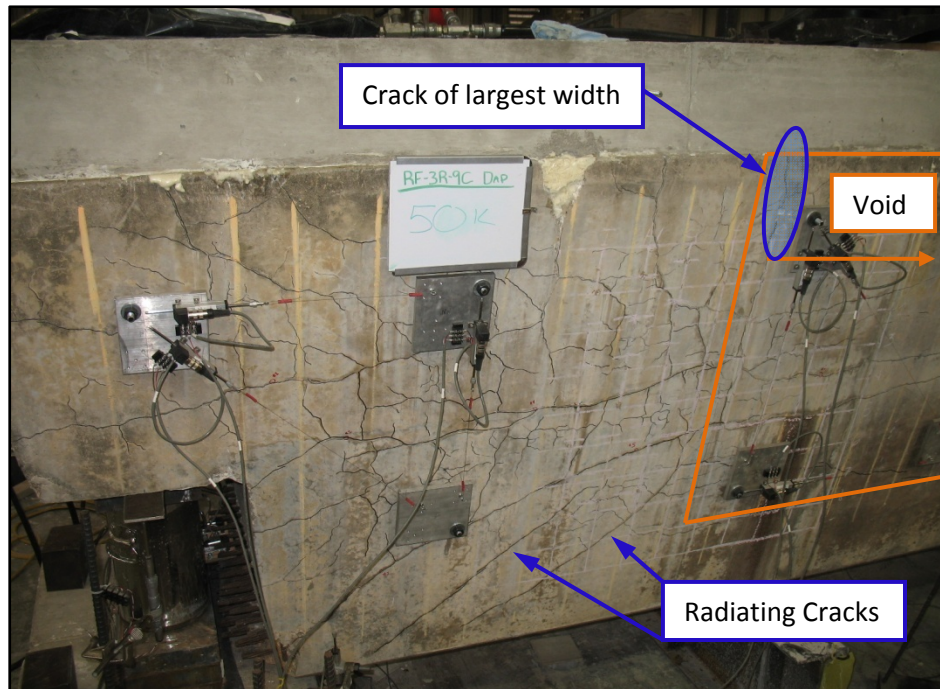


Figure 3-8 Moderately damaged end region of RF-3R-9(a).

#### 3.2.2.3.2 *RF-3R-9(c)*

RF-3R-9(c) measured 35.9 ft in total length. Void floatation resulted in little affect on web or flange thicknesses as the webs both measured 5 inches and the flange thicknesses ranged from 4 ½ inches to 5 1/8 inches. These dimensions matched or exceeded specified cross-section dimensions; therefore, void floatation resulted in minimal visible geometric changes from design. However, it did appear that void floatation was greater near the dapped end. The concrete was poorly placed on the top of the beam and the compression bars were visibly higher than intended. This presented problems in casting the deck as concrete and shear reinforcement had to be removed in order to cast the deck.

Examination of RF-3R-9(c) revealed moderate concrete deterioration. Map cracking was extensive in the end regions, with crack widths ranging from hairline to 0.06 inches. Figure 3-9 shows the extent of the cracking on the west side of the dapped end. Both sides appeared to experience about the same cracking. Cracking did not appear as extensive as in RF-3R-9(a), but cracks of large width appeared in critical shear regions. Hence, like RF-3R-9(a), RF-3R-9(c) was considered to be moderately deteriorated. Similar to RF-3R-9(a), the majority of cracking occurred within the region of the end block, except for a large horizontal crack at mid-depth that continued along the length of the beam. Again, the widest cracks appeared across the top of the beam with the widest crack located across the top of the beam at the end of the end block. Additionally, the same cracks noted in RF-3R-9(a) radiating from the bottom corner of the beam appeared in RF-3R-9(c). These cracks became horizontal away from the dapped end. As stated in Chapter 2, cracks due to ASR often act parallel to the compression stress trajectories. The developing prestressing force introduces compression into the beam and causes the cracks to become horizontal moving away from the ends.



**Figure 3-9 Moderately damaged end region of RF-3R-9(c).**

### 3.2.2.3.3 *Overview of assessment*

Reviewing the crack patterns of RF-3R-9(a) and RF-3R-9(c), cracking appears more orderly than initially deduced. Both beams appear to have developed extensive cracking originating from the top and bottom and continuing in a diagonal fashion towards mid-depth where the cracks turn horizontal. These cracks support the concept that ASR/DEF-related cracking follows stress patterns. The diagonal cracks propagating from the top of the beam are similar to spalling cracks often experienced in prestressed beams. The diagonal cracks at the top of the beam form due to compatibility issues near the end of the beam, and then become vertical as tension cracks become prominent. The diagonal cracks at the bottom of the beam may result from initial bursting stresses from the prestressing strands. The cracks appear along stress trajectories for prestress beams following the pattern (referenced in Chapter 2) of ASR/DEF-related cracks aligning with the stresses in the beam. There is no record of cracking after fabrication and before the beams were shipped to FSEL.

It should be noted that no information on release strengths was available for beam RF-3R-9; therefore, it is unknown whether the concrete achieved adequate strength at release since the beam was rejected. This could explain, to some degree, the large tension-like cracking apparent across the top of the beam. These tension cracks may have formed at stress release thereby facilitating DEF growth.

### **3.2.3 Deck Casting**

Preliminary analysis of the trapezoidal box beams showed that a deck slab had to be added in order to provide adequate flexural capacity. The large number of unbonded strands and variability in top flange thickness due to void floatation significantly altered the flexural capacity of the beams along the length. Additionally, the top surface of some beams was not finished and would have caused difficulties when applying load to test the beam. The deck slab provided a flat, even surface to set the load plates and enough thickness to ensure that the neutral axis was in the top flange at flexural failure.

Wood forms were fabricated to produce a slab that measured 8 ½ inches above the ledge at the top of the trapezoidal shape of the box beam (Figure 3-4). The cast-in-place deck thickness was 4 inches above the top flange of the box beam producing a final top flange thickness of 8 ½ inches. The actual thickness varied depending on void floatation in a given beam. The forms were fabricated in 8-foot long segments with 5 per side creating a total length of 40 feet. These general dimensions allowed the formwork to be used for any beam segment tested. Individual pieces were bolted together and placed on ¾ inch of the ledge creating a total width of 58 ¼ in. for the deck. Threaded rod passing through the deck to be cast tied together the formwork on either edge of the beam. The rods held the forms in place as the concrete was placed. A 4-inch deck thickness required only one layer of reinforcing bars. Typical deck reinforcing called for #4 bars spaced at 9 inches longitudinally and #5 bars spaced at 6 inches transversely. Figure 3-10 shows the forms in place ready for casting.



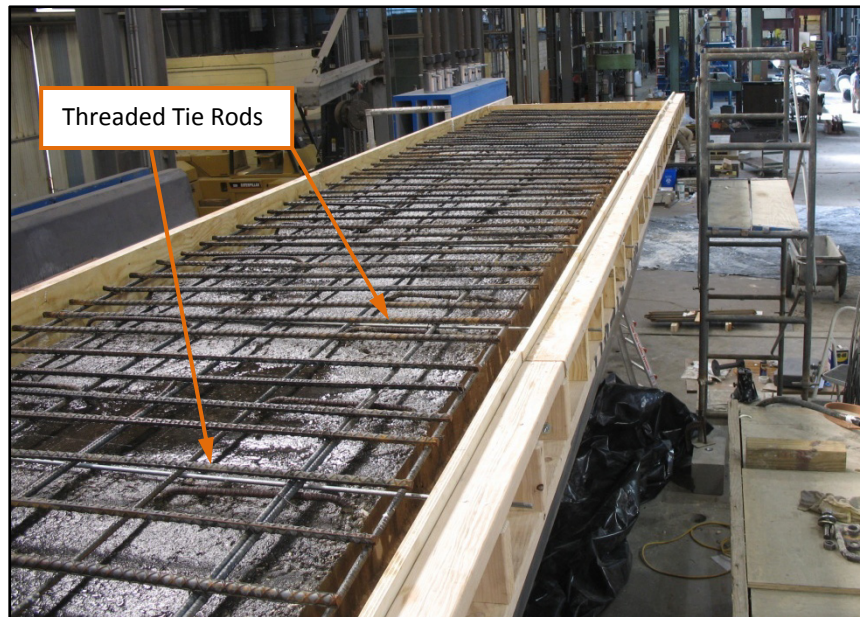


**Figure 3-10 Formwork installed ready for pour.**

The deck was cast using a 10 ksi concrete mix. The abnormally high strength concrete for a deck was used in order to test the beam as quickly as possible. An additional advantage of the high strength concrete was a slight increase in larger flexural capacity. The top of the beam was wetted before casting to prevent the dry surface of the box beam from absorbing moisture from the fresh concrete. A screed was used to level the concrete, and further surface preparation was performed near the load points (Figure 3-11).





**Figure 3-11 Casting of beam RF-3R-9(c).**

Void floatation caused problems when casting beam RF-3R-9(c). The void floatation resulted in raised longitudinal and shear transfer bars. The shear transfer bars extended above the formwork necessitating removal by torch cutting. In addition, some concrete had to be removed to provide at least two inches of cast-in-place deck concrete above the existing flange. Two inches was determined to be sufficient for bonding with the existing concrete and for aggregate suspension.

### **3.3 SHEAR TEST**

#### **3.3.1 Shear Test Set-up**

Testing took place at the Phil M. Ferguson Structural Engineering Laboratory (FSEL). The test set-up was designed specifically for shear testing of large-scale bridge girders. Figure 3-12 and Figure 3-13 contain a side view and end view of the test set-up, respectively. Figure 3-14 shows a beam in the test set-up. Load was applied via the twin 2,000 kip hydraulic rams. Attached to the ram head was a 12-inch diameter spherical head. The spherical head reacted against a steel plate set in Hydrostone on the beam. The Hydrostone eliminated small imperfections at the slab surface and aided in leveling

the plate. The rams reacted against the white transverse steel spreader beam, which subsequently transmitted the load into the brown longitudinal steel hold-down beams. Nuts placed above the hold down beams and below the elevated strong floor transferred the load from the hold-down beams, through three steel rods on each side of the beam, and into the reinforced concrete strong floor.

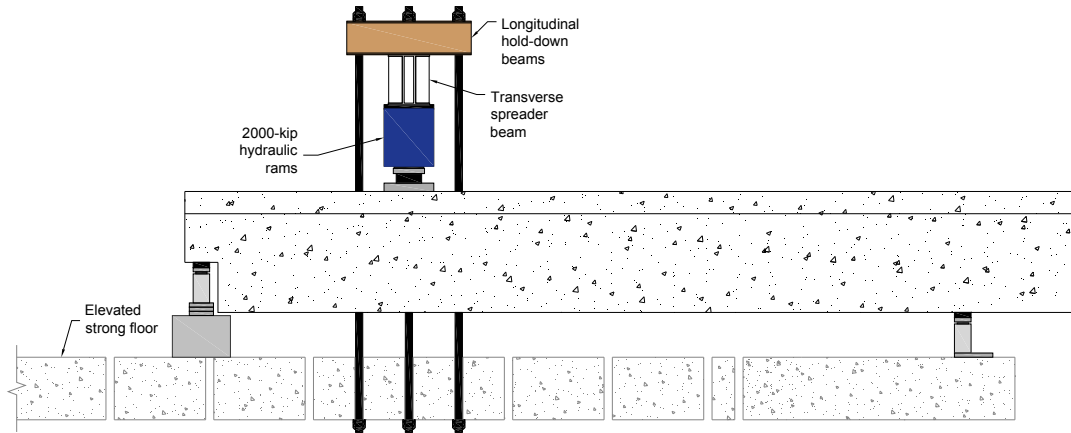


**Figure 3-12 Longitudinal cut through test set-up looking west.**

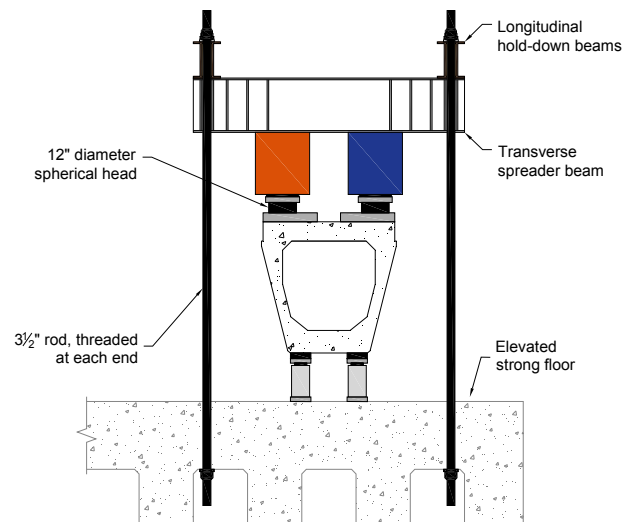


**Figure 3-13 Transverse cut through test set-up looking north.**

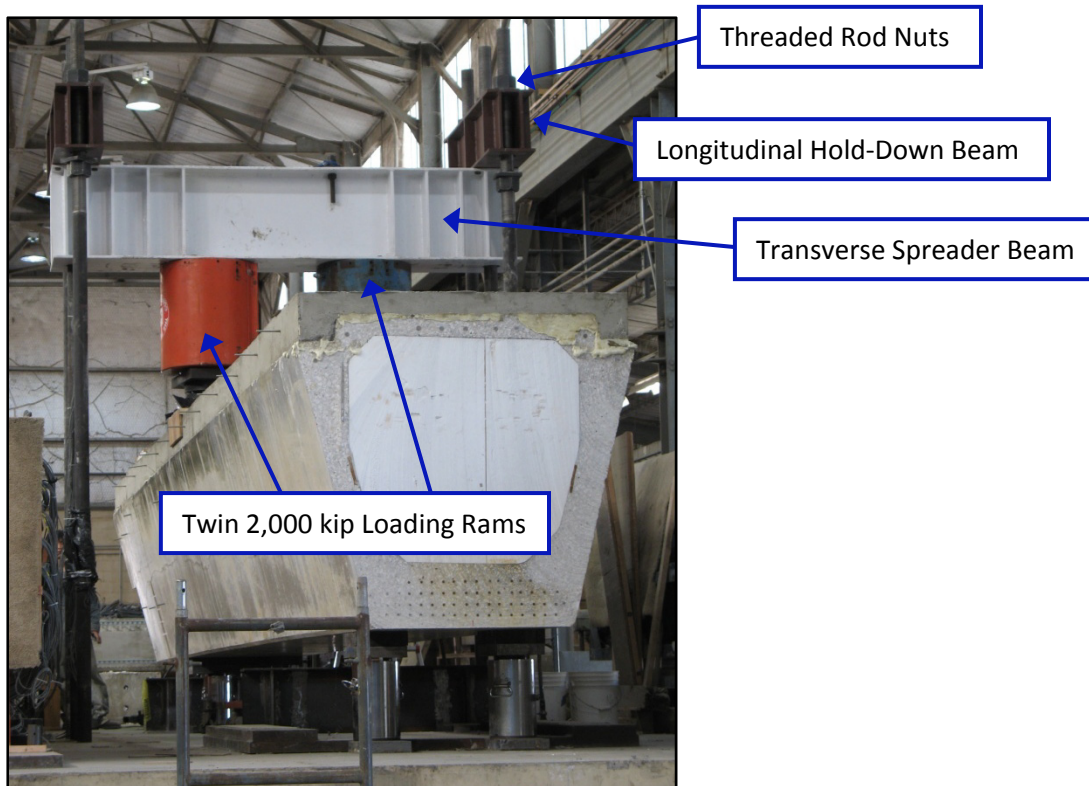


**Figure 3-14 Beam in test set-up looking north.**

The beam rested on four load cells used to measure the applied load. In total, three bearing plates supported the beam: one at the dapped end and two below the webs at the cut end. The single bearing plate measured 32 x 9 inches and the twin plates measured 16 x 9 inches. The single bearing plate had the long direction perpendicular to the longitudinal axis of the beam, whereas the twin plates were placed so the long dimension ran in the longitudinal direction. Each load cell was topped with one 2-inch thick steel plate containing a 7-inch diameter circle counter bored 3/8-inch into the plate (Figure 3-15). With the top of the load cell being slightly convex, the counter-bore prevented significant slippage between the steel plate and load cell. Atop the steel plate was a 2 ½-inch, 5-laminate elastomeric bearing pad aiding to evenly distribute the load between the load cell and the concrete box beam. The elastomeric bearing pads matched the dimensions of the corresponding steel plate. A bolt connected the load cells to 2-inch thick steel plates at the bottom completing the supports. Figure 3-16 shows entire set-up for the single plate bearing and twin plates bearing.

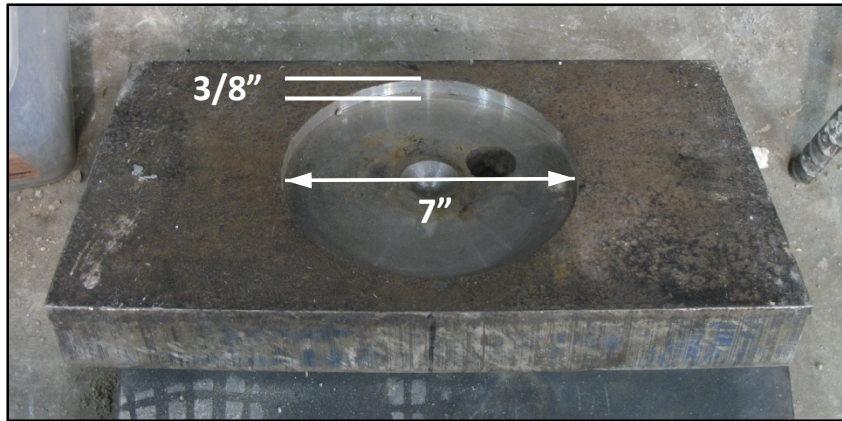


**Figure 3-15 Typical steel plate with 7-inch diameter, 3/8 inch deep counter-bored hole.**

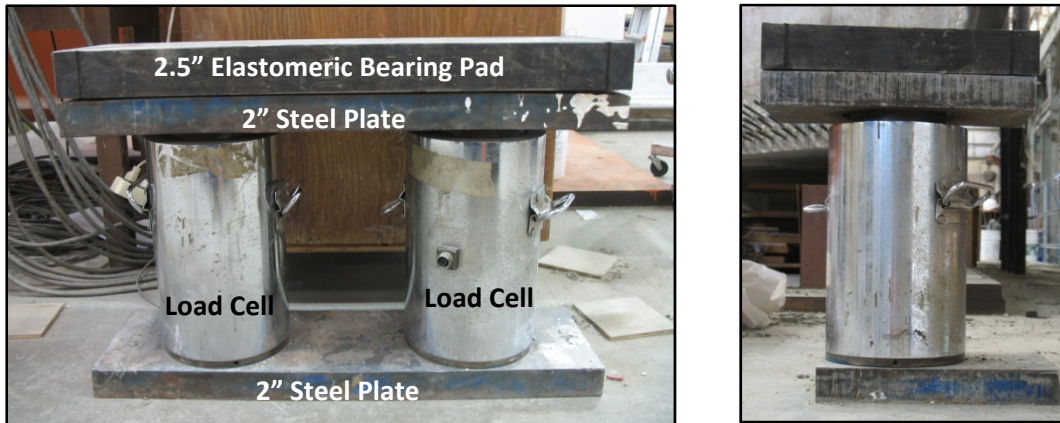


**Figure 3-16 Dapped end supports (left). One of the two supports for the non-dapped end (right).**

The load cells at the dapped end were supported on two concrete blocks and steel plates in order to reach the bottom of the nib. The bottom of the dapped end of RF-3R-9(c) was not flat due to insufficient formwork support. To adjust for this condition, a 2-inch steel plate replaced the elastomeric bearing pad and grout was used to fill the gap and distribute the load from the concrete to the steel plate. Figure 3-17 shows the support with the steel plate.

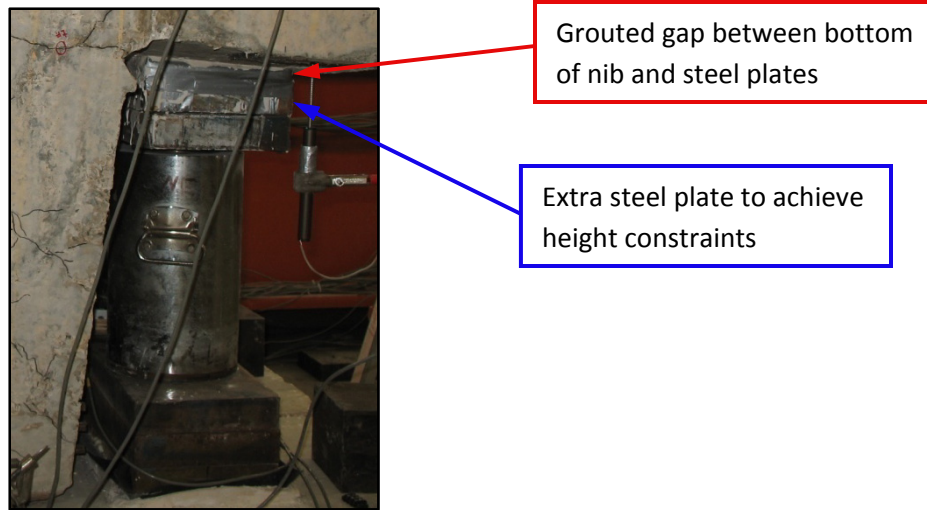


Figure 3-17 Grouted support for bowed dapped end bearing for RF-3R-9(c).

### 3.3.2 Shear Span

In contrast to using shear span-to-depth ratios between the support and the load point, many dapped end studies reported in the literature specify the distance from the vertical hanger reinforcement to the support as the governing dimension affecting shear strength. Because the distance between the support and hanger reinforcement was set for all beams in this study, the shear span ( $a_d$ ) was taken as the distance from the centroid of the vertical hanger reinforcement to the location of the applied load. As the shear span increased, a larger portion of the hollow section was engaged increasing the probability of failure in the thin web sections.

Load plate and bearing pad locations for each beam are shown in Figure 3-18. The depth to the centroid of the prestressing strands in each beam was about 53.2 in. from the top of the slab, resulting in an  $a_d/d$  of 0.94 and 1.58 for beams RF-3R-9(a) and RF-3R-9(c), respectively. The two shear spans values were close to the minimum and median of the desired range. Furthermore, a shear span of  $0.94d$  corresponds to a shear span-to-depth ratio of about 2.0 with respect to the effective depth of the nib. The shear span of  $0.94d$  was used to investigate the effect of the ASR/DEF-related concrete deterioration on the nib portion of the beam. A shear span of  $1.58d$  engaged a larger



portion of the hollow section of the beam while still applying the point load near the disturbed end region.

The elevated testing slab ended about 24 ft. from the load point on the opposite side of the tested span. Hence, a distance of 22.5 ft. was used for the long shear span creating a total span of 27 ft. 10 in. for RF-3R-9(a) and 30 ft. 8 in. for RF-3R-9(c) as shown in Figure 3-18.

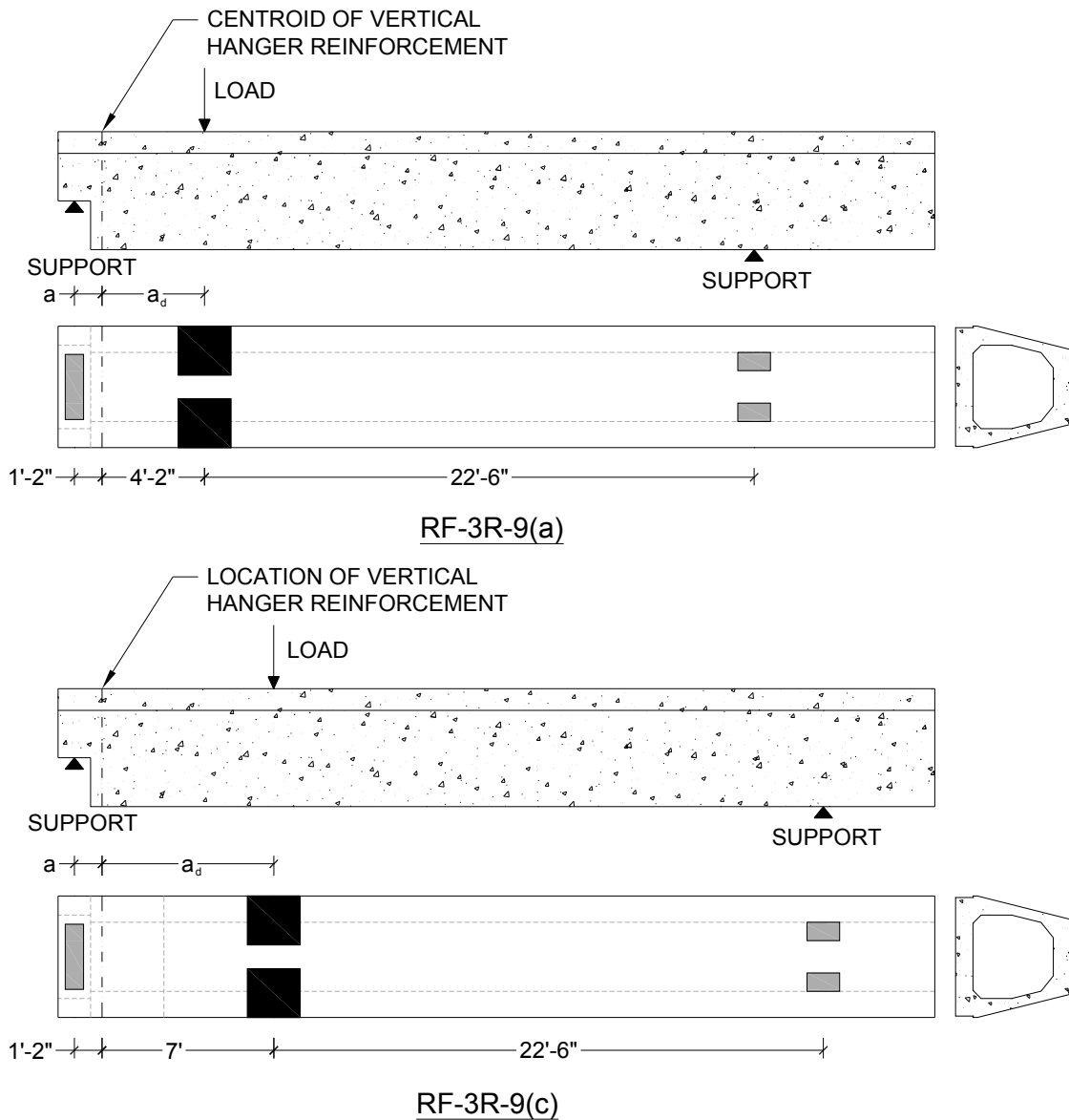


Figure 3-18 Load plate and bearing pad locations.

### 3.3.3 Instrumentation

#### 3.3.3.1 RF-3R-9(a)

Deflection, load, and crack opening at the reentrant corner were measured. Deflection was measured in four different locations along the length of the beam using linear potentiometers ranging from 2 to 6 inches stroke. Linear potentiometers were placed at each support, at the bottom of the beam near the reentrant corner, and at the load point. Steel plates were glued to the bottom of the beam to facilitate deflection measurements and protect the linear potentiometers from spalling concrete. Figure 3-19 shows a linear potentiometer installation. Two 1,000 kip load cells were placed at each support to measure support loads.

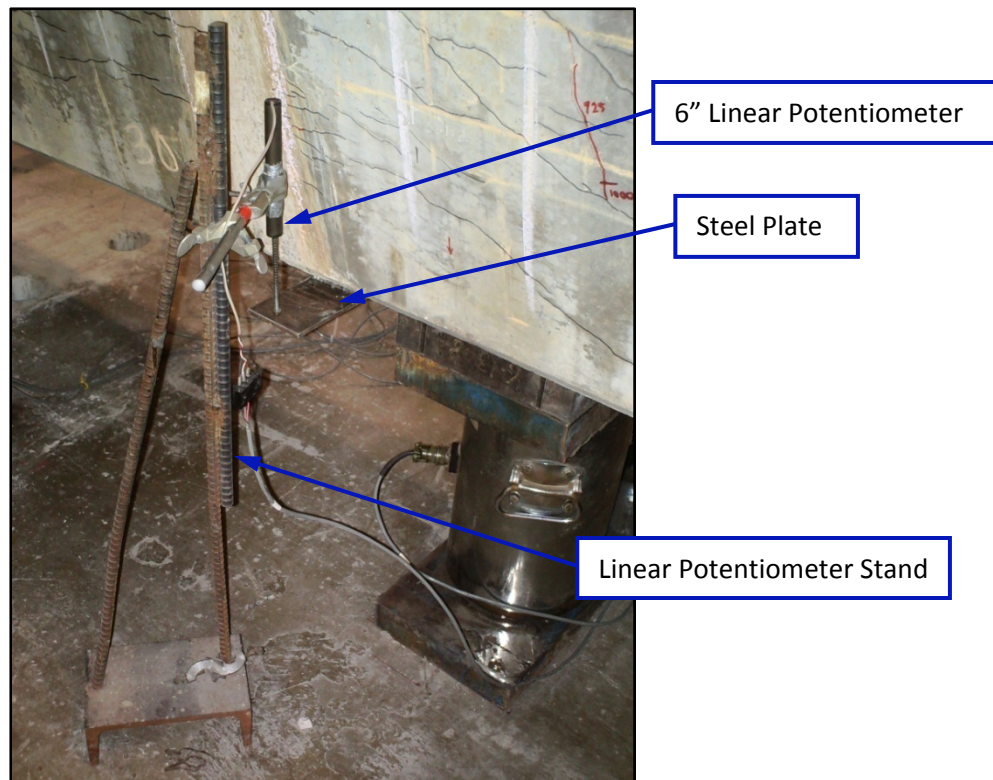
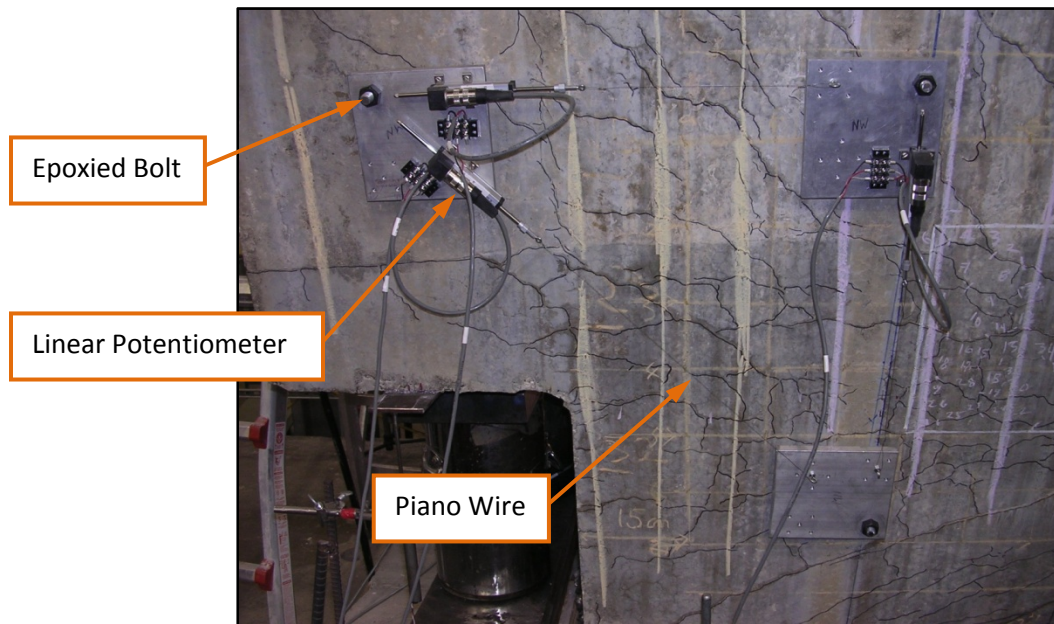


Figure 3-19 Linear potentiometer installed at support.

In addition, linear potentiometers measured opening of cracks at the reentrant corner. Three linear potentiometers attached to three aluminum plates were arranged to form a 45-degree right triangle with the diagonal near the reentrant corner (Figure 3-20). Piano wire connected the linear potentiometers to eye screws on the aluminum plates. To attach the plates to the beam, three ½-inch holes were drilled into the concrete to form a 45-degree right triangle with leg lengths of two feet. The holes extended past the exterior shear reinforcement into the core concrete. Bolts were then epoxied into the holes as seen in Figure 3-21. Once the epoxy had set, two nuts and washers connected the plates to form this crack and shear distortion measuring apparatus. The plates were aligned in the same plane. The linear potentiometers, eye screws, and piano wire were arranged such that the centerline of linear potentiometers intersected the bolts. As such, the linear potentiometers measure the relative movement of the bolts with respect to one another. Originally constructed to measure shear deformations, in this application, the diagonal provides a measure of the opening of cracks at the reentrant corner, and the horizontal and vertical potentiometers measure opening of any cracks that cross the gaged length. The shear distortion apparatus was only installed on the west side of the beam.



**Figure 3-20 Set-up to measure crack opening at the reentrant corner.**





**Figure 3-21 Threaded rod epoxied into predrilled hole in trapezoidal box beam.**

### **3.3.3.2 RF-3R-9(c)**

The same instrumentation used for beam RF-3R-9(a) was placed on beam RF-3R-9(c). The longer shear span and information from the first test lead to additional instrumentation for this beam. The shear distortion instrumentation was used to measure crack openings at the reentrant corner on both sides of the beam and shear deformations and crack openings in the web portion within the shear span. Using a longer shear span resulted in engagement of a larger portion of the thin web of the box section. Distinguishing the area as a possible failure zone, and a potential location for large cracks, measuring the elongations in the region provided a further understanding of behavior. Installation was identical to the device at the reentrant corner from beam RF-3R-9(a). Figure 3-22 shows the crack measuring instrumentation installed and Figure 3-23 gives dimensions.



Figure 3-22 Crack measuring/shear distortion instrumentation installed at reentrant corner and in web.

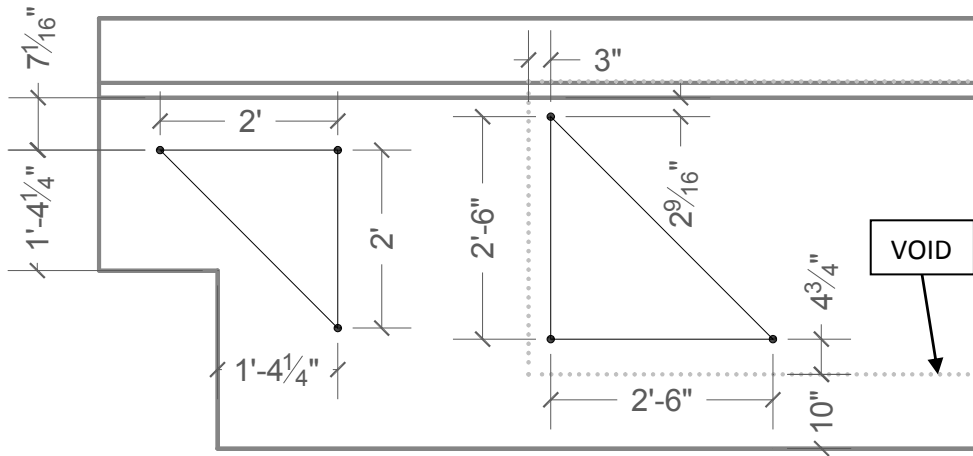


Figure 3-23 Dimensions of shear distortion instrumentation.

After testing RF-3R-9(a), strand slip appeared to be an important factor in the beam failure. In addition, according to the strut-and-tie model for RF-3R-9(c), shear induced anchorage was a possible governing failure mechanism. As such, two additional linear potentiometers were attached to strands. Figure 3-24 shows installed strand slip

linear potentiometers. The potentiometers were fixed to the strands while the measuring rod butted against the concrete. As the strand moved relative to the concrete, the linear potentiometer measured the corresponding differential movement.



**Figure 3-24 Linear potentiometers installed to measure strand slip.**

### **3.4 OVERVIEW**

Two dapped end sections of beam RF-3R-9(a) were tested at FSEL in order to evaluate the response of the dapped end, which exhibited significant concrete cracking due to ASR and DEF. Tests were conducted at shear span-to-depth ratios of  $0.94d$  and  $1.58d$ , representing the minimum and maximum of the desired testing range. A deck was added to the beams to ensure that failure occurred within the dapped end section. Instrumentation was installed to measure the response of the dapped end under applied load. Chapter 4 continues with results from the dapped end testing.

## CHAPTER 4

### Testing and Results

#### 4.1 INTRODUCTION

The two dapped ends of beam RF-3R-9 were tested. The two ends were cut from the original beam and labeled RF-3R-9(a) and RF-3R-9(c). Each beam measured 35.9 ft. in length and 58 in. in total depth (a 54 in. deep trapezoidal box beam with a 4 in. composite deck) with identical reinforcement details at both dapped ends. Cracks associated with ASR/DEF deterioration were marked prior to testing in order to distinguish them from cracks that formed under load.

Load increments varied throughout the test. Initially, increments of 50 kips were used. As loading approached critical points in the loading history, such as the shear cracking, flexural cracking, and failure load, increments were decreased to 25 kips in order to accurately record the critical loads. In both specimens, failure loads exceeded those calculated using strut-and-tie modeling and the PCI Design Handbook. Only a few shear cracks formed before failure resulting in little warning of failure.

Beams were oriented in the north-south direction in the test-set up with the dapped end to the north. Future references to beam faces will refer to the west and east sides of the beam accordingly.

Loads reported in Chapter 4 are applied loads. The reported failure loads and shear forces do not include the self-weight of the beam or the weight of the loading frame, 11 kips, which contribute to the total loads resisted by the beams. A free body diagram showing the loads reported is shown in Figure 4-1. Self-weight reactions are presented in Appendix A.

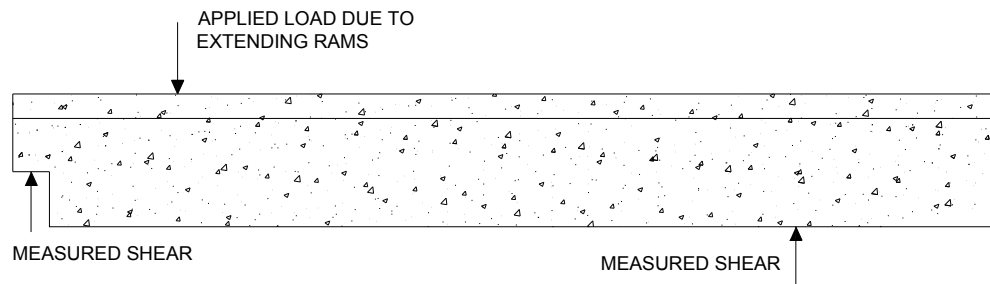


**Figure 4-1 Free body diagram showing loads reported in Chapter 4.**

## **4.2 TEST RESULTS**

### **4.2.1 Test of Dapped End RF-3R-9(a)**

The shear span from the centroid of the hanger reinforcement to the load point was set at 50 inches to create a shear span-to-depth ratio of 0.94 with respect to the depth to the centroid of 62 prestressing strands (Figure 3-18). The pre-test condition of the beam was assessed as moderately damaged as shown in Figure 4-2 and Figure 4-3. The vertical cracks near the start of the void, labeled 5 and 8, were the widest cracks while the cracks near the reentrant corner, labeled 2 and 6, were the smallest of the recorded crack widths. The large amount of reinforcement at the reentrant corner restrained cracking and resulted in the smallest crack widths. Throughout the section, crack widths ranged from hairline to 0.06 in.

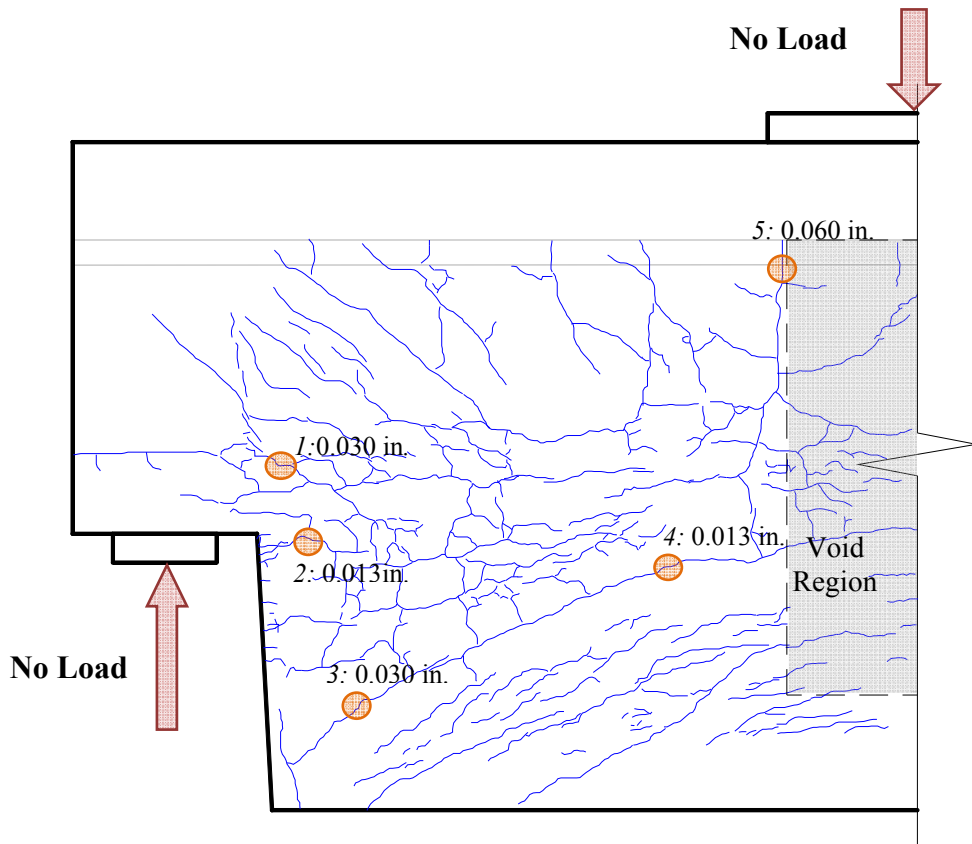


**Figure 4-2 Pre-test cracking and crack widths due to ASR and DEF on the west side of the tested shear span of beam RF-3R-9(a).**

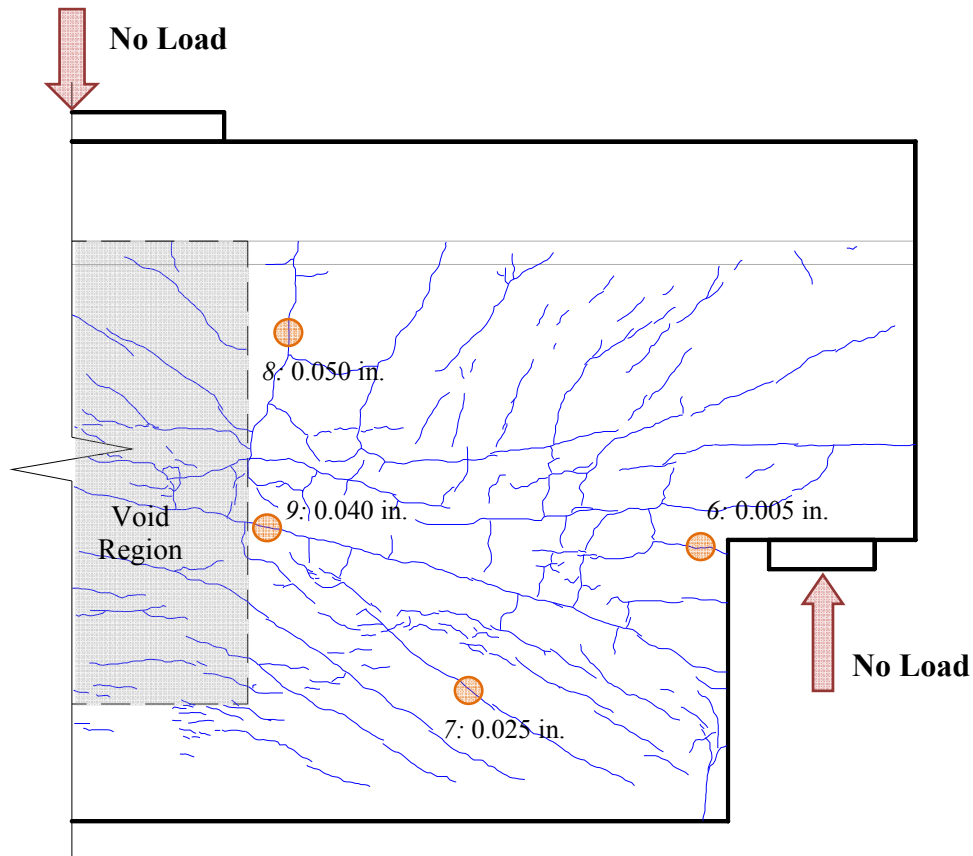


Figure 4-3 Pre-test cracking and crack widths due to ASR and DEF on the east side of the tested shear span of beam RF-3R-9(a).

#### 4.2.1.1 Dapped End Behavior

The first visible cracks occurred at an applied load of 300 kip. The new cracking was minimal with existing cracks extending and connecting. Small crack extensions, less than 3 in. long, were the only visible new cracks up to an applied load of 900 kips. At 900 kips, a few new cracks were 6 in. long, but overall shear cracking was still minimal. When loading reached 1,030 kip, there was a 40 kip load drop. Figure 4-4 shows the condition of the beam under 1,000 kip load just before the load drop occurred. After inspection, no distinct failure was visible and loading continued up to 1,083 kips when a loud noise was heard accompanied by a load drop of 70 kips.

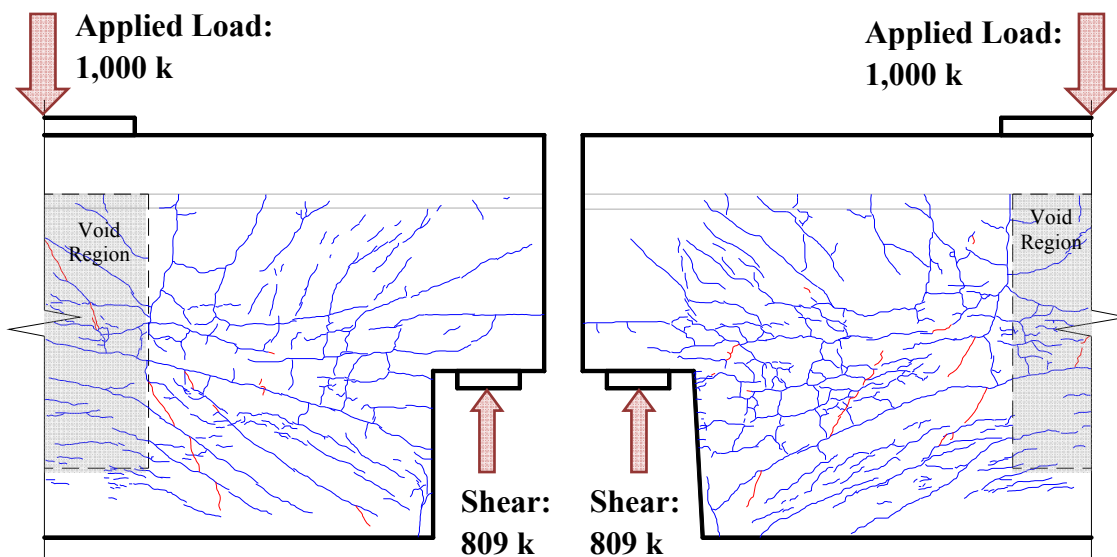


Figure 4-4 Cracking in beam on the east (left) and west (right) sides of the beam at a load of 1,000 kips.

Figure 4-5 shows cracking just before failure. Figure 4-6 and Figure 4-7 show cracking after failure. Minimal shear cracking due to the load was visible pre-failure. The new shear cracks, plotted in red, align with existing ASR/DEF cracks. The thick red lines in Figure 4-6 and Figure 4-7 highlight existing cracks that opened significantly at failure. Crack 7 on the east side opened to 0.125 in. at failure from an initial width of 0.025 in. No crack measured greater than 0.06 in. on the west side of the beam.

The failure of beam RF-3R-9(a) can be attributed to a shear induced bond failure. Shear cracks extended downward from the load point towards the bottom corner of the beam. A shear induced bond failure occurred since there was a very short (or no) length of embedment to anchor the tendons. As the strand slipped, there was a loss of load. ASR/DEF cracking in the strand anchorage zone may have contributed to the failure by reducing the bond stresses that could be developed along the strand. Additionally, bond failure may have been exacerbated by the lack of compression across the development length at the end of the beam.



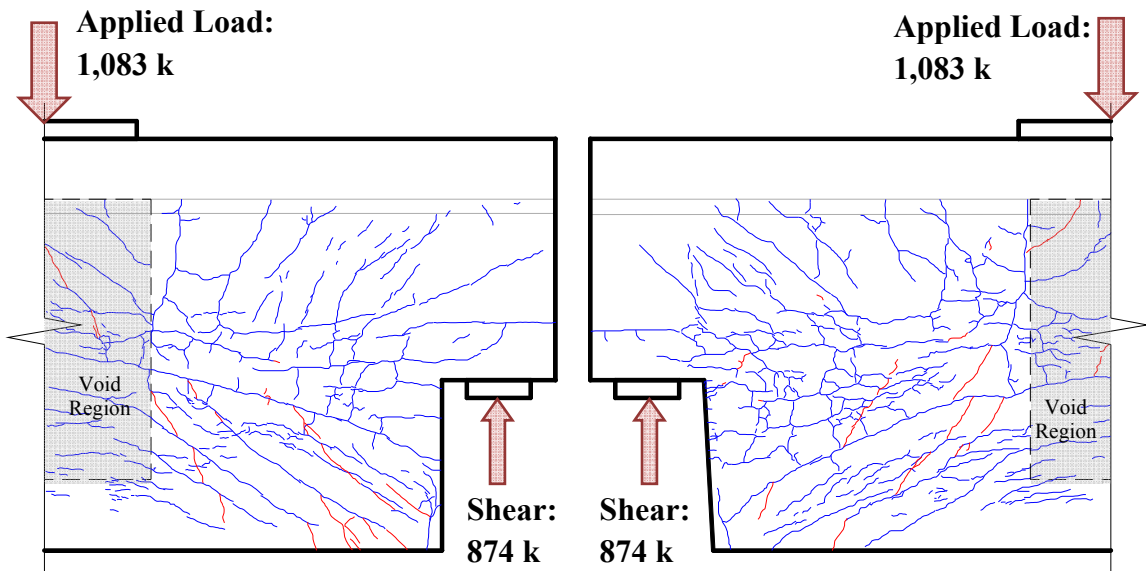


Figure 4-5 Cracking in beam on the east (left) and west (right) sides of the beam prior to failure.

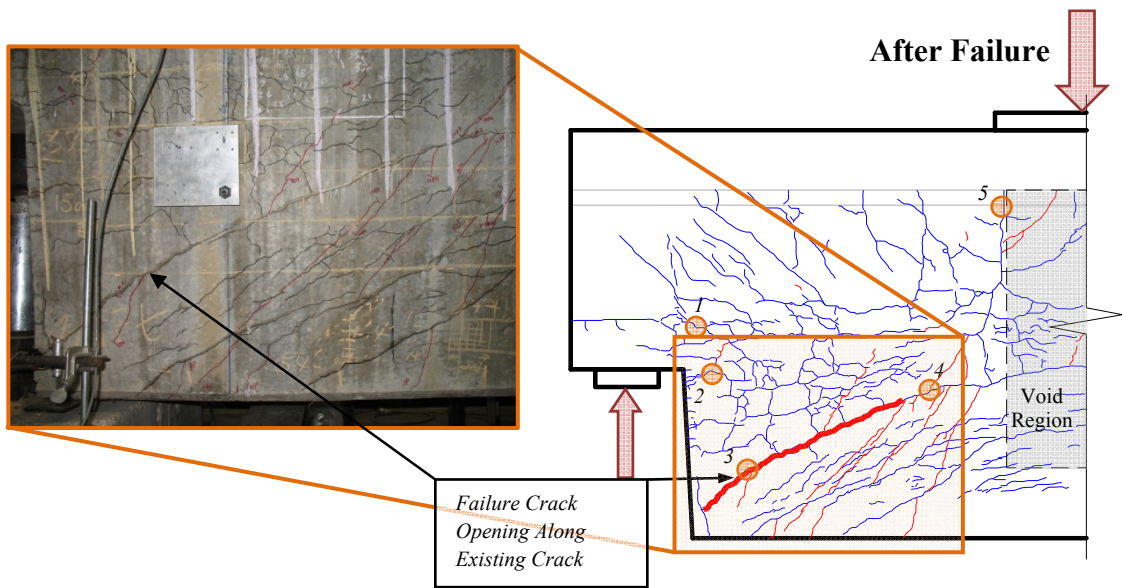


Figure 4-6 Cracking on the west side of beam RF-3R-9(a) after failure.

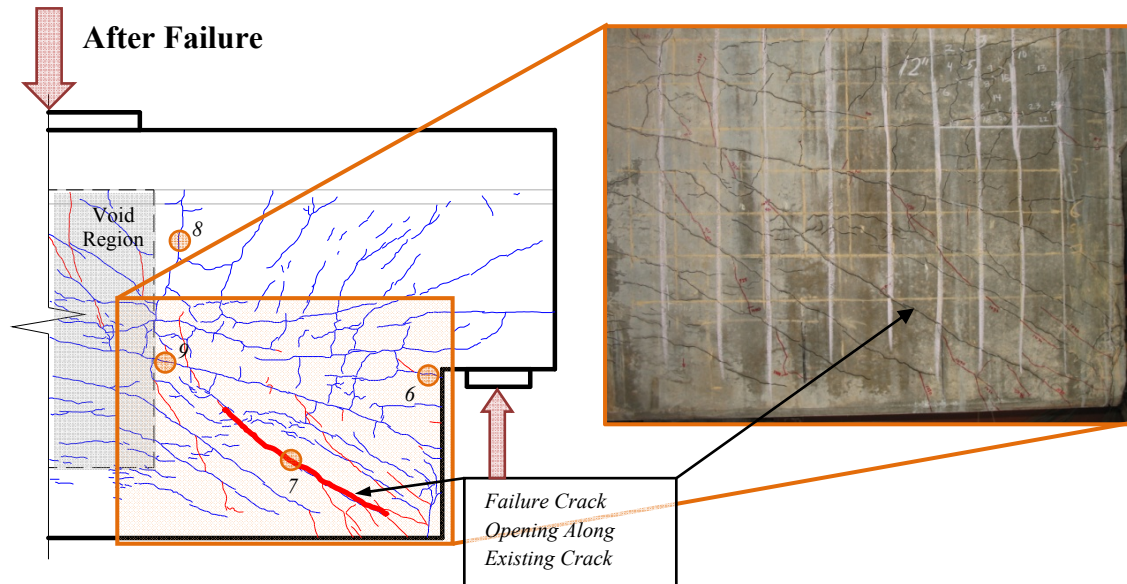


Figure 4-7 Cracking on the east side of beam RF-3R-9(a) after failure.

Table 4-1 Crack widths of existing cracks before and after failure for beam RF-3R-9(a).

Crack	1	2	3	4	5	6	7	8	9
Width Before Testing	0.030	0.013	0.030	0.013	0.060	0.005	0.025	0.050	0.040
Width at Failure	0.025	0.016	0.040	0.013	0.060	0.016	0.125	0.050	0.040

The shear crack pattern closely followed the ASR/DEF cracking pattern in the area. Additionally, the east side of the beam experienced a limited amount of shear cracking even at failure due to the single large failure crack labeled 7 in Figure 4-7. The two cracking patterns provided minimal warning before failure. Additionally, there was no significant cracking distinguishable from the ASR/DEF-related cracking that indicated failure had occurred.

#### 4.2.1.2 Measured Data

##### 4.2.1.2.1 Load- Deflection

Load-deflection data at the load point relative to the supports is presented in Figure 4-8. The graph is linear up to 900 kips where the first slope change occurs. The slope change at 900 kips corresponded with the observation of significant cracking in the beam. At 1,030 kips, the first load drop occurred. At this point the load-deflection plot became nearly horizontal with large deflections under little additional load. The beam failed at a load of about 1,083 kips and deflection of about 0.26 inches.

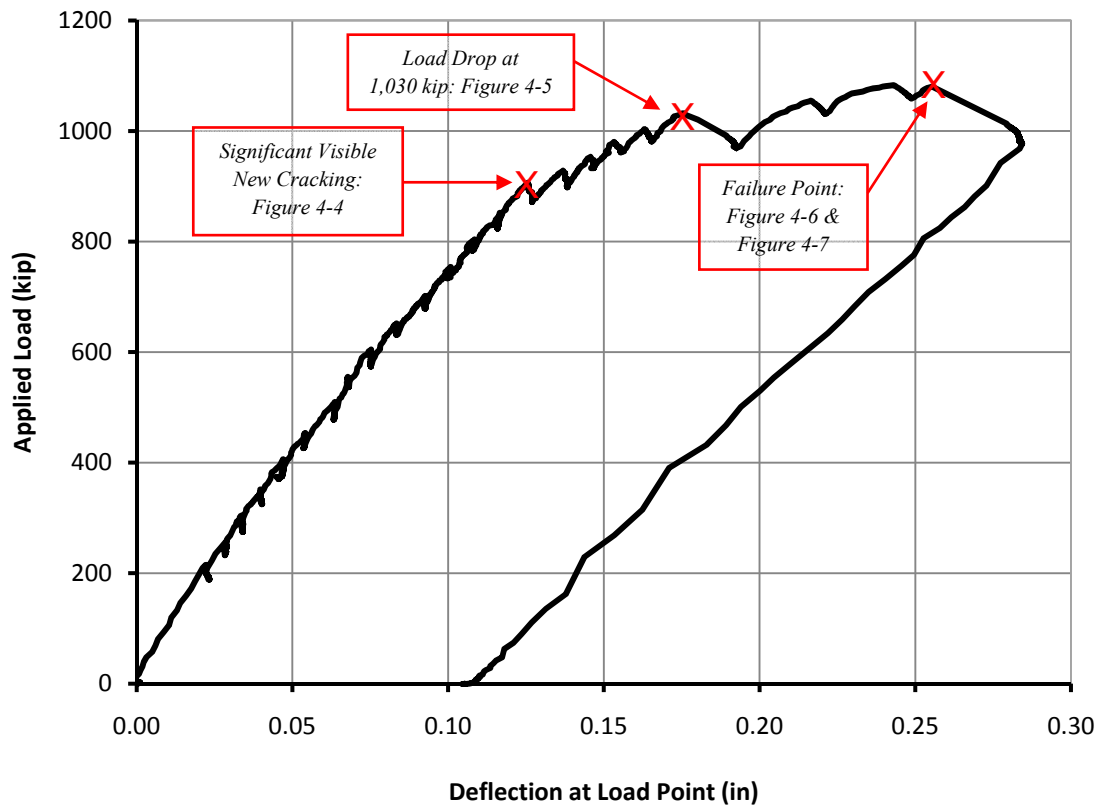


Figure 4-8 Load-deflection plot for beam RF-3R-9(a) at load point relative to supports.

##### 4.2.1.2.2 Crack Opening

The apparatus for measuring shear deformation provided an indication of the crack widths at the reentrant corner on the west side of beam RF-3R-9(a). Figure 4-9

shows the results gathered from the shear distortion apparatus during testing. The length of the diagonal increased by 0.005 in. over a gage length of 34 1/8 in. The small extension would indicate that the steel at reentrant corner did not yield. This data supports the observations that no additional cracks formed or opened at the reentrant corner.

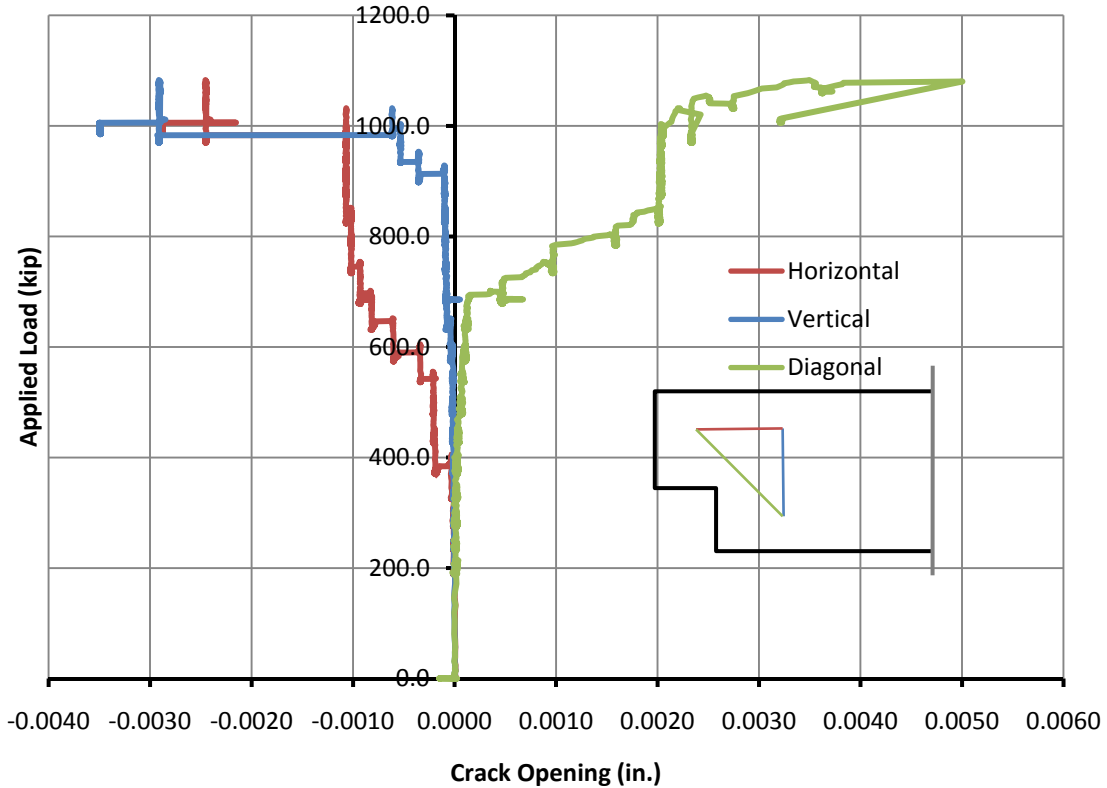


Figure 4-9 Measurements of crack opening at reentrant corner on west side.

#### 4.2.2 Shear Test Dapped End RF-3R-9(c)

RF-3R-9(c) was loaded at a shear span of 84 inches from the centroid of the hanger reinforcement to the load point creating a shear span-to-depth ratio of 1.58 with respect to the depth to the centroid of the 62 prestressing strands (Figure 3-18). The larger shear span tested in beam RF-3R-9(c) engaged a larger portion of the hollow section of the box beam increasing the probability of shear failure occurring in the 5 in. thick webs. The beam was classified as moderately damaged. ASR/DEF cracking in the

shear span can be seen in Figure 4-10 and Figure 4-11 along with crack widths. Pre-existing cracks had large widths ranging from hairline to 0.06 in.

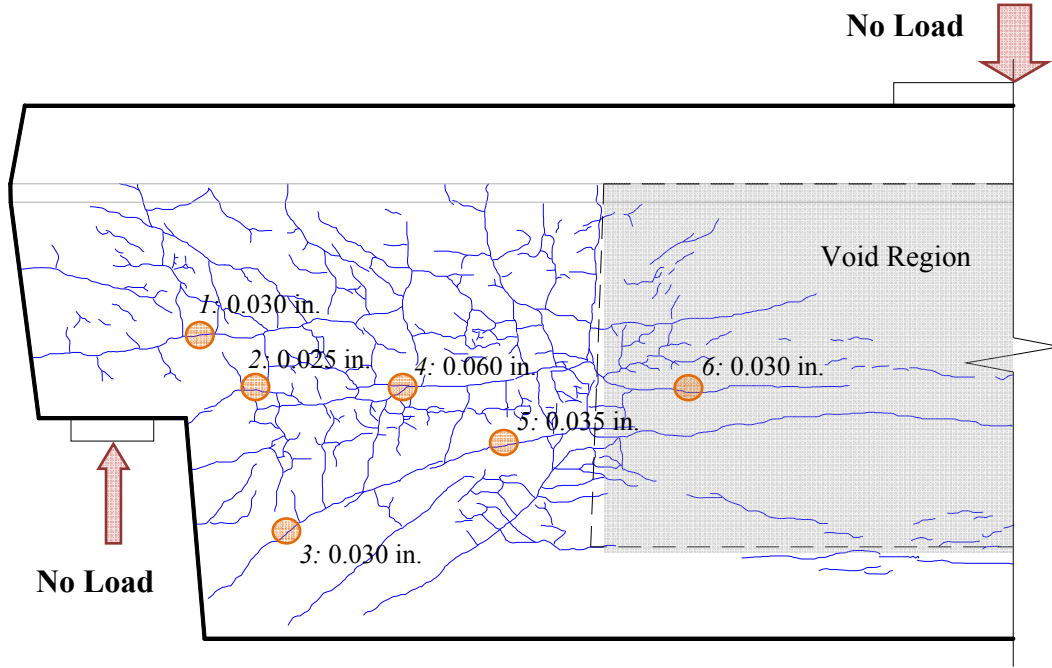


Figure 4-10 Pre-test cracking and crack widths due to ASR and DEF on the west side of the tested shear span of beam RF-3R-9(c).

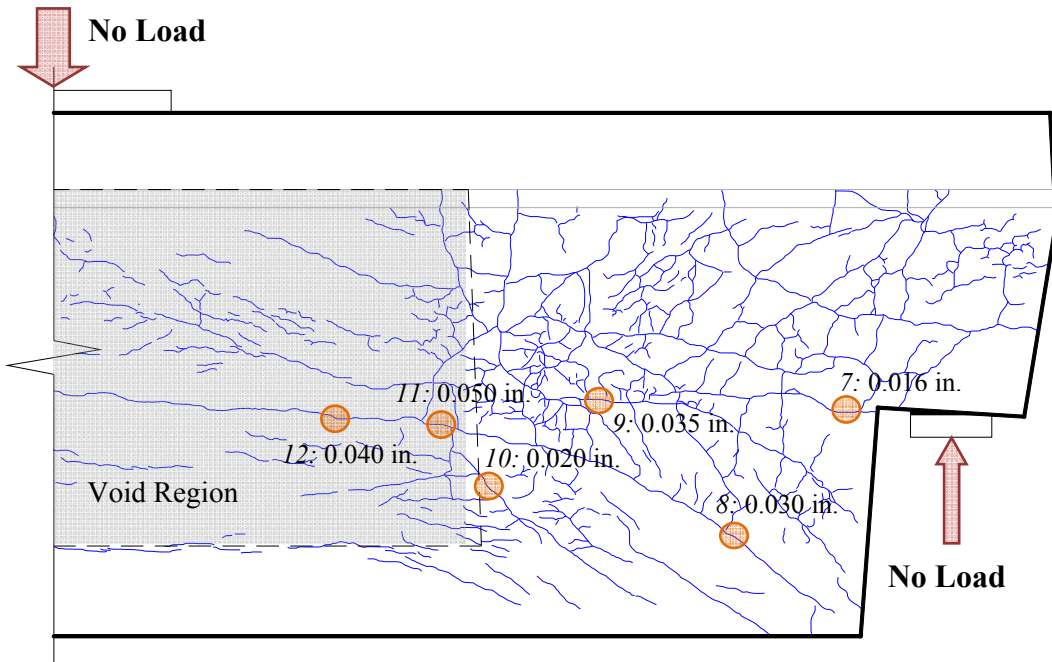


Figure 4-11 Pre-test cracking and crack widths due to ASR and DEF on the east side of the tested shear span of beam RF-3R-9(c).

#### ***4.2.2.1 Dapped End Behavior***

The first new cracking originated in the thin web and was visible at a load of 600 kips. At 750 kip, existing cracks began visibly widening. Specifically, cracks at locations 3, 5, 8, and 10. Flexural cracking became visible at a load of 850 kips. Just prior to failure, the flexural cracks extended into the web of the beam. Figure 4-12 shows cracking before failure. Figure 4-13 and Figure 4-14 show cracking after failure. Again, minimal shear cracking due to the applied load was visible before failure. It was difficult to distinguish between the new shear cracks, shown in red, and the existing ASR/DEF cracks, shown in blue. Similar to beam RF-3R-9(a), the inability to distinguish between ASR/DEF cracks and shear cracks results in minimal warning of impending failure. The thick red lines in Figure 4-13 and Figure 4-14 highlight existing cracks that opened significantly at failure. Widest cracks on the east side of the beam were the result of existing cracks opening whereas widest cracks on the west side of the beam were associated with new shear cracking. As such, existing cracks on the west side opened less than cracks on the east side.

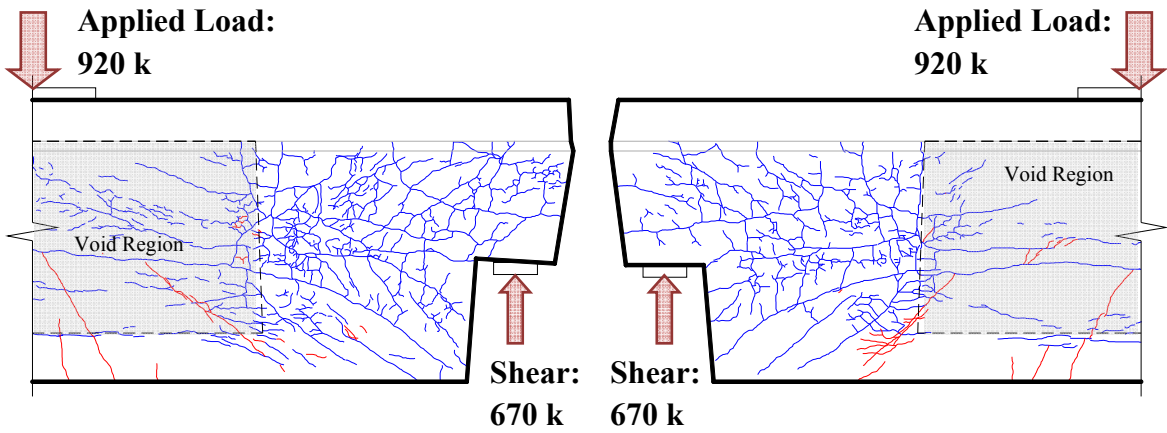


Figure 4-12 Cracking in beam RF-3R-9(c) on the east (left) and west (right) sides prior to failure.

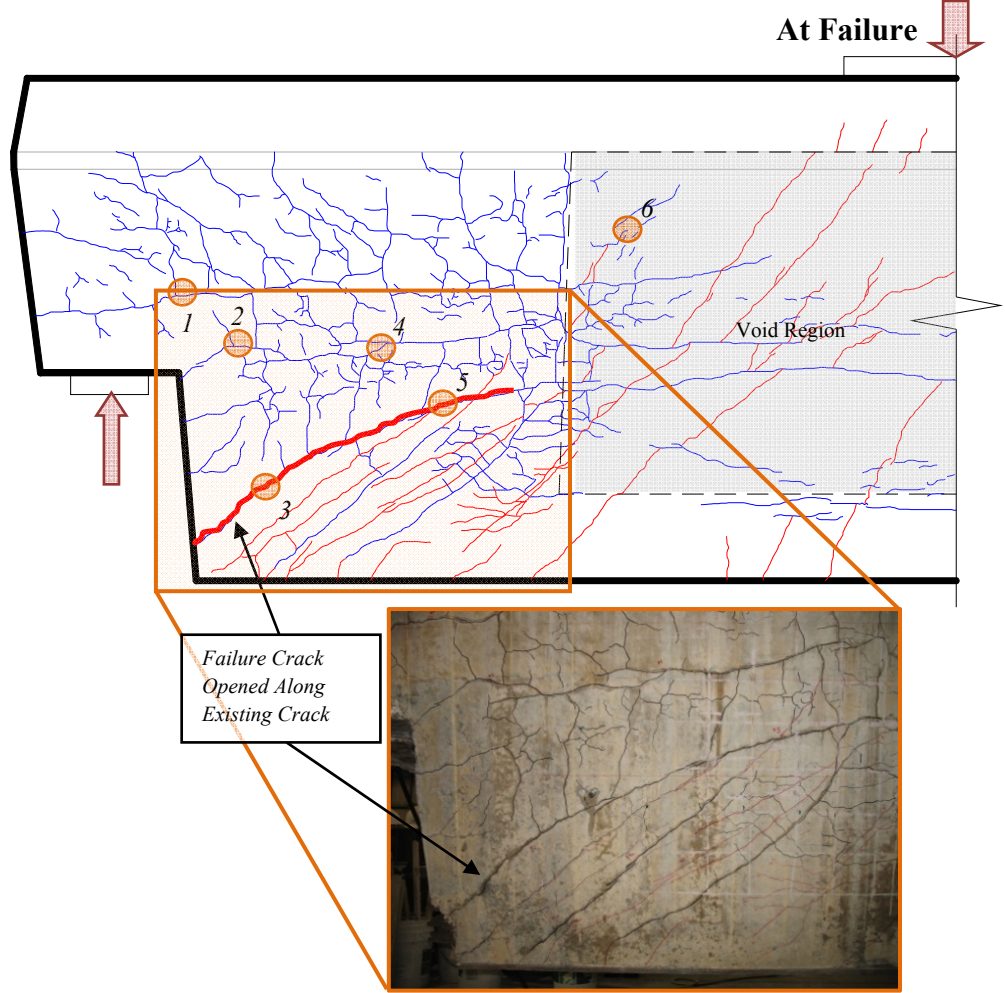


Figure 4-13 Cracking on the west side of beam RF-3R-9(c) after failure.



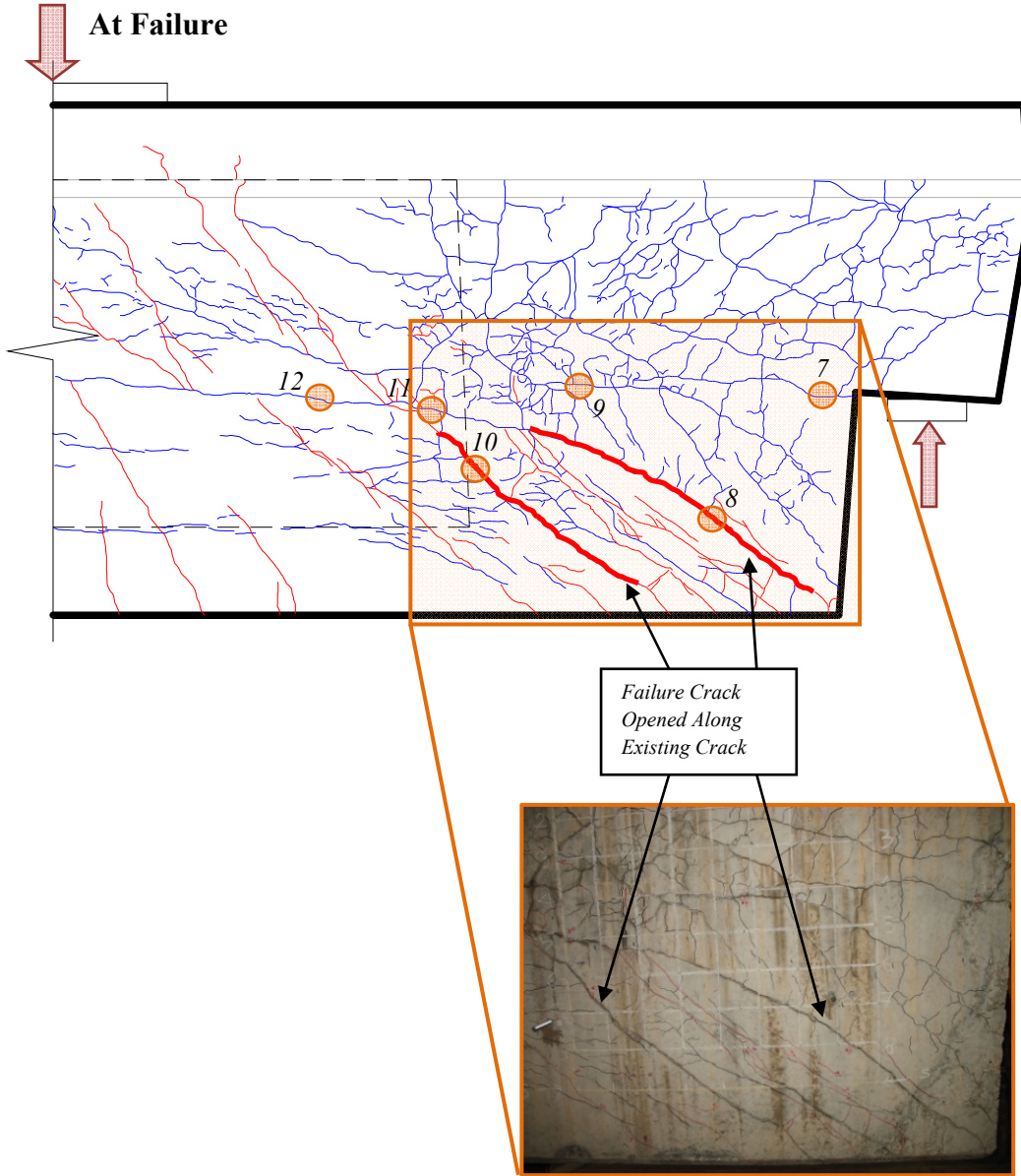


Figure 4-14 Cracking on the east side of beam RF-3R-9(c) after failure.

Table 4-2 Crack widths of existing cracks before and after testing for beam RF-3R-9(c).

Crack	1	2	3	4	5	6	7	8	9	10	11	12
Initial Width	0.030	0.025	0.030	0.060	0.035	0.030	0.016	0.030	0.035	0.020	0.050	0.040
Final Width	0.030	0.025	0.050	0.060	0.060	0.035	0.020	0.080	0.035	0.125	0.040	0.050



Again, the shear crack pattern from the applied load closely follows the ASR/DEF cracking pattern in the area. However, cracking at failure in beam RF-3R-9(c) is more typical of a shear failure than that exhibited by beam RF-3R-9(a). There was evidence of movement along the wide cracks located in the critical failure region.

Beam RF-3R-9(c) resisted a maximum load of 920 kips before failing due to a shear induced bond failure. Cracks extended and opened within the transfer length of the strands. Cracks opened much wider than in beam RF-3R-9(a), indicating greater engagement of the vertical reinforcement in the section. Again, there was little evidence of distress before the beam failed.

#### **4.2.2.2 Measured Data**

##### *4.2.2.2.1 Load vs. Deflection*

Load plotted against deflection at the load point relative to the supports is shown in Figure 4-15. The graph is linear up to 600 kips where a change in slope is evident. The slope change coincided with first visible shear cracking. A significant slope change occurred at a load of 850 kips where first flexural cracking was seen. At a load of 900 kips, the load-deflection plot became nearly horizontal. The load drop at about 0.42 in. deflection corresponds to the point in the test when loading was stopped because significant deflection was occurring with little load increase. The load dropped gradually while the condition of the beam was being assessed. No failure was discovered, so loading continued. At about 0.56 in. deflection, failure occurred accompanied by a loud noise and a 15% load drop.

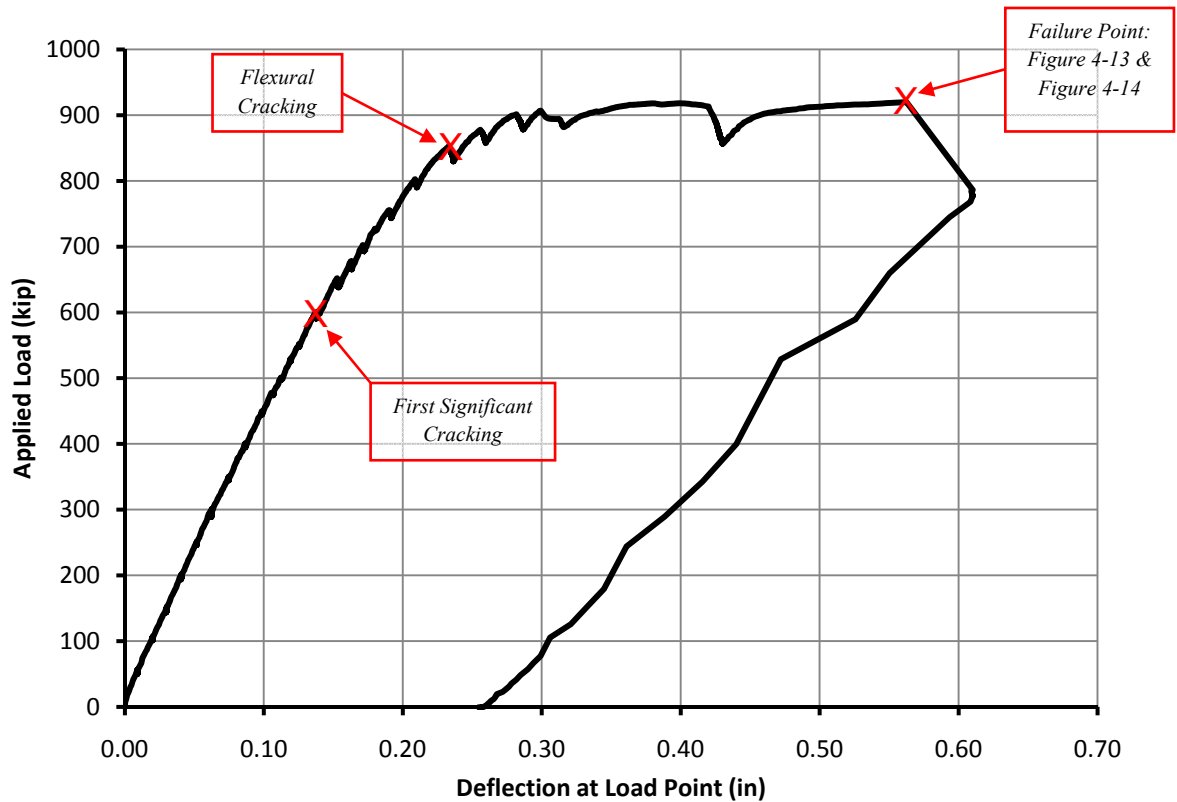


**Figure 4-15 Load-deflection plot for beam RF-3R-9(c) adjusted for rigid body movement.**

#### 4.2.2.2.2 Crack Opening

The shear distortion instrumentation provided an indication of crack opening at the reentrant corner on both sides of the beam. Figure 4-16 shows the results gathered from the shear distortion apparatuses during testing of beam RF-3R-9(c). Crack openings, measured in inches, are reported because strains are negligible in this case. The extension along the diagonal was 0.0014 in. over a gage length of 35 3/8 in. The small extension would indicate that the steel crossing the crack at the reentrant corner did not yield due to the applied load. The data supports the results from the crack patterns, which also showed no indication of additional cracking or crack opening in the area.

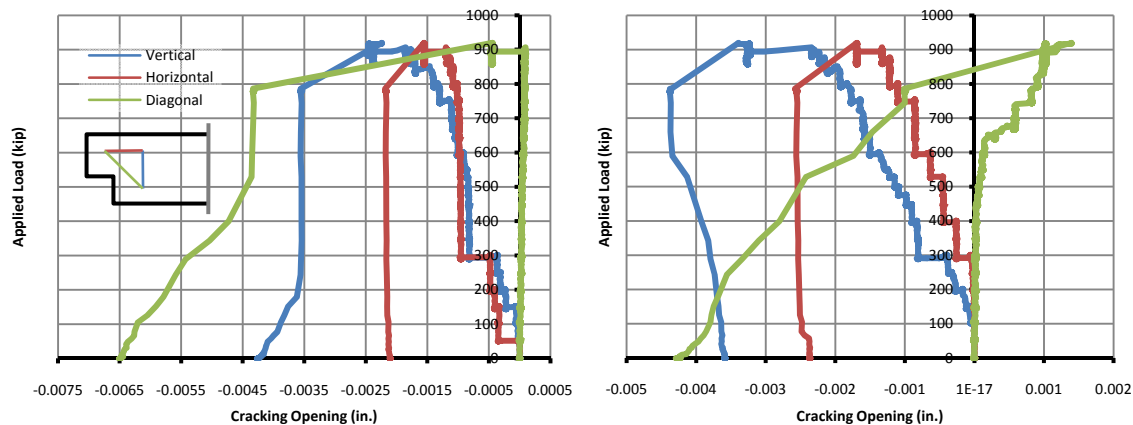


**Figure 4-16 Crack opening measurements at reentrant corner for west (left) and east (right) sides of beam RF-3R-9(c).**

The shear distortion instrumentation placed in the web portion on the east and west sides of the box section produced significantly different results than at the reentrant corner. Results of crack opening measurements are reported as strains because the strains provide pertinent information on behavior of the reinforcement in the web region. Figure 4-17 shows the measurements gathered from the shear distortion apparatus on the west side of beam RF-3R-9(c) during testing. At 600 kips, the vertical transducer began to exhibit deformations which corresponds to the load at which a new crack crossing the vertical was first noticed. This was also the point of first slope change in the load-deflection plot. Figure 4-18 shows the crack passing through the vertical measurement distance. Upon reaching the failure load, strains in the vertical leg reached 0.2% signifying that the vertical reinforcement in the region had yielded. However, the onset of yield appeared to occur at a strain of 0.12%, which indicates that the steel may have experienced strain due to ASR/DEF expansions before loading. Strains of 0.2% in the horizontal and diagonal directions do not directly indicate yield because the steel was not oriented in those directions. Additionally, deflection along the horizontal leg began extending near the failure load indicating that cracking had become more widespread at failure.

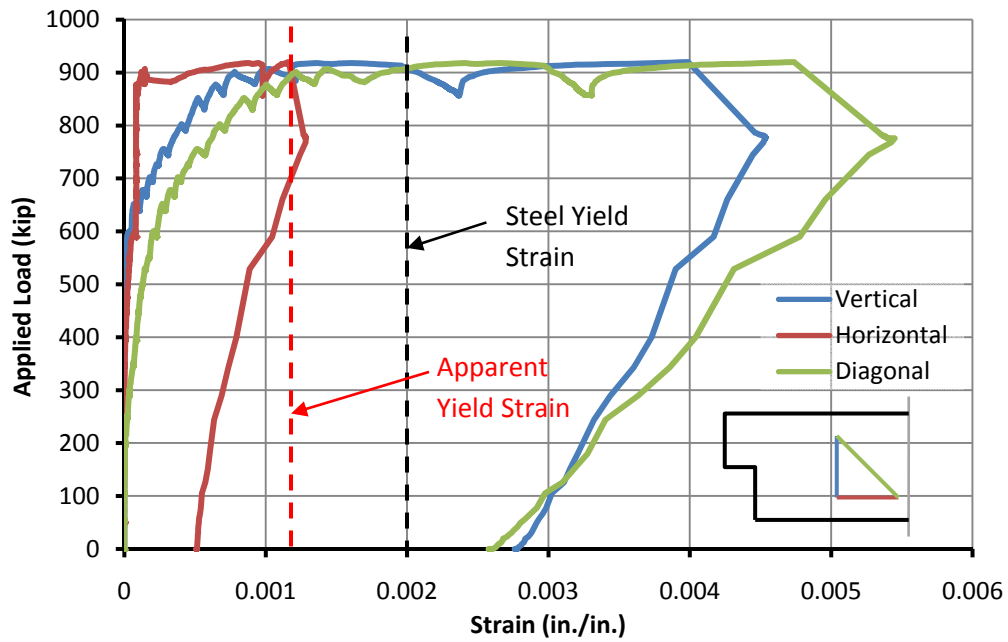


Figure 4-17 Strain measurements from shear distortion apparatus at the web on the west side of beam RF-3R-9(c).

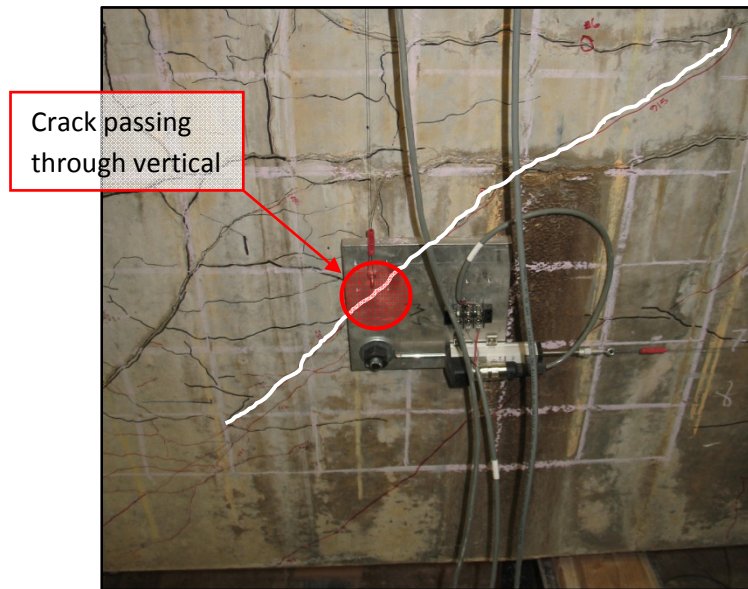


Figure 4-18 Picture highlighting the new shear crack passing through the vertical measuring leg.

The shear distortion apparatus placed in the web portion on the east side of the box section produced similar results to the apparatus on the west side. Figure 4-19 shows the measurements gathered from the shear distortion apparatus on the east side of beam

RF-3R-9(c) during testing. Results are again reported in terms of strain. On the east side of the beam, the horizontal transducer began recording measurable cracks at a load of 600 kips. This corresponds to the load when a crack crossed the horizontal leg as seen in Figure 4-20. At 650 kips, the diagonal transducer also began recording significant crack openings. The horizontal and diagonal legs continued to measure deformations at the same rate indicating that the new cracks across the horizontal were the main cracks opening up to a load of about 900 kips. Vertical measurements were unchanged until a load of 900 kips was reached where significant crack openings were measured although very little load was added. Two scenarios could explain the rapid increase in crack widths in the vertical direction.

1. ASR/DEF expansion resulted in yielding of the vertical ties in the area resulting in significant deformations once the vertical ties began taking additional load.
2. Inability of the beam to take additional load was governed by other systems within the beam preventing load increase while the stirrups began taking load. Eventually the stirrups reached yield further hindering the ability of the beam to resist load.

Insufficient evidence could be gathered to confirm either hypothesis, but enough deformation occurred at the failure load to determine that stirrups had yielded. Again, the ASR/DEF expansion appeared to have caused strain in the stirrups resulting in an apparent yield strain of 0.08% versus the expected steel yield strain of 0.2%. At failure, a new crack had developed through the vertical leg (Figure 4-20) which connected to an existing crack that opened to 0.125 in. causing large strains in the vertical leg.

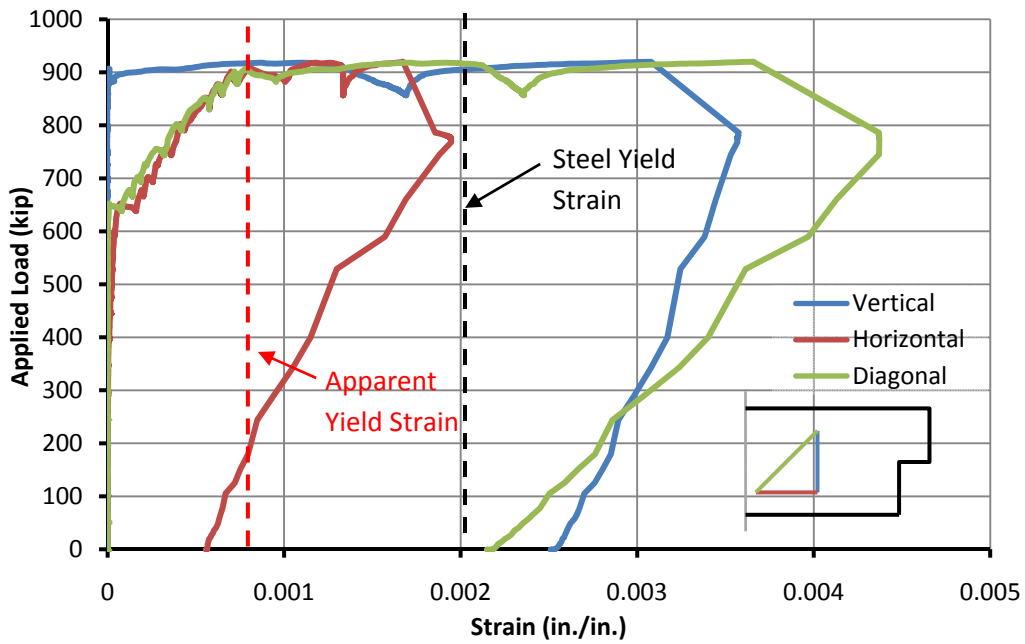


Figure 4-19 Strain measurements from the shear distortion apparatus at the web on the east side of beam RF-3R-9(c).

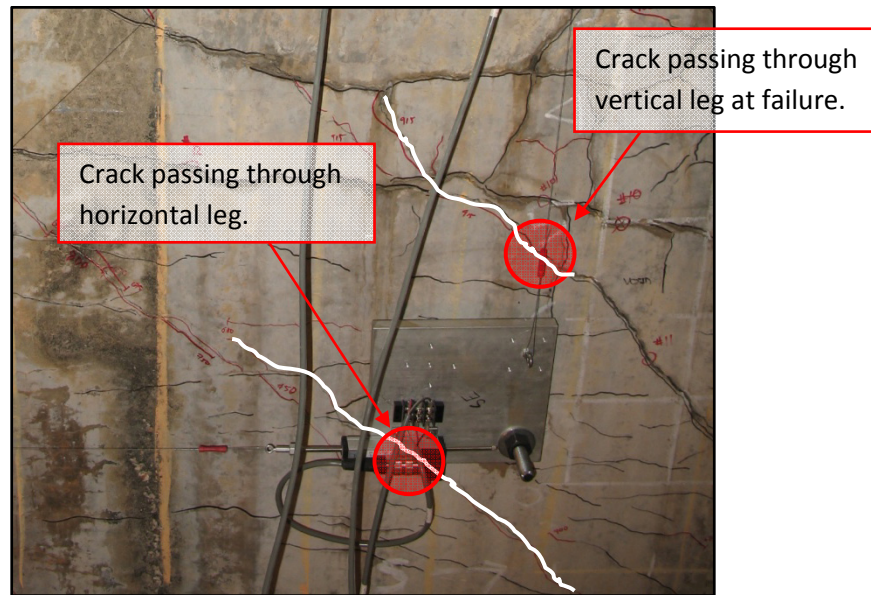


Figure 4-20 Picture highlighting shear cracks passing through the horizontal and vertical legs of the shear distortion apparatus.

#### 4.2.2.2.3 Strand Slip

As indicated earlier, strand slip occurred during failure of beam RF-3R-9(a) and led to the decision to measure strand slip for beam RF-3R-9(c). Figure 4-21 shows the results of the strand slip measurements. The strand that was debonded 3 ft. into the section, started to slip before the fully bonded strand. However, both strands slipped earlier than expected based on strand development calculations. The early strand slip supports the assumption that a shear crack formed across the strands forcing the strands to develop more stress than would be required under purely flexural loads. The fact that there is little difference between the slip load of the two strands also supports the finding. Under normal flexural loadings, the critical flexural section fell within the development length of the debonded strand, whereas the bonded strand was fully developed. As such, if debonding occurred due to purely flexural loads, the debonded strand would have started slipping at a much lower load than the bonded strand.

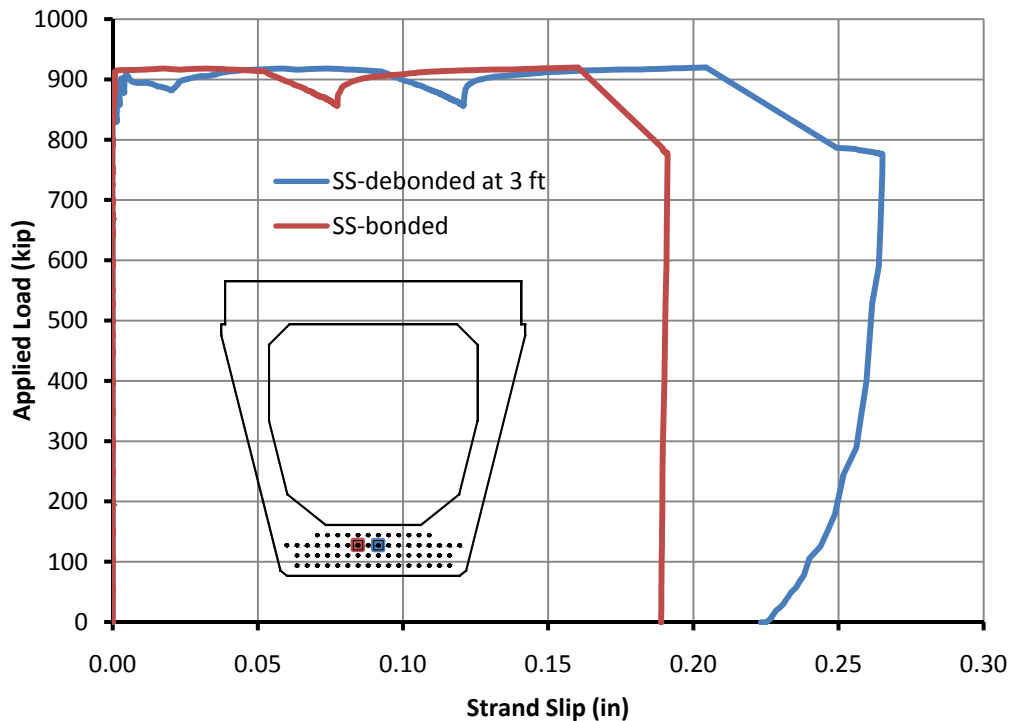
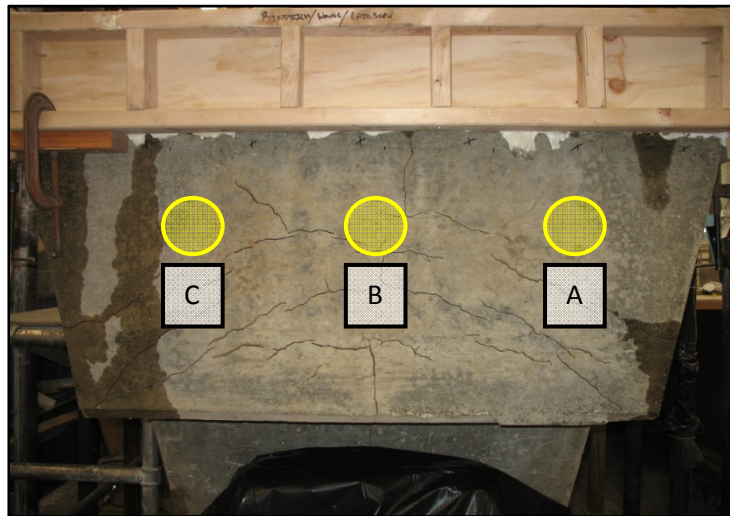


Figure 4-21 Measured strand slip under loading.

### 4.3 CYLINDER TESTS

Each beam was cored following testing to obtain cylinders for compressive strength tests of the concrete in the 13-year-old beams. The cores measured 3 ¾ in. in diameter and anywhere from 7 in. to 7.5 in. in length at testing. Extracted cores measured anywhere from 7 in. to 9 in. in length. The cores were cut to a length of 7.5 in. when possible to create a 2-to-1 aspect ratio with respect to the diameter. The cut also removed the rough surface created when the core broke from the beam. Cylinders from both beams were extracted from the end of the dap where reinforcement could be easily avoided as shown in Figure 4-22. Cores were unable to be taken in other regions without hitting reinforcement or shear damaged regions.



**Figure 4-22 Location of cores taken from beam RF-3R-9(a).**

Results from cylinder tests of beam RF-3R-9(a) are provided in Table 4-3. The average core strength was 10.1 ksi. The exterior of the end regions of beam RF-3R-9(a) appeared relatively uncracked. Core strengths were very similar to the original estimated compressive strength of 10 ksi.



**Table 4-3 Concrete cylinder core strengths from beam RF-3R-9(a).**

Cylinder	Load (lbs)	Strength (ksi)	Length (in)
A	112690	10.2	7.0625
B	109030	9.87	7.4375
C	111690	10.1	7.5

Results from cylinder core tests of beam RF-3R-9(c) are provided in Table 4-4. In contrast to beam RF-3R-9(a), the exterior of the core locations exhibited substantial cracking from ASR/DEF as seen in Figure 4-23. Core strengths from beam RF-3R-9(c) were significantly less than those from beam RF-3R-9(a). Average compressive stress was 7.05 ksi. Damaged cores fail at lower loads than undamaged cores and the compressive strength of damaged cores does not accurately represent the strength of the in situ concrete. As such, it is assumed that concrete strength of beam RF-3R-9(c) is greater than the 7.05 ksi measured from the cores and closer to the strengths from beam RF-3R-9(a).

**Table 4-4 Concrete cylinder core strengths from beam RF-3R-9(c).**

Cylinder	Load (lbs)	Strength (ksi)	Length (in)
A	80942	7.33	7.0625
B	75684	6.85	7.4375
C	77072	6.98	7.5

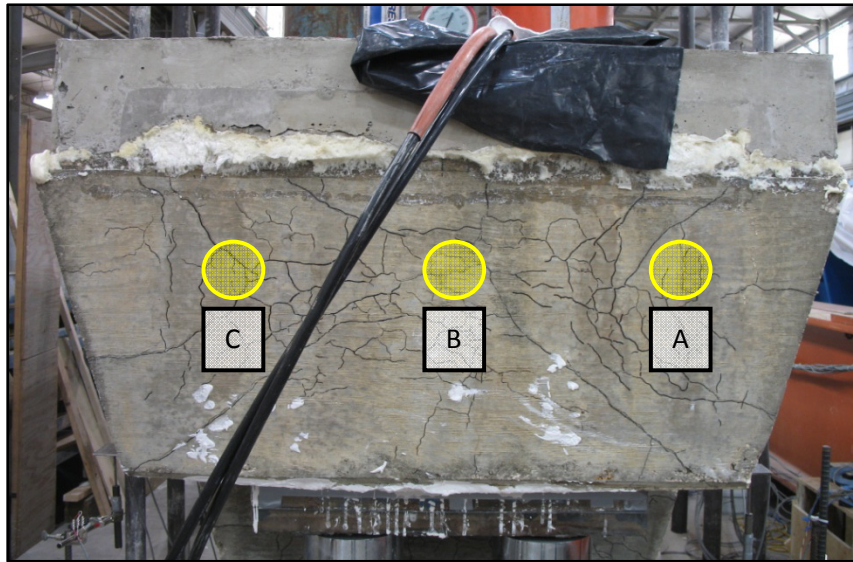


Figure 4-23 Location of cores taken from beam RF-3R-9(c).

#### 4.4 SUMMARY

Two tests were conducted on dapped end specimens RF-3R-9(a) and RF-3R-9(c) at shear spans of  $0.94d$  and  $1.58d$ , respectively, where  $d$  is the effective depth of the flexural reinforcement for the full-depth beam. Beam RF-3R-9(a) exhibited a larger load-carrying capacity than beam RF-3R-9(c) with both beams failing by a shear induced bond slip mechanism. No new cracks or widening of existing cracks were measureable within the dapped end region of the beam suggesting that the dapped end did not control the capacity. Additionally, neither beam experienced extensive cracking until after failure, which provided little warning that the beam was near capacity. Chapter 5 includes a comparison of the results to calculated loads based on code provisions.

## CHAPTER 5

### Comparison of Measured Failure Loads with Code Provisions

#### 5.1 INTRODUCTION

Few design codes outline specific methods to compute dapped end capacities. *ACI318-08 Building Code Requirements for Structural Concrete and Commentary* and *2007 AASHTO LRFD Bridge Design Specifications* strut-and-tie modeling provisions are utilized to design reinforcement in disturbed regions, such as a dapped end. Strut-and-tie models require a significant amount of engineering discretion in design with various possible models. The *PCI Design Handbook* (2004), on the other hand, contains set guidelines and equations used to determine the required reinforcement in the dapped end portion of a beam. PCI, ACI318-08, and AASHTO LRFD design methods are intended as lower bound equations for detailing reinforcement, not to determine failure loads or mechanisms. However, these are the only methods available today to estimate dapped end capacities. In this chapter, PCI, ACI318-08, and AASHTO LRFD design procedures will be used to compare computed dapped end capacities to experimental failure loads. Additionally, a cut section analysis will be developed based on the post failure condition of the beam.

Shear forces reported in Chapter 5 are total shear forces experienced by the section. The reported shear loads include: measured shear due to the self-weight of the beam, calculated shear from weight of the loading frame (11 kips), and measured shear from the extension of the rams. A free body diagram displaying contributing shear forces is shown in Figure 5-1. Shear contribution from the weight of the loading frame was calculated using on statics whereas shear contribution from the weight of the beam and extension of the beams was measured by the load cells. Beam weight reactions are presented in Appendix A.

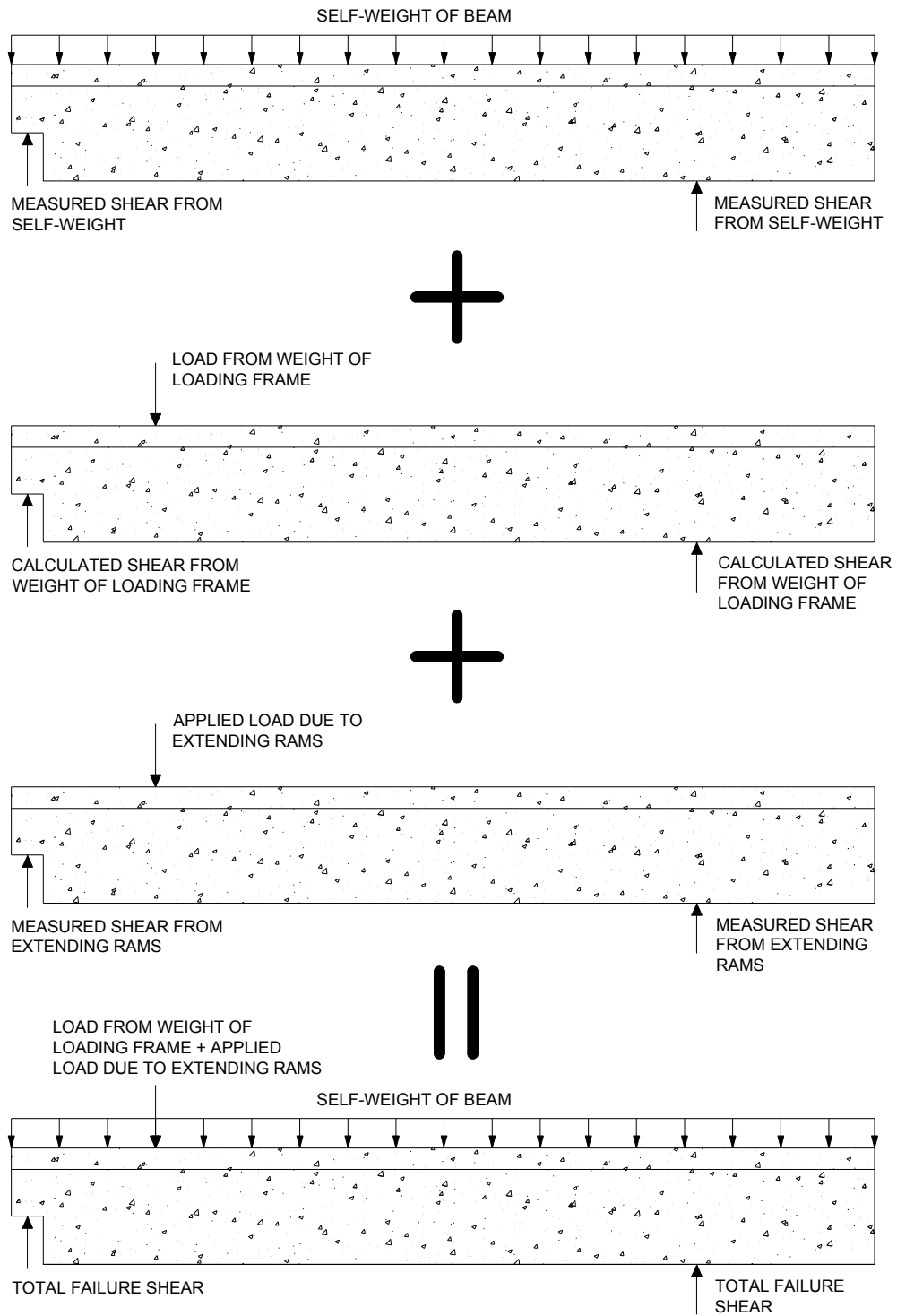


**Figure 5-1 Free body diagrams showing total failure load of beam.**

## 5.2 CALCULATED FAILURE LOADS

### 5.2.1 Strut-and-Tie Model

Strut-and-tie models are generally used in design to provide a lower bound solution for the reinforcement layout in disturbed beam regions. In this section, strut-and-tie models are used in an attempt to estimate the failure load for the beams tested with existing reinforcement layouts. In the strut-and-tie models presented herein, struts, ties, and critical singular nodes were checked to determine failure loads. Calculations can be found in Appendix C. The load determined in this section provides a lower bound estimate of the load carrying capacity of the beams.

#### *5.2.1.1 ACI 318-08 Building Code Strut-and-Tie Model Provisions*

##### *5.2.1.1.1 RF-3R-9(a)*

Beam RF-3R-9(a) was tested at a shear span of 50 inches with the distance from the centroid of the hanger reinforcement to the load point creating the shear span. The shear span-to-depth ratio ( $a_d/d$ ) was  $0.94d$ , where  $d$  is the effective depth of the flexural reinforcement for the full-depth beam as seen in Figure 5-2. The typical dapped end strut-and-tie model proved insufficient due to the large forces anticipated in tie 3 (Figure 5-2). These large stresses resulted in beam failure at unrealistically low loads. The lack of a localized second vertical tie in the reinforcement layout required adjustment of tie location in the model to engage as much reinforcement as possible (Figure 5-3). An additional strut, S5 (Figure 5-4), reduced the stresses in tie 3 allowing for greater load carrying capacity of the section, while balancing the additional horizontal force in node 4 produced from the angle change of strut S3.

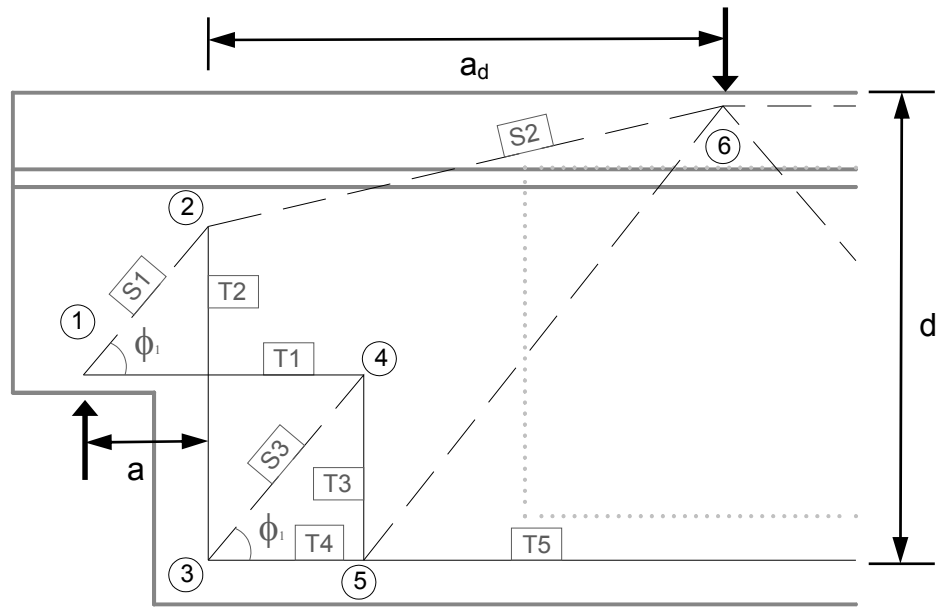


Figure 5-2 Typical strut and tie model for a dapped end section.

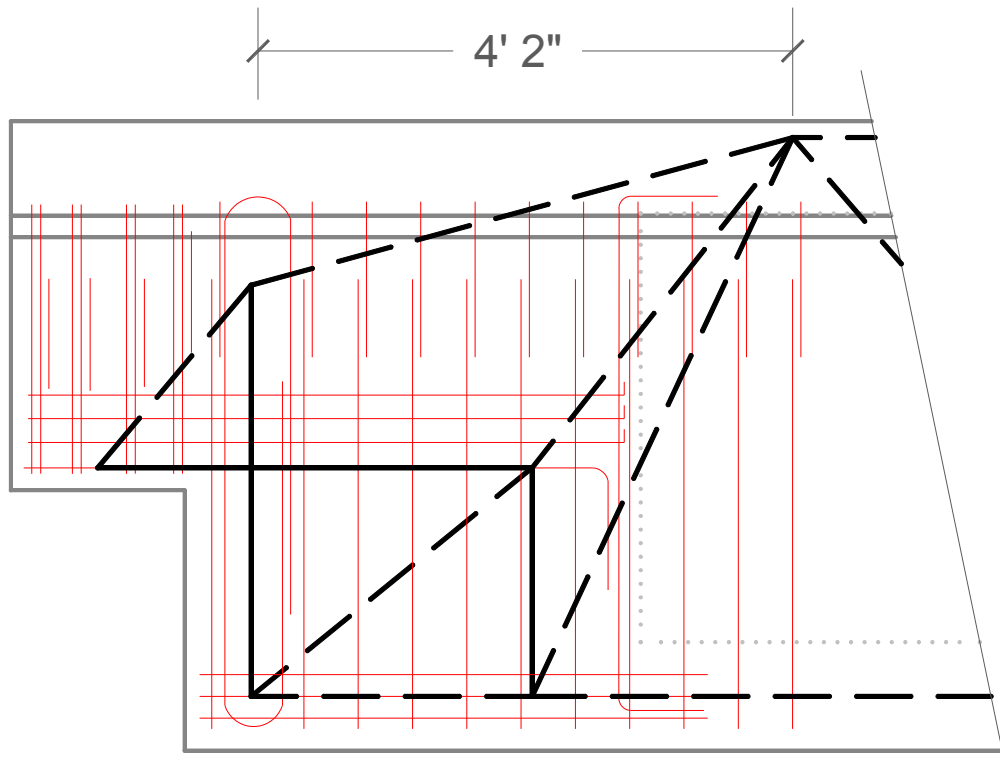
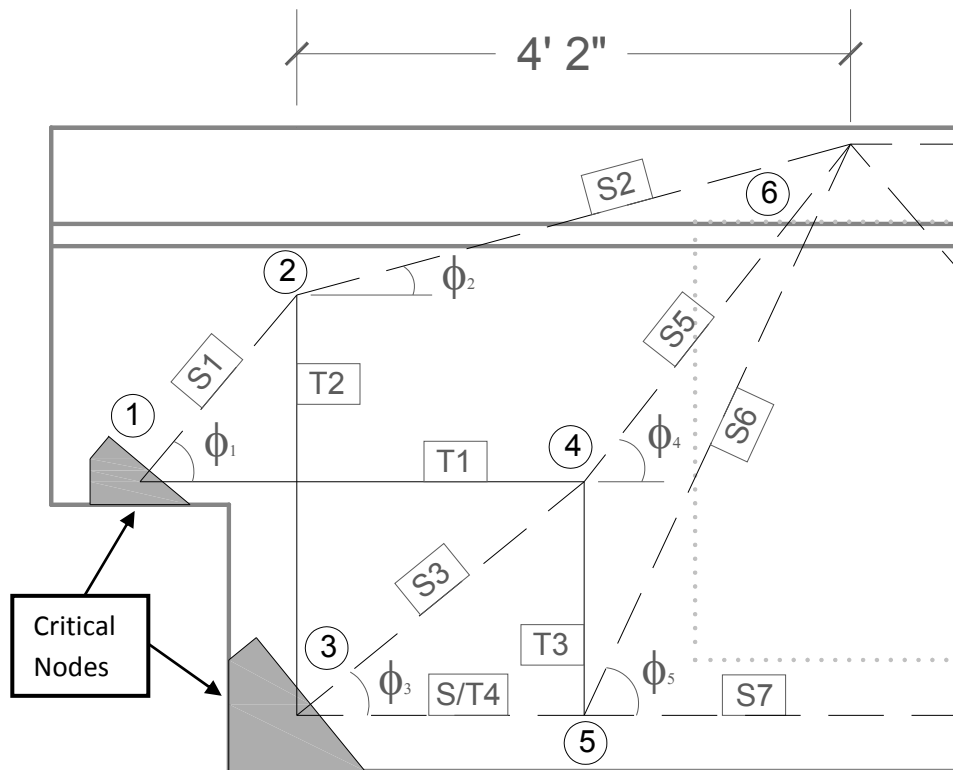


Figure 5-3 Non-prestressed reinforcement (red) with strut-and-tie model overlay for beam RF-3R-9(a).



**Figure 5-4 Proposed ACI strut-and-tie model for beam RF-3R-9(a).**

The action of member S/T4 in the strut-and-tie model (Figure 5-4) is not intuitive. Initially, the member acted as a strut due to the compression in the concrete from the prestress force. The prestress force must be overcome in order for member S/T4 to begin acting as a tie. Once overcome, the only additional tension force that can be carried by the tie would be from the three 2-legged #6 non-prestressed reinforcement shown in Figure 5-3. Because node 3 is located within the transfer length of the prestressing strands, the strands cannot develop any additional stress and failure will result when the non-prestressed reinforcement yields.

The forces induced by the straight prestressing strands were handled similar to the procedure proposed in the thesis by Mader (1990). Mader proposed applying half of the total prestressing force at each of the two bottom nodes, 3 and 5. However, in the models included herein, forces were applied to nodes 3 and 5 according to the amount of force that could be transferred by the prestressing strands over the length from the end of the

beam to the node. In order to develop additional force at node 3, the extended nodal region defined the point at which the prestressing strand anchorage commenced. The extended nodal zone represents the extension of the strut width until it intersects with the ties anchored in the node, as shown in Figure 5-5. Anchorage of the ties begins at the strut-tie intersection. Thus, for node 3, the length available to develop the prestressing force from the end of the beam to the end of the extended nodal region is 18 3/8 inches. Total effective prestressing force after allowances for losses from the 38 fully bonded strands stressed at 22.7 kips was 863 kips, with 529 kips or  $\left(\frac{18.375in}{30in}\right) \times (879kip)$  applied at node 3. The use of the extended nodal region produced more realistic failure loads. The remaining effective prestress force was applied at node 5.

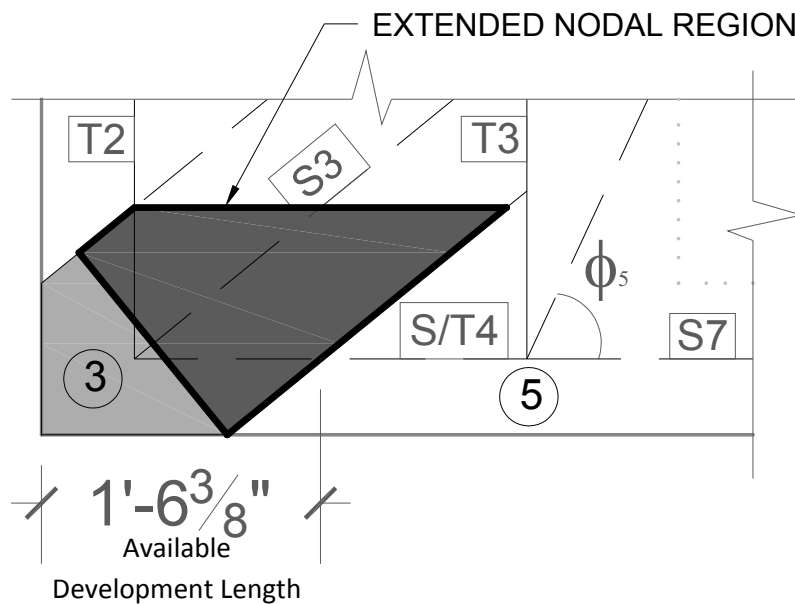


**Figure 5-5 Extended nodal region at node 3.**

Due to the large amount of concrete in the dapped end region, it was found that a tie failure mechanism would govern. Analysis of the model reveals a maximum shear force of 395 kip governed by yield of tie 3. Table 5-1 provides the shear forces corresponding to the yielding of a given tie. All struts and nodes provided sufficient strength to confirm that tie 3 controlled failure of the dapped end region of beam RF-3R-9(a). Complete calculations are available in Appendix C.



**Table 5-1 Tie capacities for beam RF-3R-9(a).**

Tie	Force per Unit Shear	Area Provided (in <sup>2</sup> )	Shear at Tie Failure (kip)	Notes
T1	0.84	7.20	515	Only includes main dap reinforcement (12 #7 bars)
T2	0.77	7.84	611	Hanger reinforcement (8-2 legged #6 bars, 2-2legged #4 bars)
T3	0.63	4.16	395	Includes 6-2 legged #4 bars and 4-1 legged #6 bar
S/T4	0.95	2.64	725	Includes nonprestressed reinforcement (3-2 legged #6 bars) and includes additional compression from extended nodal region

5.2.1.1.2 *RF-3R-9(c)*

Beam RF-3R-9(c) was tested at a shear span of 84 inches with the distance from the centroid of the hanger reinforcement to the load point creating the shear span. The shear span-to-depth ratio ( $a_d/d$ ) was 1.58d, where d is the effective depth of the flexural reinforcement for the full-depth beam (Figure 5-2). The strut-and-tie model was analyzed using the same assumptions as the previous model with the sole difference being the change in the shear span. Figure 5-6 represents the proposed model including critical nodes. In contrast to the model in Figure 5-4, the second vertical tie, 3 in Figure 5-4, is broken into two separate ties in an attempt to spread the vertical force to as much of the reinforcement as possible in the region between the hanger reinforcement and load point (Figure 5-7). Additionally, since the vertical reinforcement does not extend into the deck slab, strut 2 becomes horizontal when connecting between the two vertical ties. Again, ties control the behavior of the beam with tie 2 yielding at a shear force of 470 kip. All struts and nodes have greater capacities confirming that tie 2 controlled failure of the dapped end region of beam RF-3R-9(c). Table 5-2 provides the shear forces corresponding to tie failure. Complete calculations are available in Appendix C.

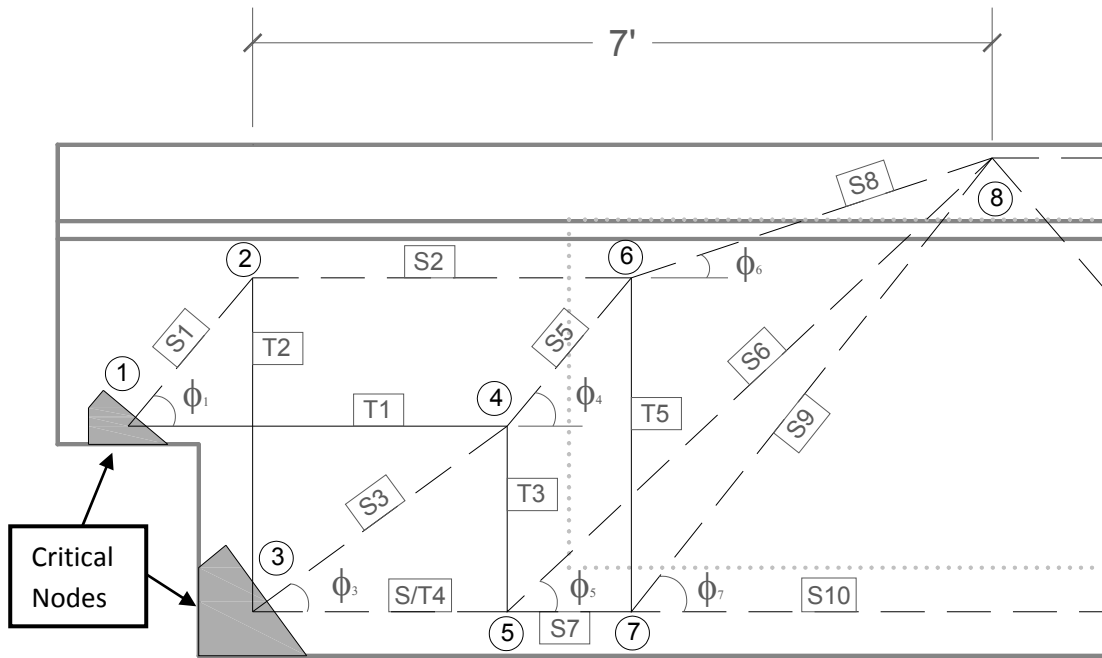


Figure 5-6 ACI strut-and-tie model proposed for beam RF-3R-9(c).

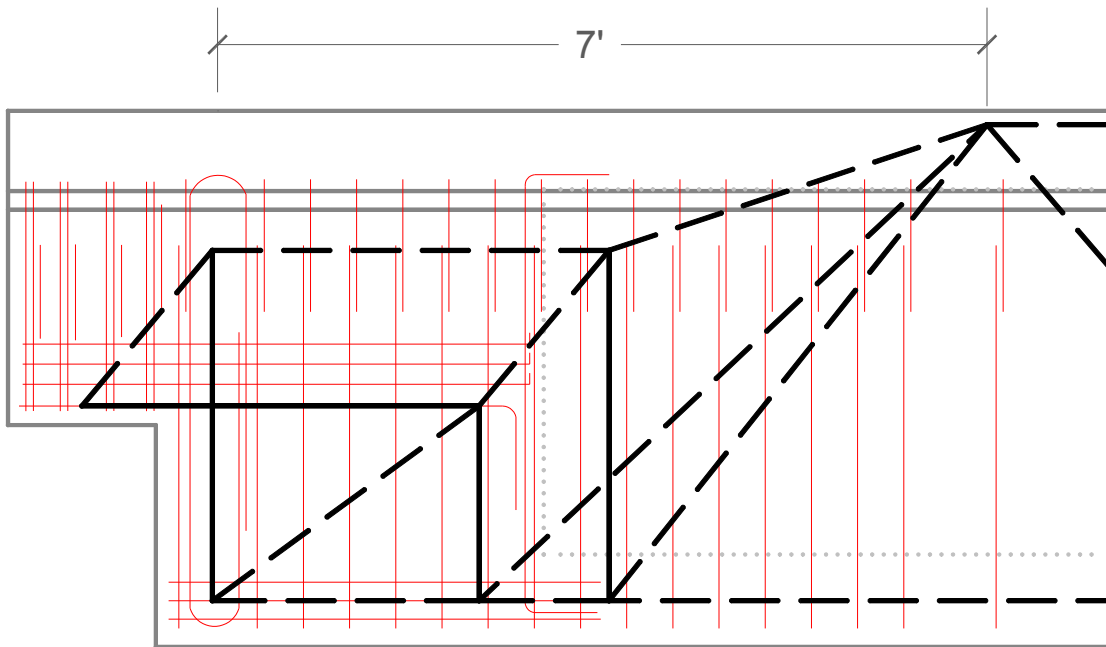


Figure 5-7 Non-prestressed reinforcement (red) with strut-and-tie model overlay for beam RF-3R-9(c).

**Table 5-2 Tie capacities for beam RF-3R-9(c).**

Tie	Force per kip Shear (kip)	Area Provided (in <sup>2</sup> )	Maximum Shear Available (kip)	Notes
T1	0.84	7.20	515	Only includes main dap reinforcement (12 #7 bars)
T2	1.00	7.84	470	Hanger reinforcement (8-2 legged #6 bars, 2-2legged #4 bars)
T3	0.37	3.36	551	Includes 6-2 legged #4 bars and 4-1 legged #6 bars
S/T4	1.37	2.64	514	Includes nonprestressed reinforcement (3-2 legged #6 bars) and includes additional compression from extended nodal region
T5	0.178	1.6	539	Includes 4-2 legged #4 bars

### ***5.2.1.2 2007 AASHTO LRFD Bridge Design Specifications***

For both beams tested, the AASHTO LRFD design provisions were applied to the same strut-and-tie geometry as in the ACI318-08 design. When analyzing an existing reinforcement layout using AASHTO LRFD and strut-and-tie modeling, the process is iterative. Therefore, to simplify the procedure, failure loads from the ACI318-08 strut-and-tie model were used in the AASHTO LRFD models as an initial guess to check the stresses in the members. The main difference between calculations in AASHTO LRFD and ACI318-08 is that AASHTO LRFD changes the efficiency factor of a strut based on the strain and angle of the crossing tie. Both a decreasing strut-to-tie angle and increasing tie strains result in decreasing strut efficiency factors. Like ACI318-08, design according to AASHTO LRFD produced failure by yielding of tie 3 in beam RF-3R-9(a) and yielding of tie 4 in beam RF-3R-9(c). All struts and nodes again proved satisfactory for the given failure modes. Complete calculations are available in Appendix C.

Figure 5-8 and Figure 5-9 represent the strut-and-tie models used for analysis according to AASHTO LRFD. The models are identical to the ACI318-08 models with only a few labeling discrepancies. Labeling of struts and ties in AASHTO LRFD is slightly different from ACI318-08 because AASHTO LRFD defines prestressing tendons as ties with zero strain until the prestressing force is overcome. As such, the bottom members were labeled as ties in the AASHTO LRFD model, in contrast to the strut/tie labels in the ACI318-08 model.

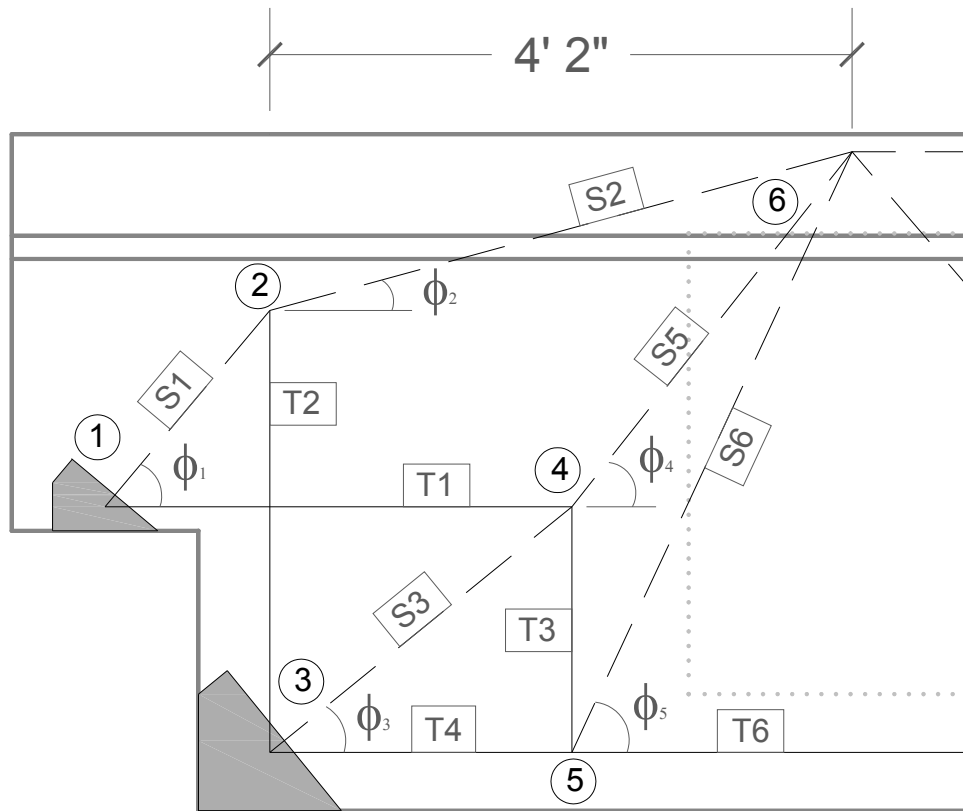


Figure 5-8 Proposed AASHTO strut-and-tie model for beam RF-3R-9(a).

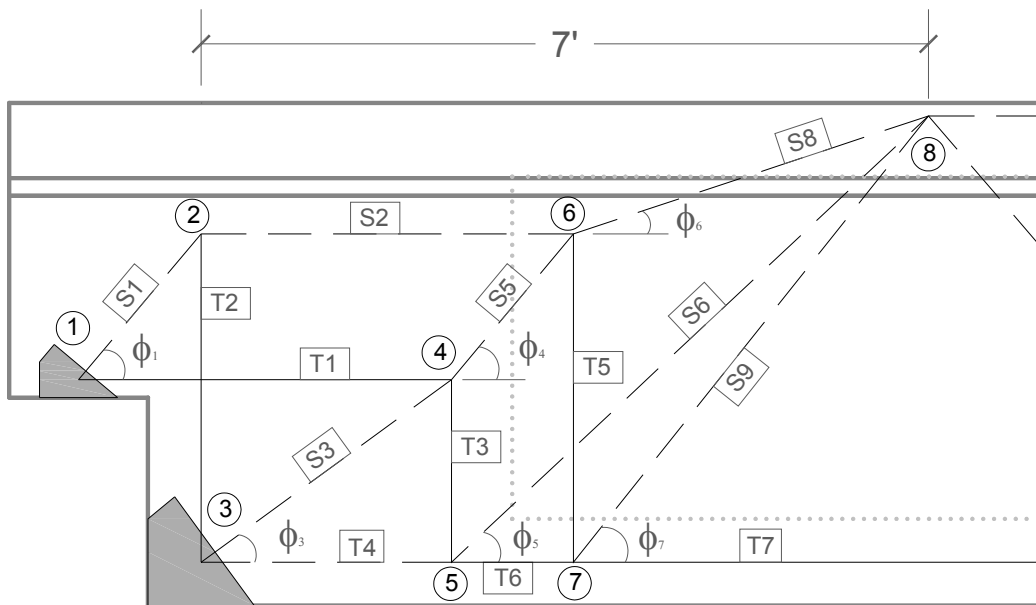


Figure 5-9 Proposed AASHTO strut-and-tie model for beam RF-3R-9(c).

### **5.2.2 PCI Handbook Design**

The *PCI Design Handbook* discusses dapped end design in Section 4.6.3. A crack emanating from the reentrant corner governs the design of this particular dapped end. According to the *PCI Design Handbook*, the shear capacity of the dapped end is 470 kip. The other handbook design provisions produce much larger failure loads. Direct shear and flexural capacity of the nib produce design shear strengths of 921 kip and 659 kip, respectively. Failure due to diagonal tension in the extended end produces a shear capacity of 827 kip. Further discussion of PCI design methods is available in Chapter 2. Calculations are available in Appendix C.

### **5.3 COMPARISON WITH CALCULATED LOADS**

Computed load carrying capacities of the dapped end sections are compared with measured capacities in Table 5-3. Calculated design shear values using ACI318-08 and AASHTO LRFD provisions are based on strut-and-tie models whereas the *PCI Design Handbook* uses straightforward provisions to calculate capacity of the beam. For beam RF-3R-9(a), the PCI design equations produced more accurate failure loads than ACI318-08 and AASHTO LRFD provisions. For beam RF-3R-9(c), all calculated failure loads were the same with yield of the hanger reinforcement controlling the capacity in each case. Neither of the beams tested failed according to the mechanisms indicated by the calculated design methods.

**Table 5-3 Calculated load carrying capacities of dapped ends compared with experimental capacities.**

Design Method	Shear Span-to-Depth Ratio	Calculated Shear ( $V_d$ in kips)	Experimental Failure Shear ( $V_f$ in kips)	$V_f/V_d$	Failure Mechanism
RF-3R-9(a)					
Strut and Tie - ACI	0.94	395	910	2.30	Yield of tie 3
Strut and Tie - AASHTO	0.94	395	910	2.30	Yield of tie 3
PCI Design Handbook	0.94	470	910	1.94	Diagonal tension at reentrant corner
RF-3R-9(c)					
Strut and Tie - ACI	1.58	470	708	1.51	Yield of tie 2
Strut and Tie - AASHTO	1.58	470	708	1.51	Yield of tie 2
PCI Design Handbook	1.58	470	708	1.51	Diagonal tension at reentrant corner

While PCI has very prescriptive provisions for dapped end sections, the strut-and-tie models used in correlation with ACI318-08 and AASHTO LRFD can perhaps be adjusted to more accurately calculate failure loads. Only adjustments to RF-3R-9(a) produced greater failure loads, while adjustments to RF-3R-9(c) did not significantly increase load carrying capacity. Improving the strut-and-tie model of RF-3R-9(a) involves changing the angle of strut 1,  $\phi_1$ , with respect to tie 1 as shown in Figure 5-10. The model appears identical to the original (Figure 5-4), but an increase of  $5^\circ$  in  $\phi_1$  to  $55^\circ$  significantly increases the load carrying capacity of the section by reducing the force in tie 1, and increasing the force in strut 5. A larger load in strut 5 reduces the force in tie 3, which governed failure in the initial model. The original angle of  $50^\circ$  was assumed based on research by Barton et al. (1991), who found acceptable angles for strut 1, with respect to tie 1, to range from  $45^\circ$  to  $55^\circ$ . The average angle of  $50^\circ$  was determined to be a viable starting point. The increase to  $55^\circ$  increases the predicted load carrying capacity to 549 kips from 395 kips and changes the failure mechanism from tie 3 to tie 2. The adjusted model increases computed failures load from strut-and-tie models and results in values closer to the measured capacity.

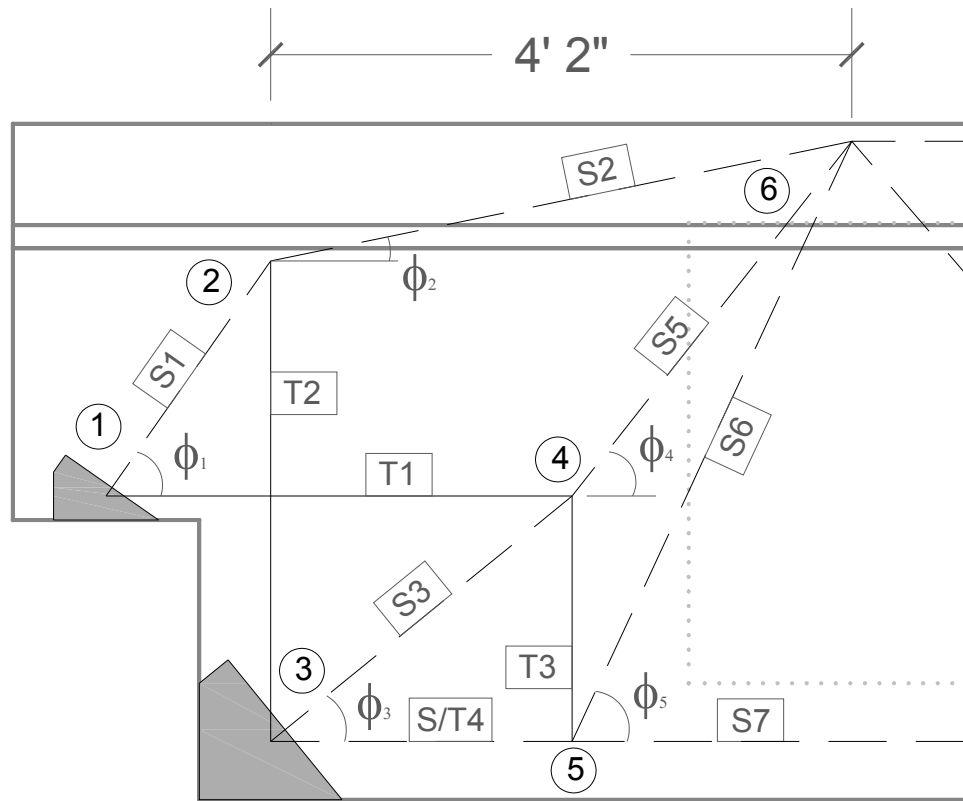


Figure 5-10 Adjusted strut-and-tie model for RF-3R-9(a).

Table 5-4 Calculated load carrying capacities of dapped ends compared with experimental capacities with adjustments to beam RF-3R-9(a).

Design Method	Shear Span-to-Depth Ratio	Calculated Shear ( $V_d$ in kip)	Experimental Failure Shear ( $V_t$ in kip)	$V_t/V_d$	Failure Mechanism
RF-3R-9(a)					
Strut and Tie - ACI	0.94	549	910	1.66	Yield of tie 2
Strut and Tie - AASHTO	0.94	549	910	1.66	Yield of tie 2
PCI Design Handbook	0.94	470	910	1.94	Diagonal tension at reentrant corner

#### 5.4 PROPOSED DIRECT STRUT MODEL

Current design methods and models for dapped ends are adequate for producing safe designs. However, calculations presented do not include  $\phi$ -factors that would increase conservativeness of design and decrease efficiency. The proposed direct strut

model is intended to improve efficiency of proven design equations while maintaining the necessary safety. The model expands on the ideas presented by Mattock and Chan (1979). The direct strut model results in lower design forces on the vertical hanger reinforcement and considers the development of prestressing strands within the extended nodal region.

#### 5.4.1 Model

The direct strut model is much simpler than the previously proposed strut-and-tie models. The model is comprised of two ties, three struts, and the bottom strut/tie depending on the prestressing force at the node. Figure 5-11 shows examples of the model for beams RF-3R-9(a) and RF-3R-9(c). In the model, it is assumed that tie 1 has sufficient development length beyond tie 2 to provide anchorage for the stress developed within the tie. The remaining elements follow typical strut-and-tie modeling procedures.

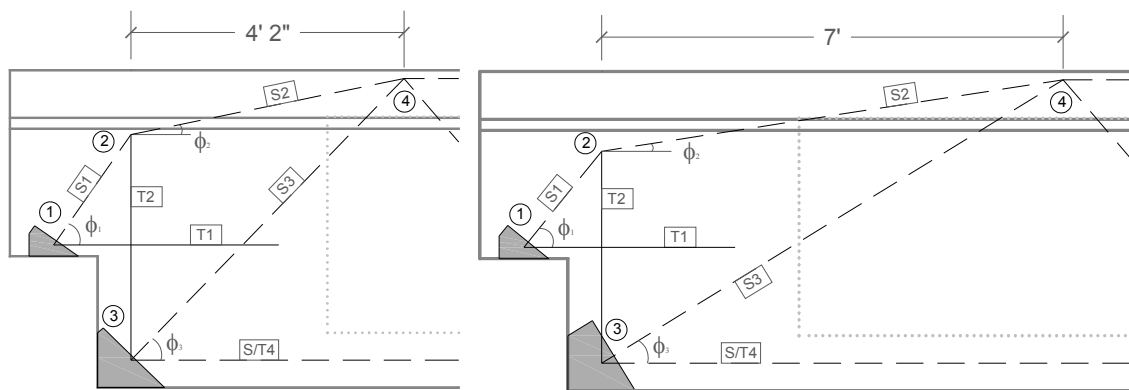


**Figure 5-11 Proposed direct strut models for beam RF-3R-9(a)[left] and beam RF-3R-9(c)[right].**

The direct strut model calculates failure loads closer to actual loads resisted by the section and closely follows the cracking pattern developed from the applied load. Computed failure loads for beams RF-3R-9(a) and RF-3R-9(c) were 571 kips and 524 kips, respectively, producing predicted-to-measured ratios –  $V_t/V_d$  – of 1.59 and 1.35. The  $V_t/V_d$  ratios found from the previous strut-and-tie models were 1.66 and 1.51 for beams RF-3R-9(a) and RF-3R-9(c), respectively. From the improvement in accuracy, the direct strut method produces more efficient strut-and-tie models than the typical models used in design today.



Two design issues would need to be addressed to complete the direct strut method:

1. development of tie 1 and
2. required steel for the full depth section beyond the hanger reinforcement.

Two design assumptions from Mattock could be incorporated into the design procedure to handle these issues. First, Mattock requires tie 1 to extend a distance of  $H - d_{nib} + l_d$  past the reentrant corner where  $H$  is the full depth of the section,  $d_{nib}$  is the depth of the main dapped end reinforcement, and  $l_d$  is the development length of the bars (Mattock & Chan, 1979). Using this requirement would take care of the anchorage of tie 1. Second, the full depth section up to a distance  $H$  beyond the reentrant corner could be designed using sectional shear design requirements, the minimum of  $V_{ci}$  and  $V_{cw}$ , at a distance  $H/2$  from the reentrant corner or using modified compression field theory based expressions in AASHTO LRFD (Mattock & Theryo, 1986). Using this requirement would aid in designing for the required amount of stirrups beyond the hanger reinforcement.

Incorporating these design provisions with the direct strut model could prove to produce efficient and safe designs for prestressed dapped end members. However, further testing is required to implement such procedures into design.

## **5.5 CUT SECTION ANALYSIS: BEAM RF-3R-9(c)**

At failure, Beam RF-3R-9(c) developed wide shear cracks from the bottom corner of the beam to the edge of the load point. These large shear cracks split the beam in two as seen in Figure 5-12. The cut section needs to satisfy equilibrium constraints using the available load-carrying elements: prestressing strands, vertical stirrups, concrete in the compression zone, and applied shear force. Herzinger and Elbadry (2007) have developed a cut analysis in correlation with shear friction and diagonal bending. The principles of their work will be utilized in this section.

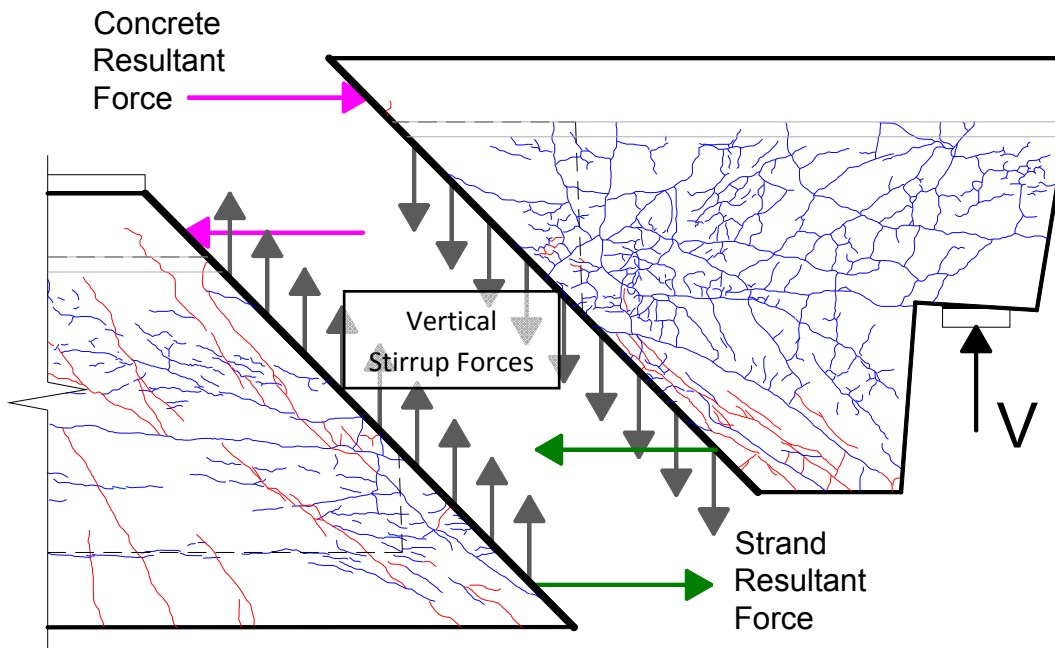
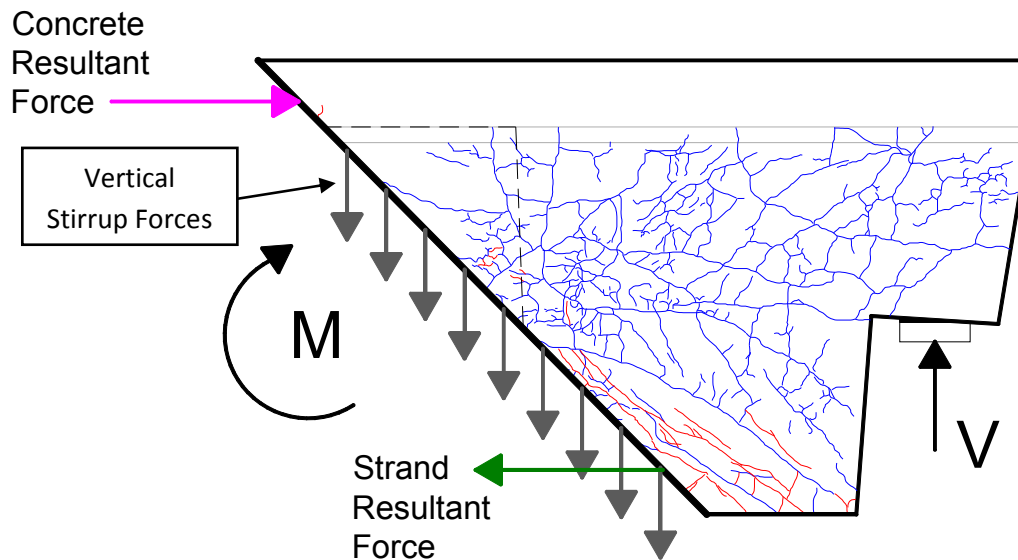


Figure 5-12 Cut section of beam RF-3R-9(c).

The top flange of the beam contained a much larger area than the webs of the section and should contribute to the flexural capacity significantly more than the rest of the section. As such, the compression resultant was assumed to act at mid-depth of the top flange. Once the location of the compression result is determined, the capacity of the cut section in Figure 5-13 can be calculated by summing the moments about the compression resultant. Forces in reinforcement were calculated based on the available stress in each bar. The strand force depended on the available development of transfer stress at the cut location. With the cut passing through the transfer length of the strands, the available stress in each strand was a portion of the effective stress after allowance for losses. In addition to the strands, six #6 reinforcing bars taken at yield contribute to the strand resultant. Vertical stirrups were included based on the bars that were intersected by the cut with sufficient ability to develop stresses. The stirrups were assumed to be yielded at failure. Yielded stirrups are reasonable after the measurements from the shear distortion apparatus revealed significant crack opening in the web region. In addition, wide cracks, up to 1/8-inch formed along the cut line.



**Figure 5-13 Cut section analyzed by summation of moments about compression resultant.**

Summing the moments about the compression resultant and solving for the shear force in the section results in a capacity of 621 kips. This closely resembles the failure shear of 708 kips with a predicted-to-measured shear ratio of 1.14. According to the cut section analysis, failure was due to a shear induced bond slip. The stirrups have reserve capacity past yield, but when the strand reaches the debonding stress, slip occurs resulting in a stress decrease and failure. Table 5-5 compares the cut section analysis results to the ACI, AASHTO, and direct strut calculations.

**Table 5-5 Comparison of adjusted final capacity calculations including cut analysis.**

Design Method	Shear Span-to-Depth Ratio	Calculated Shear ( $V_d$ in kip)	Experimental Failure Shear ( $V_t$ in kip)	$V_t/V_d$	Failure Mechanism
RF-3R-9(a)					
Strut and Tie - ACI	0.94	549	910	1.66	Yield of tie 2
Strut and Tie - AASHTO	0.94	549	910	1.66	Yield of tie 2
PCI Design Handbook	0.94	470	910	1.94	Diagonal tension at reentrant corner
Direct Strut Model - ACI	0.94	571	910	1.59	Yield of tie 2
RF-3R-9(c)					
Strut and Tie - ACI	1.58	470	708	1.51	Yield of tie 2
Strut and Tie - AASHTO	1.58	470	708	1.51	Yield of tie 2
PCI Design Handbook	1.58	470	708	1.51	Diagonal tension at reentrant corner
Direct Strut Model - ACI	1.58	524	708	1.35	Shear induced bond/strand slip
Cut Analysis Method	1.58	621	708	1.14	Shear induced bond/strand slip

## 5.6 OVERVIEW

Reviewing the results in Table 5-5, it is first evident that load prediction at the shorter shear span, beam RF-3R-9(a), is more conservative than at larger shear span. The extra conservatism in the short shear span may result from the lack of understanding of how much load can flow directly into the support versus following the dapped end models. As the shear span increases, the ability of load to go directly into the support decreases because the angle of inclination from the support to the load point decreases, making a direct strut to the support less likely. It is conservative to assume that the direct strut into the support does not exist, requiring design of the beam based solely on the dapped end model.

Second, PCI calculations produced the same failure load, independent of the shear span. ACI318-08 and AASHTO LRFD, using strut-and-tie modeling, calculate different failure loads depending on the location of the point load. Therefore, PCI produced more

accurate failure loads at larger shear spans and more conservative failure loads at shorter shear spans.

Third, the direct strut may produce more applicable and efficient design procedures than the current available dapped end strut-and-tie models. The direct strut provides a simple model to assess dapped end capacities while generating more accurate estimated loads than current models. Integrating the direct strut model with selected guidelines from Mattock and Chan (1979), Mattock and Theryo (1986), and the *PCI Design Handbook* (2004) could prove to create a simple, efficient design procedure for design of prestressed dapped end sections.

Finally, the cut analysis provided an accurate post-failure load and mechanism prediction method for beam RF-3R-9(c). However, assessment using the cut analysis pre-failure or to place reinforcement would be challenging. Beam RF-3R-9(a) could not be analyzed using the cut analysis because no distinct failure crack existed, proving the limitation of the cut analysis.

## CHAPTER 6

### Summary and Conclusions

#### 6.1 SUMMARY

Testing was conducted to investigate the effects of concrete cracking due alkali-silica reaction (ASR) and delayed-ettringite formation (DEF) on the shear strength of trapezoidal box beams. The trapezoidal box beams of this study were fabricated in 1995 for the US 59 corridor between IH 610 and BW 8 in Houston, Texas. Five full-scale beams rejected because of fabrication errors were available for testing. Four beams experienced significant cracking due to ASR and DEF. In this thesis, the effects of ASR/DEF cracking on the structural performance of the dapped ends of the beams are described. Two dapped end sections have been tested at Phil M. Ferguson Structural Engineering Laboratory.

Observed and measured behavior from the two dapped end tests were used to analyze the response of the beams and determine if there was a loss of strength as a result of premature concrete cracking to due ASR/DEF. Test results were compared against design methods of the *PCI Design Handbook*, ACI 318-08, and AASHTO LRFD. Additionally, models were developed in an attempt to more accurately compute failure loads of dapped end sections.

#### 6.2 CONCLUSIONS

Upon completion of testing, two conclusions can be inferred from the tests on beam RF-3R-9 which exhibited moderate damage due to ASR and DEF.

- (1) Capacities of the dapped end region of the prestressed trapezoidal box beams with moderate ASR/DEF-related cracking were greater than the capacities computed based on available design methods. Both beams failed by shear

induced bond slip and reached loads at least 35% greater than calculated by any given design method. The lack of new visible cracks or widening of existing cracks within the dapped end region signified that the dapped end did not control beam capacity. No design method produced failure by the same mechanism as witnessed in testing.

(2) In the presence of ASR/DEF cracking, little additional cracking due to the applied load was visible before failure. Furthermore, the cracking due to the applied load often aligned with existing cracks. This phenomenon made it difficult to distinguish between ASR/DEF-related cracking and cracking due to the applied load. The lack of additional cracking, along with the indistinguishable differences between the two types of cracking, provided little warning that the concrete was under distress as the section approached the failure load.

(3) A modified strut-and-tie model was proposed for design of dapped end sections.

### **6.3 FURTHER INVESTIGATIONS**

Testing of ASR/DEF cracked beams should continue in order to reach a firm conclusion on the effect of the cracking on the shear capacity of prestressed members. Further testing should focus on mildly and heavily damaged beams. Additionally, testing should be continued to investigate the validity of various strut-and-tie models. Finally, a review of literature revealed that most studies on dapped end specimens were conducted on a small scale. Further tests should be conducted on full-scale beams to determine if size affects dapped end response.

# APPENDIX A

## Beam Weights

Table A-1 Measurements for beam weight of RF-3R-9(a).

	Load Cell			
	NW	NE	SW	SE
Load Reading	19.5	7.4	12.0	22.8
Beam Weight (Sum)	61.7			

Table A-1 Measurements for beam weight of RF-3R-9(c).

	Load Cell			
	NW	NE	SW	SE
Load Reading	25.5	4.6	8.7	22.9
Beam Weight (Sum)	61.7			



## APPENDIX B

### Calculations for Prestress Losses

#### ***AASHTO Estimation of Loss in Prestressing Strands:***

##### **Prestressing Strand Properties**

$$f_{pu} := 270 \text{ksi} \quad f_{pbed} := 202.5 \text{ksi} \quad d_b := 0.5 \text{in} \quad E_p := 28500 \text{ksi}$$

$$f_{pj} := 0.75 f_{pu} \quad f_{pj} = 202.5 \text{ksi} \quad f_{py} := 0.9 f_{pu} \quad f_{py} = 243 \text{ksi}$$

$$n_{strands} := 62 \quad A_{strand} := 0.153 \text{in}^2 \quad A_{ps} := n_{strands} \cdot A_{strand}$$

$$P_i := A_{ps} \cdot f_{pbed} \quad P_i = 1921 \text{kip}$$

$$d_p := \frac{16 \cdot A_{strand} \text{in}^2 \cdot 52 \text{in} + 16 \cdot A_{strand} \text{in}^2 \cdot 50 \text{in} + 18 \cdot A_{strand} \text{in}^2 \cdot 48 \text{in} \dots + (n_{strands} - 50) \cdot A_{strand} \text{in}^2 \cdot 46 \text{in}}{n_{strands} \cdot A_{strand} \text{in}^2} \quad d_p = 49.161 \text{in}$$

##### **Concrete Section Properties**

$$A_g := 1108 \text{in}^2 \quad I_g := 404968 \text{in}^4 \quad y_t := 27.29 \text{in} \quad e := d_p - y_t$$

$$f_{ci} := 6385 \text{psi} \quad E_{ci} := 57000 \cdot \sqrt{f_{ci}} \text{psi}$$

##### **Beam Properties**

$$w_{sw} := 1.154 \frac{\text{kip}}{\text{ft}} \quad L := 111 \text{ft} \quad M_{sw} := \frac{w_{sw} \cdot L^2}{8} \quad M_{sw} = 1777 \text{kip}\cdot\text{ft}$$

### Loss Calculations

$$\text{Percent} := 0.913$$

$$f_{cgp} := \frac{\text{Percent} \cdot P_1}{A_g} + \frac{\text{Percent} \cdot P_1 \cdot e^2}{I_g} - \frac{M_{sw} \cdot e}{I_g} \quad f_{cgp} = 2.503 \text{ ksi}$$

$$\Delta f_{pES} := \frac{E_p}{E_{ci}} \cdot f_{cgp} \quad \Delta f_{pES} = 15.66 \text{ ksi}$$

$$t := 1$$

$$\Delta f_{pR1} := \frac{\log(24.0 \cdot t)}{40} \cdot \left( \frac{f_{pj}}{f_{py}} - 0.55 \right) \cdot f_{pj} \quad \Delta f_{pR1} = 1.98 \text{ ksi}$$

$$\Delta f_{pi} := \Delta f_{pES} + \Delta f_{pR1}$$

$$p\Delta f_{pi} := 100 \cdot \left( \frac{\Delta f_{pi}}{f_{pj}} \right) \quad p\Delta f_{pi} = 8.711 \quad \frac{100 - p\Delta f_{pi}}{100} = 0.913 \quad \text{Percent} = 0.913$$

$$H := 80 \quad (\text{Humidity estimation})$$

$$\Delta f_{pSR} := 17 \text{ ksi} - 0.15 \text{ ksi} \cdot H \quad \Delta f_{pSR} = 5 \text{ ksi}$$

$$w_{slab} := \frac{12 \text{ kip}}{L} \quad (\text{Weight of slab concrete over length})$$

$$M_{slab} := \frac{w_{slab} \cdot L^2}{8} \quad M_{slab} = 166.5 \text{ kip} \cdot \text{ft} \quad \Delta f_{cdp} := \frac{M_{slab} \cdot e}{I_g}$$

$$\Delta f_{pCR} := 12 \cdot f_{cgp} - 7 \cdot \Delta f_{cdp} \quad \Delta f_{pCR} = 29.276 \text{ ksi}$$

$$\Delta f_{pR2} := 0.3 \cdot [20.0 \text{ ksi} - 0.4 \cdot \Delta f_{pES} - 0.2 \cdot (\Delta f_{pSR} + \Delta f_{pCR})] \quad \Delta f_{pR2} = 2.064 \text{ ksi}$$

$$\Delta f_{pT} := \Delta f_{pES} + \Delta f_{pSR} + \Delta f_{pCR} + \Delta f_{pR1} + \Delta f_{pR2} \quad \Delta f_{pT} = 53.98 \text{ ksi}$$

$$f_{pj} - \Delta f_{pT} = 148.52 \text{ ksi} \quad f_{se} := f_{pj} - \Delta f_{pT}$$

$$f_{se} = 148.52 \text{ ksi}$$

# APPENDIX C

## Calculations for Code Provisions

### C.1 ACI CALCULATION: RF-3R-9(a)

#### RF-3R-9(a) Original Strut-and-Tie Model

##### Parameters

$$\begin{array}{llll}
 f_c := 10\text{ksi} & f_y := 60\text{ksi} & f_{se} := 148.5\text{ksi} & A_{ps} := 0.153\text{in}^2 \\
 A_{4b} := 0.20\text{in}^2 & A_{5b} := 0.31\text{in}^2 & A_{6b} := 0.44\text{in}^2 & A_{7b} := 0.60\text{in}^2
 \end{array}$$

##### Angles

$$\phi_1 := 50\text{deg} \quad \phi_2 := 15.3\text{deg} \quad \phi_3 := 39.1\text{deg} \quad \phi_4 := 51.7\text{deg} \quad \phi_5 := 65.0\text{deg}$$

#### Strut and Tie Check (ACI Appendix A-3 & A-4 pg. 388)

Check if struts reinforced:

$$\begin{array}{llll}
 b_s := 8\text{in} & \text{(smallest expected strut width)} & s := 5\text{in} & \text{(spacing of stirrups)} \\
 \alpha_1 := 65\text{deg} & \alpha_2 := 25\text{deg} & & \text{Maximum and minimum strut angles.} \\
 0.003 \cdot b_s \cdot s \cdot \sin(\alpha_1) = 0.109\text{in}^2 & & 0.003 \cdot b_s \cdot s \cdot \sin(\alpha_2) = 0.051\text{in}^2 & A_{prov} := 2 \cdot A_{4b} \\
 & & & A_{prov} = 0.4\text{in}^2
 \end{array}$$

$\beta_s := 0.75$  All struts have enough reinforcement with the vertical stirrups to be classified as reinforced struts.

$$V := 1\text{kip}$$

##### **Strut 1:**

$$\text{Strut}_1 := \frac{V}{\sin(\phi_1)} \quad \boxed{\text{Strut}_1 = 1.305\text{kip}}$$

Strut Width                      Minimum beam width                      Strut Efficiency Factor

$$w_1 := 9.5625\text{in} \quad \boxed{b_1 := 48\text{in}} \quad \beta_s := 0.75$$

$$V_{s1} := \frac{0.85 \cdot \beta_s \cdot f_c \cdot b_1 \cdot w_1}{\frac{\text{Strut}_1}{\text{kip}}} \quad \boxed{V_{s1} = 2241.5\text{kip}} \quad \text{Shear capacity based on strut 1}$$

**Tie 1:**

$$Tie_1 := \frac{V}{\tan(\phi_1)} \quad \boxed{Tie_1 = 0.839 \text{ kip}}$$

$$V_{t1} := \frac{12 \cdot A_{7b} \cdot f_y}{\frac{Tie_1}{\text{kip}}} \quad \boxed{V_{t1} = 514.8 \text{ kip}} \quad \text{Shear capacity based on tie 1}$$

**Strut 2:**

$$Strut_2 := \frac{V}{\tan(\phi_1) \cos(\phi_2)} \quad \boxed{Strut_2 = 0.87 \text{ kip}}$$

Strut Width

$$w_2 := 8 \cdot \text{in}$$

Minimum beam width

$$\boxed{b_2 := 54 \text{ in}}$$

Strut Efficiency Factor

$$\beta_s := 0.75$$

$$V_{s2} := \frac{0.85 \cdot \beta_s \cdot f_c \cdot b_2 \cdot w_2}{\frac{Strut_2}{\text{kip}}} \quad \boxed{V_{s2} = 3165.8 \text{ kip}} \quad \text{Shear capacity based on strut 2}$$

**Tie 2:**

$$Tie_2 := V - V \cdot \frac{\tan(\phi_2)}{\tan(\phi_1)} \quad \boxed{Tie_2 = 0.77 \text{ kip}}$$

$$V_{t2} := \frac{(2 \cdot 8 \cdot A_{6b} + 2 \cdot 2 \cdot A_{4b}) \cdot f_y}{\frac{Tie_2}{\text{kip}}} \quad \boxed{V_{t2} = 610.6 \text{ kip}} \quad \text{Shear capacity based on tie 2}$$

**Strut 3:**

$$Strut_3 := \frac{V - V \cdot \frac{\tan(\phi_2)}{\tan(\phi_1)}}{\sin(\phi_3)} \quad \boxed{Strut_3 = 1.222 \text{ kip}}$$

Strut Width

$$w_3 := 15 \cdot \text{in}$$

Minimum beam width

$$\boxed{b_3 := 36 \text{ in}}$$

Strut Efficiency Factor

$$\beta_s := 0.75$$

$$V_{s3} := \frac{0.85 \cdot \beta_s \cdot f_c \cdot b_3 \cdot w_3}{\frac{Strut_3}{\text{kip}}} \quad \boxed{V_{s3} = 2818 \text{ kip}} \quad \text{Shear capacity based on strut 3}$$

**Strut/Tie 4:**

$$S_{T4} := \text{Strut}_3 \cdot \cos(\phi_3)$$

$$S_{T4} = 0.948 \text{ kip} \quad \text{Without concentrated prestressed load applied}$$

$$V_{s_{t4}} := \frac{6 \cdot A_{6b} \cdot f_y + f_{se} \cdot A_{ps} \cdot 38 \cdot \frac{6.125 \text{ in}}{30 \text{ in}}}{\frac{S_{T4}}{\text{kip}}}$$

$$V_{s_{t4}} = 353 \text{ kip} \quad \text{Shear capacity based on strut that turns into tie \#4}$$

$$V_{s_{t4\_1}} := \frac{6 \cdot A_{6b} \cdot f_y + f_{se} \cdot A_{ps} \cdot 38 \cdot \frac{18.375 \text{ in}}{30 \text{ in}}}{\frac{S_{T4}}{\text{kip}}}$$

$$V_{s_{t4\_1}} = 724.9 \text{ kip} \quad \text{Shear capacity based on strut that turns into tie \#4 at the edge of the extended nodal region.}$$

**Strut 5:**

$$\text{Strut}_5 := \frac{\text{Strut}_3 \cdot \cos(\phi_3) - \text{Tie}_1}{\cos(\phi_4)}$$

$$\text{Strut}_5 = 0.176 \text{ kip}$$

Strut WidthMinimum beam widthStrut Efficiency Factor

$$w_5 := 8 \text{ in}$$

$$b_5 := 15 \text{ in}$$

$$\beta_s := 0.75$$

$$V_{s5} := \frac{0.85 \cdot \beta_s \cdot f_c \cdot b_5 \cdot w_5}{\frac{\text{Strut}_5}{\text{kip}}}$$

$$V_{s5} = 4352.3 \text{ kip} \quad \text{Shear capacity based on strut 5}$$

**Tie 3:**

$$\text{Tie}_3 := \text{Strut}_3 \cdot \sin(\phi_3) - \text{Strut}_5 \cdot \sin(\phi_4)$$

$$\text{Tie}_3 = 0.633 \text{ kip}$$

$$V_{t3} := \frac{(2 \cdot 6 \cdot A_{4b} + 4 \cdot A_{6b}) \cdot f_y}{\frac{\text{Tie}_3}{\text{kip}}}$$

$$V_{t3} = 394.6 \text{ kip} \quad \text{Shear capacity based on tie 3}$$

**Strut 6:**

$$\text{Strut}_6 := \frac{\text{Tie}_3}{\sin(\phi_5)}$$

$$\text{Strut}_6 = 0.698 \text{ kip}$$

Strut WidthMinimum beam widthStrut Efficiency Factor

$$w_6 := 15 \text{ in}$$

$$b_6 := 10 \text{ in}$$

$$\beta_s := 0.75$$

$$V_{s6} := \frac{0.85 \cdot \beta_s \cdot f_c \cdot b_6 \cdot w_6}{\frac{\text{Strut}_6}{\text{kip}}}$$

$$V_{s6} = 1370.2 \text{ kip} \quad \text{Shear capacity based on strut 6}$$

**Strut 7:**

$$\text{Strut}_7 := S_{T4} + \text{Strut}_6 \cdot \cos(\phi_5)$$

$$\text{Strut}_7 = 1.243 \text{ kip}$$

Without concentrated prestressed load applied

Strut Width

$$w_7 := 10 \text{ in}$$

Minimum beam width

$$b_7 := 36 \text{ in}$$

Strut Efficiency Factor

$$\beta_s := 0.75$$

$$V_{s7} := \frac{31 \cdot \text{kip} \cdot 38}{\frac{\text{Strut}_7}{\text{kip}}}$$

$$V_{s7} = 947.7 \text{ kip}$$

Shear capacity based on Strut 7, strands provide the original force on the section that needs to be overcome by the force on Strut 7 due to the applied load.

**Nodal Check (ACI Appendix A.5 pg. 392)**

**Check singular nodes:**

**Node 1:**

C-C-T node at bearing.

$$\beta_n := 0.80$$

$$f_{ce} := 0.85 \cdot \beta_n \cdot f_c$$

**Tie 1 Face:**

Node Width

$$w_{t1} := 4.125 \text{ in}$$

Minimum beam width

$$b_{t1} := 32 \text{ in}$$

Shear at node failure:

$$V_{t1\_n} := \frac{f_{ce} \cdot w_{t1} \cdot b_{t1}}{\frac{\text{Tie}_1}{\text{kip}}}$$

$$V_{t1\_n} = 1070 \text{ kip}$$

**Strut 1 Face:**

Node Width

$$w_{s1} := 9.5626 \text{ in}$$

Minimum beam width

$$b_{s1} := 32 \text{ in}$$

Shear at node failure:

$$V_{s1\_n} := \frac{f_{ce} \cdot w_{s1} \cdot b_{s1}}{\frac{\text{Strut}_1}{\text{kip}}}$$

$$V_{s1\_n} = 1594 \text{ kip}$$



**Bearing Face:**Node WidthMinimum beam width

$w_{b1} := 9\text{in}$

$b_{b1} := 32\text{in}$

Shear at node failure:

$V_{b1\_n} := f_{ce} \cdot w_{b1} \cdot b_{b1}$

$V_{b1\_n} = 1958 \text{ kip}$

**Node 3:**

C-T-T node at bearing.

$\beta_n := 0.80$

$f_{ce} := 0.85 \cdot \beta_n \cdot f_c$

**Tie 2 Face:**Node WidthMinimum beam width

$w_{t2} := 12.25\text{in}$

$b_{t2} := 36\text{in}$

Shear at node failure:

$$V_{t2\_n} := \frac{f_{ce} \cdot w_{t2} \cdot b_{t2}}{\frac{\text{Tie}_2}{\text{kip}}}$$

$V_{t2\_n} = 3892 \text{ kip}$

**Strut 3 Face:**Node WidthMinimum beam width

$w_{s3} := 15.5\text{in}$

$b_{s3} := 36\text{in}$

Shear at node failure:

$$V_{s3\_n} := \frac{f_{ce} \cdot w_{s3} \cdot b_{s3}}{\frac{\text{Strut}_3}{\text{kip}}}$$

$V_{s3\_n} = 3106 \text{ kip}$

**S/T4 Face:**Node WidthMinimum beam width

$w_{t4} := 10\text{in}$

$b_{t4} := 36\text{in}$

Shear at node failure:

$$V_{t4\_n} := \frac{f_{ce} \cdot w_{t4} \cdot b_{t4}}{\frac{\text{S}_T4}{\text{kip}}}$$

$V_{t4\_n} = 2582 \text{ kip}$

**Note:** Node under load is singular, but since it is a C-C-C node, previous experience and research indicates it will not control.

**Bearing Check (ACI 10.14 pg. 152)**

$$A_1 := 32\text{in} \cdot 9\text{in} \quad A_1 = 288 \text{ in}^2 \quad \text{Bearing area}$$

$$A_2 := 48\text{in} \cdot 16\text{in} \quad A_2 = 768 \text{ in}^2 \quad \text{Available area}$$

$$m := \begin{cases} \sqrt{\frac{A_2}{A_1}} & \text{if } \sqrt{\frac{A_2}{A_1}} \leq 2.0 \\ 2.0 & \text{otherwise} \end{cases} \quad m = 1.633$$

$$P_n := 0.85f'_c \cdot A_1 \cdot m \quad P_n = 3998 \text{ kip} \quad \text{Shear force achievable with provided bearing.}$$



## C.2 ACI CALCULATION: RF-3R-9(c)

### RF-3R-9(c) Original Strut-and-Tie Model

#### Parameters

$$\begin{array}{llll}
 f'_c := 10\text{ksi} & f_y := 60\text{ksi} & f_{se} := 148.5\text{ksi} & A_{ps} := 0.153\text{in}^2 \\
 A_{4b} := 0.20\text{in}^2 & A_{5b} := 0.31\text{in}^2 & A_{6b} := 0.44\text{in}^2 & A_{7b} := 0.60\text{in}^2 \\
 d_{4b} := 0.5\text{in} & d_{5b} := 0.625\text{in} & d_{6b} := 0.75\text{in} & d_{7b} := 0.875\text{in}
 \end{array}$$

#### Angles

$$\begin{array}{lllll}
 \phi_1 := 50\text{deg} & \phi_2 := 0\text{deg} & \phi_3 := 36.1\text{deg} & \phi_4 := 50\text{deg} & \phi_5 := 43.1\text{deg} \\
 \phi_6 := 18.4\text{deg} & \phi_7 := 51.5\text{deg} & & & 
 \end{array}$$

### Strut and Tie Check (ACI Appendix A-3 & A-4 pg. 388)

Check if struts reinforced:

$$b_s := 8\text{in} \quad (\text{smallest expected strut width}) \quad s := 5\text{in} \quad (\text{spacing of stirrups})$$

$$\alpha_1 := 65\text{deg} \quad \alpha_2 := 25\text{deg} \quad \text{Maximum and minimum strut angles.}$$

$$\begin{array}{lll}
 0.003 \cdot b_s \cdot s \cdot \sin(\alpha_1) = 0.109\text{in}^2 & 0.003 \cdot b_s \cdot s \cdot \sin(\alpha_2) = 0.051\text{in}^2 & A_{prov} := 2 \cdot A_{4b} \\
 & & A_{prov} = 0.4\text{in}^2
 \end{array}$$

$\beta_s := 0.75$  All struts have enough reinforcement with the vertical stirrups to be classified as reinforced struts.

$$V := 1\text{kip}$$

#### **Strut 1:**

$$\text{Strut}_1 := \frac{V}{\sin(\phi_1)} \quad \boxed{\text{Strut}_1 = 1.305\text{kip}}$$

Strut Width                      Minimum beam width                      Strut Efficiency Factor

$$w_1 := 9.5625\text{in} \quad \boxed{b_1 := 48\text{in}} \quad \beta_s := 0.75$$

$$V_{s1} := \frac{0.85 \cdot \beta_s \cdot f'_c \cdot b_1 \cdot w_1}{\text{Strut}_1} \quad \boxed{V_{s1} = 2241.5\text{kip}} \quad \text{Shear capacity based on strut 1}$$

**Tie 1:**

$$Tie_1 := \frac{V}{\tan(\phi_1)}$$

$$Tie_1 = 0.839 \text{ kip}$$

$$V_{t1} := \frac{12 \cdot A_{7b} \cdot f_y}{\frac{Tie_1}{\text{kip}}}$$

$$V_{t1} = 514.8 \text{ kip}$$

Shear capacity based on tie 1

**Strut 2:**

$$Strut_2 := \frac{V}{\tan(\phi_1) \cos(\phi_2)}$$

$$Strut_2 = 0.839 \text{ kip}$$

Strut Width

Minimum beam width

Strut Efficiency Factor

$$w_2 := 8 \cdot \text{in}$$

$$b_2 := 54 \text{ in}$$

$$\beta_s := 0.75$$

$$V_{s2} := \frac{0.85 \cdot \beta_s \cdot f_c \cdot b_2 \cdot w_2}{\frac{Strut_2}{\text{kip}}}$$

$$V_{s2} = 3282.1 \text{ kip}$$

Shear capacity based on strut 2

**Tie 2:**

$$Tie_2 := V - V \cdot \frac{\tan(\phi_2)}{\tan(\phi_1)}$$

$$Tie_2 = 1 \text{ kip}$$

$$V_{t2} := \frac{(2 \cdot 8 \cdot A_{6b} + 2 \cdot 2 \cdot A_{4b}) \cdot f_y}{\frac{Tie_2}{\text{kip}}}$$

$$V_{t2} = 470.4 \text{ kip}$$

Shear capacity based on tie 2

**Strut 3:**

$$Strut_3 := \frac{V - \left( V \cdot \frac{\tan(\phi_2)}{\tan(\phi_1)} \right)}{\sin(\phi_3)}$$

$$Strut_3 = 1.697 \text{ kip}$$

Strut Width

Minimum beam width

Strut Efficiency Factor

$$w_3 := 15 \cdot \text{in}$$

$$b_3 := 36 \text{ in}$$

$$\beta_s := 0.75$$

$$V_{s3} := \frac{0.85 \cdot \beta_s \cdot f_c \cdot b_3 \cdot w_3}{\frac{Strut_3}{\text{kip}}}$$

$$V_{s3} = 2028.3 \text{ kip}$$

Shear capacity based on strut 3

**Strut/Tie 4:**

$$S_{T4} := \text{Strut}_3 \cdot \cos(\phi_3)$$

$$S_{T4} = 1.371 \text{ kip}$$

Without concentrated prestressed load applied

$$V_{s_{t4}} := \frac{6 \cdot A_{6b} \cdot f_y + f_{se} \cdot A_{ps} \cdot 38 \cdot \frac{6.125 \text{ in}}{30 \text{ in}}}{\frac{S_{T4}}{\text{kip}}}$$

$$V_{s_{t4}} = 244 \text{ kip}$$

Shear capacity based on strut that turns into tie #4

$$V_{s_{t4_1}} := \frac{6 \cdot A_{6b} \cdot f_y + f_{se} \cdot A_{ps} \cdot 38 \cdot \frac{19 \text{ in}}{30 \text{ in}}}{\frac{S_{T4}}{\text{kip}}}$$

$$V_{s_{t4_1}} = 514.2 \text{ kip}$$

Shear capacity based on strut that turns into tie #4 at the edge of the extended nodal region.

**Strut 5:**

$$\text{Strut}_5 := \frac{\text{Strut}_3 \cdot \cos(\phi_3) - \text{Tie}_1}{\cos(\phi_4)}$$

$$\text{Strut}_5 = 0.828 \text{ kip}$$

Strut Width

Minimum beam width

Strut Efficiency Factor

$$w_5 := 8 \cdot \text{in}$$

$$b_5 := 48 \text{ in}$$

$$\beta_s := 0.75$$

$$V_{s5} := \frac{0.85 \cdot \beta_s \cdot f_c \cdot b_5 \cdot w_5}{\text{Strut}_5}$$

$$V_{s5} = 2956.4 \text{ kip}$$

Shear capacity based on strut 5

**Tie 3:**

$$\text{Tie}_3 := \text{Strut}_3 \cdot \sin(\phi_3) - \text{Strut}_5 \cdot \sin(\phi_4)$$

$$\text{Tie}_3 = 0.366 \text{ kip}$$

$$V_{t3} := \frac{(2 \cdot 4 \cdot A_{4b} + 4 \cdot A_{6b}) \cdot f_y}{\frac{\text{Tie}_3}{\text{kip}}}$$

$$V_{t3} = 551.3 \text{ kip}$$

Shear capacity based on tie 3

**Strut 6:**

$$2 \cdot 4 \cdot A_{4b} + 4 \cdot A_{6b} = 3.36 \text{ in}^2$$

$$\text{Strut}_6 := \frac{\text{Tie}_3}{\sin(\phi_5)}$$

$$\text{Strut}_6 = 0.535 \text{ kip}$$

Strut Width

Minimum beam width

Strut Efficiency Factor

$$w_6 := 10 \cdot \text{in}$$

$$b_6 := 10 \text{ in}$$

$$\beta_s := 0.75$$

$$V_{s6} := \frac{0.85 \cdot \beta_s \cdot f_c \cdot b_6 \cdot w_6}{\text{Strut}_6}$$

$$V_{s6} = 1191.1 \text{ kip}$$

Shear capacity based on strut 6

**Strut 7:**

$$\text{Strut}_7 := S_{T4} + \text{Strut}_6 \cdot \cos(\phi_5)$$

$$\text{Strut}_7 = 1.762 \text{ kip}$$

Without concentrated prestressed load applied

Strut Width

Minimum beam width

Strut Efficiency Factor

$$w_7 := 10 \text{ in}$$

$$b_7 := 36 \text{ in}$$

$$\beta_s := 0.75$$

$$V_{s7} := \frac{31 \cdot \text{kip} \cdot 38}{\frac{\text{Strut}_7}{\text{kip}}}$$

$$V_{s7} = 668.5 \text{ kip}$$

Shear capacity based on Strut 7, strands provide the original force on the section that needs to be overcome by the force on Strut 7 due to the applied load.

**Strut 8:**

$$\text{Strut}_8 := \frac{\text{Strut}_2 + \text{Strut}_5 \cdot \cos(\phi_4)}{\cos(\phi_6)}$$

$$\text{Strut}_8 = 1.445 \text{ kip}$$

Strut Width

Minimum beam width

Strut Efficiency Factor

$$w_8 := 10 \text{ in}$$

$$b_8 := 15 \text{ in}$$

$$\beta_s := 0.75$$

$$V_{s8} := \frac{0.85 \cdot \beta_s \cdot f_c \cdot b_8 \cdot w_8}{\frac{\text{Strut}_8}{\text{kip}}}$$

$$V_{s8} = 661.7 \text{ kip}$$

Shear capacity based on strut 8

**Tie 5:**

$$\text{Tie}_5 := \text{Strut}_5 \cdot \sin(\phi_4) - \text{Strut}_8 \cdot \sin(\phi_6)$$

$$\text{Tie}_5 = 0.178 \text{ kip}$$

$$V_{t5} := \frac{(2 \cdot 4 \cdot A_{4b}) \cdot f_y}{\frac{\text{Tie}_5}{\text{kip}}}$$

$$V_{t5} = 539 \text{ kip}$$

Shear capacity based on tie 5

**Strut 9:**

$$\text{Strut}_9 := \frac{\text{Tie}_5}{\sin(\phi_7)}$$

$$\text{Strut}_9 = 0.228 \text{ kip}$$

Strut Width

Minimum beam width

Strut Efficiency Factor

$$w_9 := 8 \text{ in}$$

$$b_9 := 10 \text{ in}$$

$$\beta_s := 0.75$$

$$V_{s9} := \frac{0.85 \cdot \beta_s \cdot f_c \cdot b_9 \cdot w_9}{\frac{\text{Strut}_9}{\text{kip}}}$$

$$V_{s9} = 2240.8 \text{ kip}$$

Shear capacity based on strut 9

**Strut 10:**

$$\text{Strut}_{10} := \text{Strut}_7 + \text{Strut}_9 \cdot \cos(\phi_7)$$

$$\text{Strut}_{10} = 1.904 \text{ kip}$$

Shear capacity based on Strut 10, strands provide the original force on the section that needs to be overcome by the force on Strut 10 due to the applied load. Strands are able to provide greater strength as they are able to pick up tension beyond the prestress in this region.

Strut Width      Minimum beam width      Strut Efficiency Factor

$$w_{10} := 10 \cdot \text{in}$$

$$b_{10} := 36 \text{ in}$$

$$\beta_s := 0.75$$

$$V_{s7} := \frac{31 \cdot \text{kip} \cdot 38}{\text{Strut}_{10}} \\ \text{kip}$$

$$V_{s7} = 618.8 \text{ kip}$$

**Nodal Check (ACI Appendix A.5 pg. 392)****Check Singular Nodes:****Node 1:**

C-C-T node at bearing.

$$\beta_n := 0.80$$

$$f_{ce} := 0.85 \cdot \beta_n \cdot f_c$$

**Tie 1 Face:**

Node Width

Minimum beam width

$$w_{t1} := 4.125 \text{ in}$$

$$b_{t1} := 32 \text{ in}$$

Shear at node failure:

$$V_{t1\_n} := \frac{f_{ce} \cdot w_{t1} \cdot b_{t1}}{\text{Tie}_1} \\ \text{kip}$$

$$V_{t1\_n} = 1070 \text{ kip}$$

**Strut 1 Face:**

Node Width

Minimum beam width

$$w_{s1} := 9.5626 \text{ in}$$

$$b_{s1} := 32 \text{ in}$$

Shear at node failure:

$$V_{s1\_n} := \frac{f_{ce} \cdot w_{s1} \cdot b_{s1}}{\text{Strut}_1} \\ \text{kip}$$

$$V_{s1\_n} = 1594 \text{ kip}$$

**Bearing Face:**

Node Width

$$w_{b1} := 9\text{in}$$

Minimum beam width

$$b_{b1} := 32\text{in}$$

Shear at node failure:

$$V_{b1\_n} := f_{cc} \cdot w_{b1} \cdot b_{b1}$$

$$V_{b1\_n} = 1958 \text{ kip}$$

**Node 3:**

C-T-T node at bearing.

$$\beta_n := 0.80$$

$$f_{ce} := 0.85 \cdot \beta_n \cdot f_c$$

**Tie 2 Face:**

Node Width

$$w_{t2} := 12.25\text{in}$$

Minimum beam width

$$b_{t2} := 36\text{in}$$

Shear at node failure:

$$V_{t2\_n} := \frac{f_{ce} \cdot w_{t2} \cdot b_{t2}}{\frac{\text{Tie}_2}{\text{kip}}}$$

$$V_{t2\_n} = 2999 \text{ kip}$$

**Strut 3 Face:**

Node Width

$$w_{s3} := 15.5625\text{in}$$

Minimum beam width

$$b_{s3} := 36\text{in}$$

Shear at node failure:

$$V_{s3\_n} := \frac{f_{ce} \cdot w_{s3} \cdot b_{s3}}{\frac{\text{Strut}_3}{\text{kip}}}$$

$$V_{s3\_n} = 2245 \text{ kip}$$

**S/T4 Face:**

Node Width

$$w_{t4} := 10\text{in}$$

Minimum beam width

$$b_{t4} := 36\text{in}$$

Shear at node failure:

$$V_{t4\_n} := \frac{f_{ce} \cdot w_{t4} \cdot b_{t4}}{\frac{S\_T4}{\text{kip}}}$$

$$V_{t4\_n} = 1785 \text{ kip}$$

**Note:** Node under load is singular, but since it is a C-C-C node, previous experience and research indicates it will not control.



### **Bearing Check (ACI 10.14 pg. 152)**

$$A_1 := 32\text{in} \cdot 9\text{in} \quad A_1 = 288 \text{ in}^2 \quad \text{Bearing area}$$

$$A_2 := 48\text{in} \cdot 16\text{in} \quad A_2 = 768 \text{ in}^2 \quad \text{Available area}$$

$$m := \begin{cases} \sqrt{\frac{A_2}{A_1}} & \text{if } \sqrt{\frac{A_2}{A_1}} \leq 2.0 \\ 2.0 & \text{otherwise} \end{cases} \quad m = 1.633$$

$$P_n := 0.85f'_c \cdot A_1 \cdot m \quad P_n = 3998 \text{ kip} \quad \text{Shear force achievable with provided bearing.}$$

$$\psi_c := 1.0 \quad \lambda := 1.0$$

$$l_{dh\_7b} := \frac{0.02 \cdot \psi_c \cdot f_y}{\lambda \cdot \sqrt{f'_c} \cdot \text{psi}} \cdot d_{7b} \quad l_{dh\_7b} = 10.5 \text{ in}$$

### C.3 AASHTO CALCULATION: RF-3R-9(a)

#### RF-3R-9(a) Original Strut-and-Tie Model

##### Parameters

$$f_c := 10\text{ksi} \quad f_y := 60\text{ksi} \quad E := 29000\text{ksi} \quad f_{se} := 148.5\text{ksi}$$

$$A_{ps} := 0.153\text{in}^2$$

$$A_{4b} := 0.20\text{in}^2 \quad A_{5b} := 0.31\text{in}^2 \quad A_{6b} := 0.44\text{in}^2 \quad A_{7b} := 0.60\text{in}^2$$

$$d_{4b} := 0.5\text{in} \quad d_{5b} := 0.625\text{in} \quad d_{6b} := 0.75\text{in} \quad d_{7b} := 0.875\text{in}$$

##### Angles

$$\phi_1 := 50\text{deg} \quad \phi_2 := 15.3\text{deg} \quad \phi_3 := 39.1\text{deg} \quad \phi_4 := 51.7\text{deg} \quad \phi_5 := 65.0\text{deg}$$

#### Strut and Tie Check (AASHTO 5.6.3.3 & 5.6.3.4 pg. 5-30)

$V := 394.8\text{kip}$  From ACI Calculations, yield of tie 3.

##### **Tie 1:**

$$Tie_1 := \frac{V}{\tan(\phi_1)}$$

$$Tie_1 = 331.277\text{kip}$$

$$\sigma_{t1} := \frac{Tie_1}{12 \cdot A_{7b}}$$

$$\sigma_{t1} = 46\text{ksi} \quad \text{Stress in tie 1 at failure.}$$

$$\epsilon_{s1} := \frac{\sigma_{t1}}{E}$$

$$\epsilon_{s1} = 1.587 \times 10^{-3}$$



**Strut 1:**

$$\text{Strut}_1 := \frac{V}{\sin(\phi_1)}$$

$$\text{Strut}_1 = 515.375 \text{ kip}$$

Strut WidthMinimum beam width

$$w_1 := 9.5625 \cdot \text{in}$$

$$b_1 := 48 \text{ in}$$

$$\epsilon_{t1} := \epsilon_{s1} + (\epsilon_{s1} + 0.002) \cdot \cot(\phi_1)^2$$

$$f_{cu1} := \begin{cases} \frac{f_c}{0.8 + 170 \cdot \epsilon_{t1}} & \text{if } \frac{f_c}{0.8 + 170 \cdot \epsilon_{t1}} \leq 0.85 \cdot f_c \\ 0.85 \cdot f_c & \text{otherwise} \end{cases} \quad f_{cu1} = 6.671 \text{ ksi}$$

*Effective available concrete stress*

$$\sigma_{s1} := \frac{\text{Strut}_1}{b_1 \cdot w_1}$$

$$\sigma_{s1} = 1.1 \text{ ksi}$$

*Stress in strut 1 at failure*

$$\text{Check} := \begin{cases} \text{"OK"} & \text{if } \sigma_{s1} \leq f_{cu1} \\ \text{"NO GOOD"} & \text{otherwise} \end{cases}$$

Check = "OK"

**Tie 2:**

$$\text{Tie}_2 := V - V \cdot \frac{\tan(\phi_2)}{\tan(\phi_1)}$$

$$\text{Tie}_2 = 304.173 \text{ kip}$$

$$\sigma_{t2} := \frac{\text{Tie}_2}{2 \cdot 8 \cdot A_{6b} + 2 \cdot 2 \cdot A_{4b}}$$

$$\sigma_{t2} = 38.8 \text{ ksi}$$

*Stress in tie 2 at failure*

$$\epsilon_{s2} := \frac{\sigma_{t2}}{E}$$

$$\epsilon_{s2} = 1.338 \times 10^{-3}$$

**Recheck Strut 1:**

$$\epsilon_{t2} := \epsilon_{s2} + (\epsilon_{s2} + 0.002) \cdot \cot(90\text{deg} - \phi_1)^2$$

$$f_{cu1} := \begin{cases} \frac{f_c}{0.8 + 170 \cdot \epsilon_{t2}} & \text{if } \frac{f_c}{0.8 + 170 \cdot \epsilon_{t2}} \leq 0.85 \cdot f_c \\ 0.85 \cdot f_c & \text{otherwise} \end{cases} \quad f_{cu1} = 5.455 \text{ ksi}$$

$$\sigma_{s1} := \frac{\text{Strut}_1}{b_1 \cdot w_1}$$

$$\sigma_{s1} = 1.1 \text{ ksi}$$

*Stress in strut 1 at failure*

$$\text{Check} := \begin{cases} \text{"OK"} & \text{if } \sigma_{s1} \leq f_{cu1} \\ \text{"NO GOOD"} & \text{otherwise} \end{cases} \quad \text{Check} = \text{"OK"}$$

**Strut 2:**

$$\text{Strut}_2 := \frac{V}{\tan(\phi_1) \cos(\phi_2)} \quad \boxed{\text{Strut}_2 = 343.449 \text{ kip}}$$

Strut Width                      Minimum beam width

$$w_2 := 8 \cdot \text{in} \quad \boxed{b_2 := 54 \text{ in}} \quad \epsilon_{t2} := \epsilon_{s2} + (\epsilon_{s2} + 0.002) \cdot \cot(90\text{deg} - \phi_2)^2$$

$$f_{cu2} := \begin{cases} \frac{f_c}{0.8 + 170 \cdot \epsilon_{t2}} & \text{if } \frac{f_c}{0.8 + 170 \cdot \epsilon_{t2}} \leq 0.85 \cdot f_c \\ 0.85 \cdot f_c & \text{otherwise} \end{cases} \quad f_{cu1} = 5.455 \text{ ksi}$$

*Effective available concrete stress*

$$\sigma_{s2} := \frac{\text{Strut}_2}{b_2 \cdot w_2} \quad \boxed{\sigma_{s2} = 0.8 \text{ ksi}} \quad \text{Stress in strut 2 at failure}$$

$$\text{Check} := \begin{cases} \text{"OK"} & \text{if } \sigma_{s2} \leq f_{cu2} \\ \text{"NO GOOD"} & \text{otherwise} \end{cases} \quad \text{Check} = \text{"OK"}$$

**Tie 4:**

$$\text{Tie}_4 := \frac{V - V \cdot \frac{\tan(\phi_2)}{\tan(\phi_1)}}{\tan(\phi_3)} \quad \boxed{\text{Tie}_4 = 374.285 \text{ kip}} \quad \text{Without concentrated prestressed load applied}$$

$$\sigma_{t4} := \frac{\text{Tie}_4 - f_{se} \cdot A_{ps} \cdot 38 \cdot \frac{6.125 \text{ in}}{30 \text{ in}}}{6 \cdot A_{6b}} \quad \boxed{\sigma_{t4} = 75 \text{ ksi}} \quad \text{Stress in reinforcing steel near prestressing steel at failure}$$

$$\sigma_{t4\_2} := \frac{\text{Tie}_4 - f_{se} \cdot A_{ps} \cdot 38 \cdot \frac{18.375 \text{ in}}{30 \text{ in}}}{6 \cdot A_{6b}} \quad \boxed{\sigma_{t4\_2} = -58.5 \text{ ksi}} \quad \text{Stress in reinforcing steel near prestressing steel at failure assuming prestressing force taken at extended nodal region.}$$

$$\epsilon_{s4} := 0 \quad \text{Use extended nodal region making steel strain 0.}$$

**Since tie still in compression, stress in tie is still 0.0 according to AASHTO.**

**Strut 3:**

$$\text{Strut}_3 := \frac{V - V \cdot \frac{\tan(\phi_2)}{\tan(\phi_1)}}{\sin(\phi_3)}$$

Strut<sub>3</sub> = 482.297 kip

Strut WidthMinimum beam width

$w_3 := 15 \cdot \text{in}$

b<sub>3</sub> := 36in

Check across tie 2:

$$\epsilon_{t2} := \epsilon_{s2} + (\epsilon_{s2} + 0.002) \cdot \cot(90\text{deg} - \phi_3)^2$$

$$f_{cu3} := \begin{cases} \frac{f_c}{0.8 + 170 \cdot \epsilon_{t2}} & \text{if } \frac{f_c}{0.8 + 170 \cdot \epsilon_{t2}} \leq 0.85 \cdot f_c \\ 0.85 \cdot f_c & \text{otherwise} \end{cases} \quad f_{cu3} = 7.132 \text{ ksi}$$

*Effective available concrete stress*

$$\sigma_{s3} := \frac{\text{Strut}_3}{b_3 \cdot w_3}$$

σ<sub>s3</sub> = 0.9 ksi

 Stress in strut 3 at failure

$$\text{Check} := \begin{cases} \text{"OK"} & \text{if } \sigma_{s3} \leq f_{cu3} \\ \text{"NO GOOD"} & \text{otherwise} \end{cases}$$

Check = "OK"

Check across tie 4:

$$\epsilon_{t4} := \epsilon_{s4} + (\epsilon_{s4} + 0.002) \cdot \cot(\phi_3)^2$$

$$f_{cu3} := \begin{cases} \frac{f_c}{0.8 + 170 \cdot \epsilon_{t4}} & \text{if } \frac{f_c}{0.8 + 170 \cdot \epsilon_{t4}} \leq 0.85 \cdot f_c \\ 0.85 \cdot f_c & \text{otherwise} \end{cases} \quad f_{cu3} = 7.606 \text{ ksi}$$

*Effective available concrete stress*

$$\sigma_{s3} := \frac{\text{Strut}_3}{b_3 \cdot w_3}$$

σ<sub>s3</sub> = 0.9 ksi

 Stress in strut 3 at failure

$$\text{Check} := \begin{cases} \text{"OK"} & \text{if } \sigma_{s3} \leq f_{cu3} \\ \text{"NO GOOD"} & \text{otherwise} \end{cases}$$

Check = "OK"

**Tie 3:**

$$\text{Tie}_3 := \text{Strut}_3 \cdot \sin(\phi_3) - (\text{Strut}_3 \cdot \cos(\phi_3) - \text{Tie}_1) \cdot \tan(\phi_4) \quad \boxed{\text{Tie}_3 = 249.715 \text{ kip}}$$

$$\sigma_{t3} := \frac{\text{Tie}_3}{2 \cdot 6 \cdot A_{4b} + 4 \cdot A_{6b}} \quad \boxed{\sigma_{t3} = 60 \text{ ksi}} \quad \text{Stress in tie 3 at failure.}$$

$$\epsilon_{s3} := \frac{\sigma_{t3}}{E} \quad \boxed{\epsilon_{s3} = 2.07 \times 10^{-3}}$$

**Recheck Strut 3:**

Check across tie 1:

$$\epsilon_{t1} := \epsilon_{s1} + (\epsilon_{s1} + 0.002) \cdot \cot(\phi_3)^2$$

$$f_{cu3} := \begin{cases} \frac{f_c}{0.8 + 170 \cdot \epsilon_{t1}} & \text{if } \frac{f_c}{0.8 + 170 \cdot \epsilon_{t1}} \leq 0.85 \cdot f_c \\ 0.85 \cdot f_c & \text{otherwise} \end{cases} \quad f_{cu3} = 5.018 \text{ ksi}$$

*Effective available concrete stress*

$$\sigma_{s3} := \frac{\text{Strut}_3}{b_3 \cdot w_3} \quad \boxed{\sigma_{s3} = 0.9 \text{ ksi}} \quad \text{Stress in strut 3 at failure}$$

$$\text{Check} := \begin{cases} \text{"OK"} & \text{if } \sigma_{s3} \leq f_{cu3} \\ \text{"NO GOOD"} & \text{otherwise} \end{cases} \quad \text{Check} = \text{"OK"}$$

Check across tie 3:

$$\epsilon_{t3} := \epsilon_{s3} + (\epsilon_{s3} + 0.002) \cdot \cot(90\text{deg} - \phi_3)^2$$

$$f_{cu3} := \begin{cases} \frac{f_c}{0.8 + 170 \cdot \epsilon_{t3}} & \text{if } \frac{f_c}{0.8 + 170 \cdot \epsilon_{t3}} \leq 0.85 \cdot f_c \\ 0.85 \cdot f_c & \text{otherwise} \end{cases} \quad f_{cu3} = 6.216 \text{ ksi}$$

*Effective available concrete stress*

$$\sigma_{s3} := \frac{\text{Strut}_3}{b_3 \cdot w_3} \quad \boxed{\sigma_{s3} = 0.9 \text{ ksi}} \quad \text{Stress in strut 3 at failure}$$

$$\text{Check} := \begin{cases} \text{"OK"} & \text{if } \sigma_{s3} \leq f_{cu3} \\ \text{"NO GOOD"} & \text{otherwise} \end{cases} \quad \text{Check} = \text{"OK"}$$

**Strut 5:**

$$\text{Strut}_5 := \frac{\text{Strut}_3 \cdot \cos(\phi_3) - \text{Tie}_1}{\cos(\phi_4)}$$

$$\text{Strut}_5 = 69.393 \text{ kip}$$

Strut Width

$$w_5 := 8 \text{ in}$$

Minimum beam width

$$b_5 := 15 \text{ in}$$

$$\varepsilon_{t1} := \varepsilon_{s1} + (\varepsilon_{s1} + 0.002) \cdot \cot(\phi_4)^2$$

*Check across tie 1:*

$$f_{cu5} := \begin{cases} \frac{f_c}{0.8 + 170 \cdot \varepsilon_{t1}} & \text{if } \frac{f_c}{0.8 + 170 \cdot \varepsilon_{t1}} \leq 0.85 \cdot f_c \\ 0.85 \cdot f_c & \text{otherwise} \end{cases} \quad f_{cu5} = 6.897 \text{ ksi}$$

*Effective available  
concrete stress*

$$\sigma_{s5} := \frac{\text{Strut}_5}{b_5 \cdot w_5}$$

$$\sigma_{s5} = 0.6 \text{ ksi}$$

Stress in strut 5 at failure

$$\text{Check} := \begin{cases} \text{"OK"} & \text{if } \sigma_{s5} \leq f_{cu5} \\ \text{"NO GOOD"} & \text{otherwise} \end{cases}$$

Check = "OK"

*Check across tie 3:*

$$\varepsilon_{t3} := \varepsilon_{s3} + (\varepsilon_{s3} + 0.002) \cdot \cot(90\text{deg} - \phi_4)^2$$

$$f_{cu5} := \begin{cases} \frac{f_c}{0.8 + 170 \cdot \varepsilon_{t3}} & \text{if } \frac{f_c}{0.8 + 170 \cdot \varepsilon_{t3}} \leq 0.85 \cdot f_c \\ 0.85 \cdot f_c & \text{otherwise} \end{cases} \quad f_{cu5} = 4.422 \text{ ksi}$$

*Effective available  
concrete stress*

$$\sigma_{s5} := \frac{\text{Strut}_5}{b_5 \cdot w_5}$$

$$\sigma_{s5} = 0.6 \text{ ksi}$$

Stress in strut 5 at failure

$$\text{Check} := \begin{cases} \text{"OK"} & \text{if } \sigma_{s3} \leq f_{cu3} \\ \text{"NO GOOD"} & \text{otherwise} \end{cases}$$

Check = "OK"

**Strut 6:**

$$\text{Strut}_6 := \frac{\text{Tie}_3}{\sin(\phi_5)} \quad \boxed{\text{Strut}_6 = 275.53 \text{ kip}}$$

Strut Width

$$w_6 := 15 \cdot \text{in}$$

Minimum beam width

$$\boxed{b_6 := 10 \text{ in}}$$

Check across tie 3:  $\epsilon_{t3} := \epsilon_{s3} + (\epsilon_{s3} + 0.002) \cdot \cot(90\text{deg} - \phi_5)^2$

$$f_{cu6} := \begin{cases} \frac{f_c}{0.8 + 170 \cdot \epsilon_{t3}} & \text{if } \frac{f_c}{0.8 + 170 \cdot \epsilon_{t3}} \leq 0.85 \cdot f_c \\ 0.85 \cdot f_c & \text{otherwise} \end{cases} \quad f_{cu6} = 2.307 \text{ ksi}$$

*Effective available concrete stress*

$$\sigma_{s6} := \frac{\text{Strut}_6}{b_6 \cdot w_6} \quad \boxed{\sigma_{s6} = 1.8 \text{ ksi}} \quad \text{Stress in strut 6 at failure}$$

$$\text{Check} := \begin{cases} \text{"OK"} & \text{if } \sigma_{s6} \leq f_{cu6} \\ \text{"NO GOOD"} & \text{otherwise} \end{cases} \quad \text{Check} = \text{"OK"}$$

Check across tie 4:  $\epsilon_{t4} := \epsilon_{s4} + (\epsilon_{s4} + 0.002) \cdot \cot(\phi_5)^2$

$$f_{cu6} := \begin{cases} \frac{f_c}{0.8 + 170 \cdot \epsilon_{t4}} & \text{if } \frac{f_c}{0.8 + 170 \cdot \epsilon_{t4}} \leq 0.85 \cdot f_c \\ 0.85 \cdot f_c & \text{otherwise} \end{cases} \quad f_{cu6} = 8.5 \text{ ksi} \quad \text{Effective available concrete stress}$$

$$\sigma_{s6} := \frac{\text{Strut}_6}{b_6 \cdot w_6} \quad \boxed{\sigma_{s6} = 1.8 \text{ ksi}} \quad \text{Stress in strut 5 at failure}$$

$$\text{Check} := \begin{cases} \text{"OK"} & \text{if } \sigma_{s6} \leq f_{cu6} \\ \text{"NO GOOD"} & \text{otherwise} \end{cases} \quad \text{Check} = \text{"OK"}$$



**Tie 6:**

$$Tie_6 := Tie_4 + Strut_6 \cdot \cos(\phi_5)$$

$$Tie_6 = 490.729 \text{ kip}$$

*Without concentrated prestressed load applied*

$$F_{t7} := Tie_6 - 31 \cdot \text{kip} \cdot 38$$

$$F_{t7} = -687.3 \text{ kip}$$

*Force in tie 6 at failure, strands provide the original force on the section that needs to be overcome by the force in Tie 6 due to the applied load.*

$$\epsilon_{s6} := 0$$

**Since tie still in compression, stress in tie is still 0.0 according to AASHTO.**

**Nodal Check (AASHTO 5.6.3.5 pg. 5-34)**

**Check Singular Nodes:**

**Node 1:**

C-C-T node at bearing.

$$f_{ce} := 0.75 \cdot f_c$$

**Tie 1 Face:**

Node Width

Minimum beam width

$$w_{t1} := 4.125 \text{ in}$$

$$b_{t1} := 32 \text{ in}$$

Shear at node failure:

$$V_{t1\_n} := \frac{f_{ce} \cdot w_{t1} \cdot b_{t1}}{Tie_1}$$

$$V_{t1\_n} = 2.988$$

Since greater than 1, ok because available force is greater than applied force.

**Strut 1 Face:**

Node Width

Minimum beam width

$$w_{s1} := 9.5626 \text{ in}$$

$$b_{s1} := 32 \text{ in}$$

Shear at node failure:

$$V_{s1\_n} := \frac{f_{ce} \cdot w_{s1} \cdot b_{s1}}{Strut_1}$$

$$V_{s1\_n} = 4.453$$

Since greater than 1, ok because available force is greater than applied force.

**Bearing Face:**

Node Width

$$w_{b1} := 9\text{in}$$

Minimum beam width

$$b_{b1} := 32\text{in}$$

Shear at node failure:

$$V_{b1\_n} := \frac{f_{ce} \cdot w_{b1} \cdot b_{b1}}{V}$$

$$V_{b1\_n} = 5$$

Since greater than 1, ok because available force is greater than applied force.

**Node 3:**

C-T-T node at bearing.

$$f_{ce} := 0.65 \cdot f_c$$

**Tie 2 Face:**

Node Width

$$w_{t2} := 12.25\text{in}$$

Minimum beam width

$$b_{t2} := 36\text{in}$$

Shear at node failure:

$$V_{t2\_n} := \frac{f_{ce} \cdot w_{t2} \cdot b_{t2}}{Tie_2}$$

$$V_{t2\_n} = 9$$

Since greater than 1, ok because available force is greater than applied force.

**Strut 3 Face:**

Node Width

$$w_{s3} := 15.5\text{in}$$

Minimum beam width

$$b_{s3} := 36\text{in}$$

Shear at node failure:

$$V_{s3\_n} := \frac{f_{ce} \cdot w_{s3} \cdot b_{s3}}{\text{Strut}_3}$$

$$V_{s3\_n} = 8$$

Since greater than 1, ok because available force is greater than applied force.

**Tie 4 Face:**

Node Width

$$w_{t4} := 10\text{in}$$

Minimum beam width

$$b_{t4} := 36\text{in}$$

Shear at node failure:

$$V_{t4\_n} := \frac{f_{ce} \cdot w_{t4} \cdot b_{t4}}{Tie_4}$$

$$V_{t4\_n} = 6.252$$

Since greater than 1, ok because available force is greater than applied force.

**Note:** Node under load is singular, but since it is a C-C-C node, previous experience and research indicates it will not control.



**Bearing Check (AASHTO 5.7.5 pg. 5-57)**

$$A_1 := 32\text{in} \cdot 9\text{in} \quad A_1 = 288 \text{ in}^2 \quad \text{Bearing area}$$

$$A_2 := 48\text{in} \cdot 16\text{in} \quad A_2 = 0.495 \text{ m}^2 \quad \text{Available area}$$

$$m := \begin{cases} \sqrt{\frac{A_2}{A_1}} & \text{if } \sqrt{\frac{A_2}{A_1}} \leq 2.0 \\ 2.0 & \text{otherwise} \end{cases} \quad m = 1.633$$

$$P_n := 0.85f_c \cdot A_1 \cdot m \quad P_n = 3998 \text{ kip} \quad \text{Shear force achievable with provided bearing.}$$

## C.4 AASHTO CALCULATION: RF-3R-9(c)

### RF-3R-9(c) Original Strut-and-Tie Model

#### Parameters

$$f_c := 10\text{ksi} \quad f_y := 60\text{ksi} \quad E := 29000\text{ksi} \quad f_{se} := 148.5\text{ksi}$$

$$A_{ps} := 0.153\text{in}^2$$

$$A_{4b} := 0.20\text{in}^2 \quad A_{5b} := 0.31\text{in}^2 \quad A_{6b} := 0.44\text{in}^2 \quad A_{7b} := 0.60\text{in}^2$$

#### Angles

$$\phi_1 := 50\text{deg} \quad \phi_2 := 0\text{deg} \quad \phi_3 := 36.1\text{deg} \quad \phi_4 := 50\text{deg}$$

$$\phi_5 := 43.1\text{deg} \quad \phi_6 := 18.4\text{deg} \quad \phi_7 := 51.5\text{deg}$$

### Strut and Tie Check (AASHTO 5.6.3.3 & 5.6.3.4 pg. 5-30)

$V := 470.4\text{kip}$  From ACI Calculations, yield of tie 3.

#### **Tie 1:**

$$Tie_1 := \frac{V}{\tan(\phi_1)} \quad \boxed{Tie_1 = 394.712 \text{ kip}}$$

$$\sigma_{t1} := \frac{Tie_1}{12 \cdot A_{7b}} \quad \boxed{\sigma_{t1} = 54.8 \text{ ksi}} \quad \text{Stress in tie 1 at failure.}$$

$$\epsilon_{s1} := \frac{\sigma_{t1}}{E} \quad \boxed{\epsilon_{s1} = 1.89 \times 10^{-3}}$$

#### **Strut 1:**

$$Strut_1 := \frac{V}{\sin(\phi_1)} \quad \boxed{Strut_1 = 614.064 \text{ kip}}$$

#### Strut Width

$$w_1 := 9.5625\text{-in}$$

#### Minimum beam width

$$\boxed{b_1 := 48\text{in}}$$

$$\epsilon_{t1} := \epsilon_{s1} + (\epsilon_{s1} + 0.002) \cdot \cot(\phi_1)^2$$

$$f_{cu1} := \begin{cases} \frac{f_c}{0.8 + 170 \cdot \epsilon_{t1}} & \text{if } \frac{f_c}{0.8 + 170 \cdot \epsilon_{t1}} \leq 0.85 \cdot f_c \\ 0.85 \cdot f_c & \text{otherwise} \end{cases} \quad f_{cu1} = 6.301 \text{ ksi}$$

*Effective available  
concrete stress*

$$\sigma_{s1} := \frac{\text{Strut}_1}{b_1 \cdot w_1}$$

$$\sigma_{s1} = 1.3 \text{ ksi} \quad \text{Stress in strut 1 at failure}$$

$$\text{Check} := \begin{cases} \text{"OK"} & \text{if } \sigma_{s1} \leq f_{cu1} \\ \text{"NO GOOD"} & \text{otherwise} \end{cases}$$

$$\text{Check} = \text{"OK"}$$

**Tie 2:**

$$\text{Tie}_2 := V - V \cdot \frac{\tan(\phi_2)}{\tan(\phi_1)}$$

$$\text{Tie}_2 = 470.4 \text{ kip}$$

$$\sigma_{t2} := \frac{\text{Tie}_2}{2 \cdot 8 \cdot A_{6b} + 2 \cdot 2 \cdot A_{4b}}$$

$$\sigma_{t2} = 60 \text{ ksi} \quad \text{Stress in tie 2 at failure}$$

$$\epsilon_{s2} := \frac{\sigma_{t2}}{E}$$

$$\epsilon_{s2} = 2.069 \times 10^{-3}$$

**Recheck Strut 1:**

$$\epsilon_{t2} := \epsilon_{s2} + (\epsilon_{s2} + 0.002) \cdot \cot(90\text{deg} - \phi_1)^2$$

$$f_{cu1} := \begin{cases} \frac{f_c}{0.8 + 170 \cdot \epsilon_{t2}} & \text{if } \frac{f_c}{0.8 + 170 \cdot \epsilon_{t2}} \leq 0.85 \cdot f_c \\ 0.85 \cdot f_c & \text{otherwise} \end{cases} \quad f_{cu1} = 4.686 \text{ ksi}$$

*Effective available concrete stress*

$$\sigma_{s1} := \frac{\text{Strut}_1}{b_1 \cdot w_1}$$

$$\sigma_{s1} = 1.3 \text{ ksi} \quad \text{Stress in strut 1 at failure}$$

$$\text{Check} := \begin{cases} \text{"OK"} & \text{if } \sigma_{s1} \leq f_{cu1} \\ \text{"NO GOOD"} & \text{otherwise} \end{cases}$$

$$\text{Check} = \text{"OK"}$$

**Strut 2:**

$$\text{Strut}_2 := \frac{V}{\tan(\phi_1) \cos(\phi_2)}$$

$$\text{Strut}_2 = 394.712 \text{ kip}$$

Strut Width

$$w_2 := 8 \cdot \text{in}$$

Minimum beam width

$$b_2 := 54 \text{ in}$$

$$\epsilon_{t2} := \epsilon_{s2} + (\epsilon_{s2} + 0.002) \cdot \cot(90\text{deg} - \phi_2)^2$$

$$f_{cu2} := \begin{cases} \frac{f_c}{0.8 + 170 \cdot \epsilon_{t2}} & \text{if } \frac{f_c}{0.8 + 170 \cdot \epsilon_{t2}} \leq 0.85 \cdot f_c \\ 0.85 \cdot f_c & \text{otherwise} \end{cases} \quad f_{cu1} = 4.686 \text{ ksi}$$

*Effective available concrete stress*

$$\sigma_{s2} := \frac{\text{Strut}_2}{b_2 \cdot w_2} \quad \sigma_{s2} = 0.9 \text{ ksi} \quad \text{Stress in strut 2 at failure}$$

$$\text{Check} := \begin{cases} \text{"OK"} & \text{if } \sigma_{s2} \leq f_{cu2} \\ \text{"NO GOOD"} & \text{otherwise} \end{cases} \quad \text{Check} = \text{"OK"}$$

**Tie 4:**

$$\text{Tie}_4 := \frac{V - V \cdot \frac{\tan(\phi_2)}{\tan(\phi_1)}}{\tan(\phi_3)} \quad \text{Tie}_4 = 645.079 \text{ kip}$$

*Without concentrated prestressed load applied*

$$\sigma_{t4} := \frac{\text{Tie}_4 - f_{se} \cdot A_{ps} \cdot 38 \cdot \frac{6.125 \text{ in}}{30 \text{ in}}}{6 \cdot A_{6b}} \quad \sigma_{t4} = 177.6 \text{ ksi}$$

*Stress in reinforcing steel near prestressing steel at failure, no good, however larger development can be used*

$$\sigma_{t4\_2} := \frac{\text{Tie}_4 - f_{se} \cdot A_{ps} \cdot 38 \cdot \frac{19 \text{ in}}{30 \text{ in}}}{6 \cdot A_{6b}} \quad \sigma_{t4\_2} = 37.2 \text{ ksi}$$

*Stress in reinforcing steel near prestressing steel at failure assuming*

$$\epsilon_{s4} := 0 \quad \text{Use extended nodal region for additional capacity. prestressing force taken at extended nodal region.}$$

**Since tie still in compression, stress in tie is still 0.0 according to AASHTO.**

**Strut 3:**

$$\text{Strut}_3 := \frac{V - V \cdot \frac{\tan(\phi_2)}{\tan(\phi_1)}}{\sin(\phi_3)} \quad \text{Strut}_3 = 798.376 \text{ kip}$$

Strut Width

Minimum beam width

$$w_3 := 15 \cdot \text{in}$$

$$b_3 := 36 \text{ in}$$

Check across tie 2:

$$\epsilon_{t2} := \epsilon_{s2} + (\epsilon_{s2} + 0.002) \cdot \cot(90 \text{ deg} - \phi_3)^2$$

$$f_{cu3} := \begin{cases} \frac{f_c}{0.8 + 170 \cdot \epsilon_{t2}} & \text{if } \frac{f_c}{0.8 + 170 \cdot \epsilon_{t2}} \leq 0.85 \cdot f_c \\ 0.85 \cdot f_c & \text{otherwise} \end{cases} \quad f_{cu3} = 6.581 \text{ ksi}$$

*Effective available concrete stress*

$$\sigma_{s3} := \frac{\text{Strut}_3}{b_3 \cdot w_3} \quad \sigma_{s3} = 1.5 \text{ ksi} \quad \text{Stress in strut 3 at failure}$$

$$\text{Check} := \begin{cases} \text{"OK"} & \text{if } \sigma_{s3} \leq f_{cu3} \\ \text{"NO GOOD"} & \text{otherwise} \end{cases} \quad \text{Check} = \text{"OK"}$$

*Check across tie 4:*

$$\epsilon_{t4} := \epsilon_{s4} + (\epsilon_{s4} + 0.002) \cdot \cot(\phi_3)^2$$

$$f_{cu3} := \begin{cases} \frac{f_c}{0.8 + 170 \cdot \epsilon_{t4}} & \text{if } \frac{f_c}{0.8 + 170 \cdot \epsilon_{t4}} \leq 0.85 \cdot f_c \\ 0.85 \cdot f_c & \text{otherwise} \end{cases} \quad f_{cu3} = 6.947 \text{ ksi}$$

*Effective available concrete stress*

$$\sigma_{s3} := \frac{\text{Strut}_3}{b_3 \cdot w_3} \quad \sigma_{s3} = 1.5 \text{ ksi} \quad \text{Stress in strut 3 at failure}$$

$$\text{Check} := \begin{cases} \text{"OK"} & \text{if } \sigma_{s3} \leq f_{cu3} \\ \text{"NO GOOD"} & \text{otherwise} \end{cases} \quad \text{Check} = \text{"OK"}$$

**Tie 3:**

$$\text{Tie}_3 := \text{Strut}_3 \cdot \sin(\phi_3) - (\text{Strut}_3 \cdot \cos(\phi_3) - \text{Tie}_1) \cdot \tan(\phi_4) \quad \text{Tie}_3 = 172.024 \text{ kip}$$

$$\sigma_{t3} := \frac{\text{Tie}_3}{2 \cdot 6 \cdot A_{4b} + 4 \cdot A_{6b}} \quad \sigma_{t3} = 41.4 \text{ ksi} \quad \text{Stress in tie 3 at failure.}$$

$$\epsilon_{s3} := \frac{\sigma_{t3}}{E} \quad \epsilon_{s3} = 1.426 \times 10^{-3}$$

**Recheck Strut 3:**

*Check across tie 1:*

$$\epsilon_{t1} := \epsilon_{s1} + (\epsilon_{s1} + 0.002) \cdot \cot(\phi_3)^2$$

$$f_{cu3} := \begin{cases} \frac{f_c}{0.8 + 170 \cdot \epsilon_{t1}} & \text{if } \frac{f_c}{0.8 + 170 \cdot \epsilon_{t1}} \leq 0.85 \cdot f_c \\ 0.85 \cdot f_c & \text{otherwise} \end{cases} \quad f_{cu3} = 4.228 \text{ ksi}$$

*Effective available concrete stress*

$$\sigma_{s3} := \frac{\text{Strut}_3}{b_3 \cdot w_3} \quad \sigma_{s3} = 1.5 \text{ ksi} \quad \text{Stress in strut 3 at failure}$$

$$\text{Check} := \begin{cases} \text{"OK"} & \text{if } \sigma_{s3} \leq f_{cu3} \\ \text{"NO GOOD"} & \text{otherwise} \end{cases} \quad \text{Check} = \text{"OK"}$$

*Check across tie 3:*

$$\epsilon_{t3} := \epsilon_{s3} + (\epsilon_{s3} + 0.002) \cdot \cot(90\text{deg} - \phi_3)^2$$

$$f_{cu3} := \begin{cases} \frac{f_c}{0.8 + 170 \cdot \epsilon_{t3}} & \text{if } \frac{f_c}{0.8 + 170 \cdot \epsilon_{t3}} \leq 0.85 \cdot f_c \\ 0.85 \cdot f_c & \text{otherwise} \end{cases} \quad f_{cu3} = 7.396 \text{ ksi}$$

*Effective available concrete stress*

$$\sigma_{s3} := \frac{\text{Strut}_3}{b_3 \cdot w_3} \quad \sigma_{s3} = 1.5 \text{ ksi} \quad \text{Stress in strut 3 at failure}$$

$$\text{Check} := \begin{cases} \text{"OK"} & \text{if } \sigma_{s3} \leq f_{cu3} \\ \text{"NO GOOD"} & \text{otherwise} \end{cases} \quad \text{Check} = \text{"OK"}$$

**Strut 5:**

$$\text{Strut}_5 := \frac{\text{Strut}_3 \cdot \cos(\phi_3) - \text{Tie}_1}{\cos(\phi_4)} \quad \text{Strut}_5 = 389.502 \text{ kip}$$

Strut Width

Minimum beam width

$$w_5 := 8 \cdot \text{in}$$

$$b_5 := 15 \text{ in}$$

$$\epsilon_{t1} := \epsilon_{s1} + (\epsilon_{s1} + 0.002) \cdot \cot(\phi_4)^2$$

*Check across tie 1:*

$$f_{cu5} := \begin{cases} \frac{f_c}{0.8 + 170 \cdot \epsilon_{t1}} & \text{if } \frac{f_c}{0.8 + 170 \cdot \epsilon_{t1}} \leq 0.85 \cdot f_c \\ 0.85 \cdot f_c & \text{otherwise} \end{cases} \quad f_{cu5} = 6.301 \text{ ksi}$$

*Effective available concrete stress*



$$\sigma_{s5} := \frac{\text{Strut}_5}{b_5 \cdot w_5} \quad \sigma_{s5} = 3.2 \text{ ksi} \quad \text{Stress in strut 5 at failure}$$

$$\text{Check} := \begin{cases} \text{"OK"} & \text{if } \sigma_{s5} \leq f_{cu5} \\ \text{"NO GOOD"} & \text{otherwise} \end{cases} \quad \text{Check} = \text{"OK"}$$

Check across tie 3:

$$\epsilon_{t3} := \epsilon_{s3} + (\epsilon_{s3} + 0.002) \cdot \cot(90\text{deg} - \phi_4)^2$$

$$f_{cu5} := \begin{cases} \frac{f_c}{0.8 + 170 \cdot \epsilon_{t3}} & \text{if } \frac{f_c}{0.8 + 170 \cdot \epsilon_{t3}} \leq 0.85 \cdot f_c \\ 0.85 \cdot f_c & \text{otherwise} \end{cases} \quad f_{cu5} = 5.349 \text{ ksi}$$

*Effective available concrete stress*

$$\sigma_{s5} := \frac{\text{Strut}_5}{b_5 \cdot w_5} \quad \sigma_{s5} = 3.2 \text{ ksi} \quad \text{Stress in strut 5 at failure}$$

$$\text{Check} := \begin{cases} \text{"OK"} & \text{if } \sigma_{s3} \leq f_{cu3} \\ \text{"NO GOOD"} & \text{otherwise} \end{cases} \quad \text{Check} = \text{"OK"}$$

**Strut 6:**

$$\text{Strut}_6 := \frac{\text{Tie}_3}{\sin(\phi_5)} \quad \text{Strut}_6 = 251.765 \text{ kip}$$

Strut Width

Minimum beam width

$$w_6 := 15 \text{ in}$$

$$b_6 := 10 \text{ in}$$

Check across tie 3:

$$\epsilon_{t3} := \epsilon_{s3} + (\epsilon_{s3} + 0.002) \cdot \cot(90\text{deg} - \phi_5)^2$$

$$f_{cu6} := \begin{cases} \frac{f_c}{0.8 + 170 \cdot \epsilon_{t3}} & \text{if } \frac{f_c}{0.8 + 170 \cdot \epsilon_{t3}} \leq 0.85 \cdot f_c \\ 0.85 \cdot f_c & \text{otherwise} \end{cases} \quad f_{cu6} = 6.442 \text{ ksi}$$

*Effective available concrete stress*

$$\sigma_{s6} := \frac{\text{Strut}_6}{b_6 \cdot w_6} \quad \sigma_{s6} = 1.7 \text{ ksi} \quad \text{Stress in strut 6 at failure}$$

$$\text{Check} := \begin{cases} \text{"OK"} & \text{if } \sigma_{s6} \leq f_{cu6} \\ \text{"NO GOOD"} & \text{otherwise} \end{cases} \quad \text{Check} = \text{"OK"}$$

Check across tie 4:

$$\epsilon_{t4} := \epsilon_{s4} + (\epsilon_{s4} + 0.002) \cdot \cot(\phi_5)^2$$

$$f_{cu6} := \begin{cases} \frac{f_c}{0.8 + 170 \cdot \epsilon_{t4}} & \text{if } \frac{f_c}{0.8 + 170 \cdot \epsilon_{t4}} \leq 0.85 \cdot f_c \\ 0.85 \cdot f_c & \text{otherwise} \end{cases} \quad f_{cu6} = 8.416 \text{ ksi}$$

*Effective available concrete stress*

$$\sigma_{s6} := \frac{\text{Strut}_6}{b_6 \cdot w_6}$$

$$\sigma_{s6} = 1.7 \text{ ksi} \quad \text{Stress in strut 5 at failure}$$

$$\text{Check} := \begin{cases} \text{"OK"} & \text{if } \sigma_{s6} \leq f_{cu6} \\ \text{"NO GOOD"} & \text{otherwise} \end{cases}$$

$$\text{Check} = \text{"OK"}$$

**Tie 6:**

$$\text{Tie}_6 := \text{Tie}_4 + \text{Strut}_6 \cdot \cos(\phi_5)$$

$$\text{Tie}_6 = 828.909 \text{ kip} \quad \text{Without concentrated prestressed load applied}$$

$$F_{t6} := \text{Tie}_6 - 31 \cdot \text{kip} \cdot 38$$

$$F_{t6} = -349.1 \text{ kip}$$

$$\epsilon_{s6} := 0$$

Force in tie 6 at failure, strands provide the original force on the section that needs to be overcome by the force in Tie 6 due to the applied load.

**Since tie still in compression, stress in tie is still 0.0 according to AASHTO.**

**Tie 5:**

$$\text{Tie}_5 := \text{Strut}_5 \cdot \sin(\phi_4) - (\text{Strut}_2 + \text{Strut}_5 \cdot \cos(\phi_4)) \cdot \tan(\phi_6) \quad \text{Tie}_5 = 83.786 \text{ kip}$$

$$\sigma_{t5} := \frac{\text{Tie}_5}{2 \cdot 4 \cdot A_{4b}}$$

$$\sigma_{t5} = 52.4 \text{ ksi} \quad \text{Stress in tie 5 at failure}$$

$$\epsilon_{s5} := \frac{\sigma_{t5}}{E}$$

$$\epsilon_{s5} = 1.806 \times 10^{-3}$$

**Recheck Strut 5:**

Check across tie 5:

$$\epsilon_{t5} := \epsilon_{s5} + (\epsilon_{s5} + 0.002) \cdot \cot(90\text{deg} - \phi_4)^2$$



$$f_{cu5} := \begin{cases} \frac{f_c}{0.8 + 170 \cdot \epsilon_{t5}} & \text{if } \frac{f_c}{0.8 + 170 \cdot \epsilon_{t5}} \leq 0.85 \cdot f_c \\ 0.85 \cdot f_c & \text{otherwise} \end{cases} \quad f_{cu5} = 4.936 \text{ ksi}$$

*Effective available concrete stress*

$$\sigma_{s5} := \frac{\text{Strut}_5}{b_5 \cdot w_5} \quad \sigma_{s5} = 3.2 \text{ ksi} \quad \text{Stress in strut 5 at failure}$$

$$\text{Check} := \begin{cases} \text{"OK"} & \text{if } \sigma_{s5} \leq f_{cu5} \\ \text{"NO GOOD"} & \text{otherwise} \end{cases} \quad \text{Check} = \text{"OK"}$$

### Recheck Strut 6:

Check across tie 6:

$$\epsilon_{t5} := \epsilon_{s5} + (\epsilon_{s5} + 0.002) \cdot \cot(\phi_5)^2$$

$$f_{cu6} := \begin{cases} \frac{f_c}{0.8 + 170 \cdot \epsilon_{t5}} & \text{if } \frac{f_c}{0.8 + 170 \cdot \epsilon_{t5}} \leq 0.85 \cdot f_c \\ 0.85 \cdot f_c & \text{otherwise} \end{cases} \quad f_{cu6} = 5.418 \text{ ksi}$$

*Effective available concrete stress*

$$\sigma_{s6} := \frac{\text{Strut}_6}{b_6 \cdot w_6} \quad \sigma_{s6} = 1.7 \text{ ksi} \quad \text{Stress in strut 6 at failure}$$

$$\text{Check} := \begin{cases} \text{"OK"} & \text{if } \sigma_{s6} \leq f_{cu6} \\ \text{"NO GOOD"} & \text{otherwise} \end{cases} \quad \text{Check} = \text{"OK"}$$

### Strut 8:

$$\text{Strut}_8 := \frac{\text{Strut}_2 + \text{Strut}_5 \cdot \cos(\phi_4)}{\cos(\phi_6)} \quad \text{Strut}_8 = 679.835 \text{ kip}$$

Strut Width

$$w_8 := 10 \text{ in}$$

Minimum beam width

$$b_8 := 15 \text{ in}$$

Check across tie 5:

$$\epsilon_{t5} := \epsilon_{s5} + (\epsilon_{s5} + 0.002) \cdot \cot(90 - \phi_6)^2$$

$$f_{cu8} := \begin{cases} \frac{f_c}{0.8 + 170 \cdot \epsilon_{t5}} & \text{if } \frac{f_c}{0.8 + 170 \cdot \epsilon_{t5}} \leq 0.85 \cdot f_c \\ 0.85 \cdot f_c & \text{otherwise} \end{cases} \quad f_{cu8} = 8.5 \text{ ksi}$$

*Effective available concrete stress*

$$\sigma_{s8} := \frac{\text{Strut}_8}{b_8 \cdot w_8}$$

$\sigma_{s8} = 4.5 \text{ ksi}$  Stress in strut 5 at failure

$$\text{Check} := \begin{cases} \text{"OK"} & \text{if } \sigma_{s8} \leq f_{cu8} \\ \text{"NO GOOD"} & \text{otherwise} \end{cases}$$

Check = "OK"

### Strut 9:

$$\text{Strut}_9 := \frac{\text{Tie}_5}{\sin(\phi_7)}$$

$\text{Strut}_9 = 107.06 \text{ kip}$

Strut Width

Minimum beam width

$$w_9 := 8 \cdot \text{in}$$

$$b_9 := 10 \text{ in}$$

Check across tie 5:

$$\epsilon_{t5} := \epsilon_{s5} + (\epsilon_{s5} + 0.002) \cdot \cot(\phi_7)^2$$

$$f_{cu9} := \begin{cases} \frac{f_c}{0.8 + 170 \cdot \epsilon_{t5}} & \text{if } \frac{f_c}{0.8 + 170 \cdot \epsilon_{t5}} \leq 0.85 \cdot f_c \\ 0.85 \cdot f_c & \text{otherwise} \end{cases} \quad f_{cu9} = 6.595 \text{ ksi}$$

*Effective available concrete stress*

$$\sigma_{s9} := \frac{\text{Strut}_9}{b_9 \cdot w_9}$$

$\sigma_{s9} = 1.3 \text{ ksi}$  Stress in strut 9 at failure

$$\text{Check} := \begin{cases} \text{"OK"} & \text{if } \sigma_{s9} \leq f_{cu9} \\ \text{"NO GOOD"} & \text{otherwise} \end{cases}$$

Check = "OK"

### Tie 7:

$$\text{Tie}_7 := \text{Tie}_6 + \text{Strut}_9 \cdot \cos(\phi_7)$$

$\text{Tie}_7 = 895.555 \text{ kip}$

$$F_{t7} := \text{Tie}_7 - 31 \cdot \text{kip} \cdot 38$$

$F_{t7} = -282.4 \text{ kip}$

$$\epsilon_{s7} := 0$$

*Force in Tie 7 for given shear, strands provide the original force on the section that needs to be overcome by the force on Tie 7 due to the applied load. Strands are able to provide greater strength as they are able to pick up tension beyond the prestress in this region.*

**Since tie still in compression, stress in tie is still 0.0 according to AASHTO.**

## Nodal Check (AASHTO 5.6.3.5 pg. 5-34)

### **Check Singular Nodes:**

#### **Node 1:**

C-C-T node at bearing.

$$f_{ce} := 0.75 \cdot f_c$$

#### **Tie 1 Face:**

Node Width

$$w_{t1} := 4.125 \text{in}$$

Minimum beam width

$$b_{t1} := 32 \text{in}$$

Shear at node failure:

$$V_{t1\_n} := \frac{f_{ce} \cdot w_{t1} \cdot b_{t1}}{Tie_1}$$

$$V_{t1\_n} = 2.508$$

Since greater than 1, ok because available force is greater than applied force.

#### **Strut 1 Face:**

Node Width

$$w_{s1} := 9.5626 \text{in}$$

Minimum beam width

$$b_{s1} := 32 \text{in}$$

Shear at node failure:

$$V_{s1\_n} := \frac{f_{ce} \cdot w_{s1} \cdot b_{s1}}{\text{Strut}_1}$$

$$V_{s1\_n} = 3.737$$

Since greater than 1, ok because available force is greater than applied force.

#### **Bearing Face:**

Node Width

$$w_{b1} := 9 \text{in}$$

Minimum beam width

$$b_{b1} := 32 \text{in}$$

Shear at node failure:

$$V_{b1\_n} := \frac{f_{ce} \cdot w_{b1} \cdot b_{b1}}{V}$$

$$V_{b1\_n} = 5$$

Since greater than 1, ok because available force is greater than applied force.

#### **Node 3:**

C-T-T node at bearing.

$$f_{ce} := 0.65 \cdot f_c$$

**Tie 2 Face:**

Node Width

$$w_{t2} := 12.25\text{in}$$

Minimum beam width

$$b_{t2} := 36\text{in}$$

Shear at node failure:

$$V_{t2\_n} := \frac{f_{ce} \cdot w_{t2} \cdot b_{t2}}{Tie_2}$$

$$V_{t2\_n} = 6$$

Since greater than 1, ok because available force is greater than applied force.

**Strut 3 Face:**

Node Width

$$w_{s3} := 15.5\text{in}$$

Minimum beam width

$$b_{s3} := 36\text{in}$$

Shear at node failure:

$$V_{s3\_n} := \frac{f_{ce} \cdot w_{s3} \cdot b_{s3}}{\text{Strut}_3}$$

$$V_{s3\_n} = 5$$

Since greater than 1, ok because available force is greater than applied force.

**Tie 4 Face:**

Node Width

$$w_{t4} := 10\text{in}$$

Minimum beam width

$$b_{t4} := 36\text{in}$$

Shear at node failure:

$$V_{t4\_n} := \frac{f_{ce} \cdot w_{t4} \cdot b_{t4}}{Tie_4}$$

$$V_{t4\_n} = 3.627$$

Since greater than 1, ok because available force is greater than applied force.

**Note:** Node under load is singular, but since it is a C-C-C node, previous experience and research indicates it will not control.

**Bearing Check (AASHTO 5.7.5 pg. 5-57)**

$$A_1 := 32\text{in} \cdot 9\text{in}$$

$$A_1 = 288\text{in}^2$$

*Bearing area*

$$A_2 := 48\text{in} \cdot 16\text{in}$$

$$A_2 = 768\text{in}^2$$

*Available area*

$$m := \begin{cases} \sqrt{\frac{A_2}{A_1}} & \text{if } \sqrt{\frac{A_2}{A_1}} \leq 2.0 \\ 2.0 & \text{otherwise} \end{cases} \quad m = 1.633$$

$$P_n := 0.85f_c \cdot A_1 \cdot m$$

$$P_n = 3998\text{ kip}$$

Shear force achievable with provided bearing.

## C.5 PCI CALCULATION

### PCI Design Provisions

#### Flexure and Axial Tension in Extended End

$$f_y := 60\text{ksi} \quad a := \frac{16\text{in}}{2} + 6.125\text{in} \quad a = 14.125\text{-in} \quad d := 34\text{in} - 2.0625\text{in} \quad d = 31.937\text{-in}$$

$$A_s := 12 \cdot 0.60\text{in}^2 \quad A_s = 7.2 \cdot \text{in}^2 \quad (\text{Typical } 701 \text{ bars}) \quad \text{Conservative to assume small axial load (20\% of } V_u)$$

$$V_f := \frac{A_s \cdot f_y}{\frac{a}{d} + 0.2 \frac{h}{d}}$$

$$V_f = 659.4 \cdot \text{kip}$$

#### Direct Shear

$$b := 4\text{ft} \quad (\text{Conservative estimate}) \quad \mu := 1.4 \frac{\text{lbf}}{\text{in}^2} \quad \lambda := 1.0$$

Guess

$$V_{ds} := 1000\text{kip}$$

Given

$$A_s = \frac{2 \cdot V_{ds}}{3f_y \cdot \frac{1000 \cdot \lambda \cdot b \cdot h \cdot \mu}{V_{ds}}} + \frac{0.2V_{ds}}{f_y} \quad \text{Conservative to assume small axial load (20\% of } V_u)$$

$$V_{ds} := \text{Find}(V_{ds}) \quad V_{ds} = 921.4 \cdot \text{kip}$$

$$\mu_e := \frac{1000 \cdot \lambda \cdot b \cdot h \cdot \mu}{V_{ds}} \quad \mu_e = 2.48$$

#### Diagonal Tension at Re-entrant Corner

$$A_{\text{hanger}} := 2 \cdot 8 \cdot 0.44\text{in}^2 \quad (\text{Typical } 602 \text{ bars}) \quad A_{hs} := 2 \cdot 2 \cdot 0.20\text{in}^2 \quad (\text{Typical } 401/402 \text{ bars})$$

$$A_{sh} := A_{\text{hanger}} + A_{hs}$$

$$V_r := A_{sh} \cdot f_y \quad V_r = 470.4 \cdot \text{kip}$$

#### Diagonal Tension in Extended End

$$A_v := 4 \cdot 4 \cdot 0.31\text{in}^2 \quad (\text{Typical } 503 \text{ \& } 504 \text{ bars}) \quad A_h := 2 \cdot 6 \cdot 0.31\text{in}^2 \quad (\text{Typical } 505 \text{ bars})$$

$$V_{dt} := A_v \cdot f_y + A_h \cdot f_y + 2 \cdot b \cdot d \cdot \lambda \cdot \sqrt{f'_c \cdot \text{psi}}$$

$$V_{dt} = 827.4 \cdot \text{kip}$$

**Check Anchorages**

$H := 58\text{in}$                        $d = 31.937\text{in}$                        $D := 52.316\text{in}$                        $l_{dh\_7} := 7\text{in}$  (*Design Aid 11.2.9*)

$\text{Extension\_Past\_Dap} := H - d + l_{dh\_7}$                        $\text{Extension\_Past\_Dap} = 33.063\text{in}$                       **OK**

$l_{d\_6} := 25\text{in}$                       (*Design Aid 11.2.9*)                      **Note: #6 bars between prestressing strands**

$\text{Bar\_Length} := H - D + l_{d\_6}$                        $\text{Bar\_Length} = 30.684\text{in}$                       **OK**



## C.6 ADJUSTED ACI CALCULATION: RF-3R-9(a)

### RF-3R-9(a) Adjusted Strut-and-Tie Model

#### Parameters

$$f_c := 10\text{ksi} \quad f_y := 60\text{ksi} \quad f_{se} := 148.5\text{ksi} \quad A_{ps} := 0.153\text{in}^2$$

$$A_{4b} := 0.20\text{in}^2 \quad A_{5b} := 0.31\text{in}^2 \quad A_{6b} := 0.44\text{in}^2 \quad A_{7b} := 0.60\text{in}^2$$

#### Angles

$$\phi_1 := 55\text{deg} \quad \phi_2 := 11.6\text{deg} \quad \phi_3 := 39.1\text{deg} \quad \phi_4 := 51.7\text{deg} \quad \phi_5 := 65.0\text{deg}$$

### Strut and Tie Check (ACI Appendix A-3 & A-4 pg. 388)

Check if struts reinforced:

$$b_s := 8\text{in} \quad (\text{smallest expected strut width}) \quad s := 5\text{in} \quad (\text{spacing of stirrups})$$

$$\alpha_1 := 65\text{deg} \quad \alpha_2 := 25\text{deg} \quad \text{Maximum and minimum strut angles.}$$

$$0.003 \cdot b_s \cdot s \cdot \sin(\alpha_1) = 0.109\text{in}^2 \quad 0.003 \cdot b_s \cdot s \cdot \sin(\alpha_2) = 0.051\text{in}^2 \quad A_{prov} := 2 \cdot A_{4b}$$

$$A_{prov} = 0.4\text{in}^2$$

$$\beta_s := 0.75 \quad \text{All struts have enough reinforcement with the vertical stirrups to be classified as reinforced struts.}$$

$$V := 1\text{kip}$$

#### **Strut 1:**

$$\text{Strut}_1 := \frac{V}{\sin(\phi_1)} \quad \boxed{\text{Strut}_1 = 1.221\text{kip}}$$

Strut Width                      Minimum beam width                      Strut Efficiency Factor

$$w_1 := 9.5625\text{in} \quad \boxed{b_1 := 48\text{in}} \quad \beta_s := 0.75$$

$$V_{s1} := \frac{0.85 \cdot \beta_s \cdot f_c \cdot b_1 \cdot w_1}{\frac{\text{Strut}_1}{\text{kip}}} \quad \boxed{V_{s1} = 2396.9\text{kip}} \quad \text{Shear capacity based on strut 1}$$

#### **Tie 1:**

$$\text{Tie}_1 := \frac{V}{\tan(\phi_1)} \quad \boxed{\text{Tie}_1 = 0.7\text{kip}}$$

$$V_{t1} := \frac{12 \cdot A_{7b} \cdot f_y}{\frac{\text{Tie}_1}{\text{kip}}} \quad \boxed{V_{t1} = 617\text{kip}} \quad \text{Shear capacity based on tie 1}$$

**Strut 2:**

$$\text{Strut}_2 := \frac{V}{\tan(\phi_1) \cos(\phi_2)} \quad \boxed{\text{Strut}_2 = 0.715 \text{ kip}}$$

Strut Width                      Minimum beam width                      Strut Efficiency Factor

$$w_2 := 8 \cdot \text{in} \quad \boxed{b_2 := 54 \text{ in}} \quad \beta_s := 0.75$$

$$V_{s2} := \frac{0.85 \cdot \beta_s \cdot f_c \cdot b_2 \cdot w_2}{\frac{\text{Strut}_2}{\text{kip}}} \quad \boxed{V_{s2} = 3852.8 \text{ kip}} \quad \text{Shear capacity based on strut 2}$$

**Tie 2:**

$$\text{Tie}_2 := V - V \cdot \frac{\tan(\phi_2)}{\tan(\phi_1)} \quad \boxed{\text{Tie}_2 = 0.856 \text{ kip}}$$

$$V_{t2} := \frac{(2 \cdot 8 \cdot A_{6b} + 2 \cdot 2 \cdot A_{4b}) \cdot f_y}{\frac{\text{Tie}_2}{\text{kip}}} \quad \boxed{V_{t2} = 549.4 \text{ kip}} \quad \text{Shear capacity based on tie 2}$$

**Strut 3:**

$$\text{Strut}_3 := \frac{V - V \cdot \frac{\tan(\phi_2)}{\tan(\phi_1)}}{\sin(\phi_3)} \quad \boxed{\text{Strut}_3 = 1.358 \text{ kip}}$$

Strut Width                      Minimum beam width                      Strut Efficiency Factor

$$w_3 := 15 \cdot \text{in} \quad \boxed{b_3 := 36 \text{ in}} \quad \beta_s := 0.75$$

$$V_{s3} := \frac{0.85 \cdot \beta_s \cdot f_c \cdot b_3 \cdot w_3}{\frac{\text{Strut}_3}{\text{kip}}} \quad \boxed{V_{s3} = 2535.5 \text{ kip}} \quad \text{Shear capacity based on strut 3}$$

**Strut/Tie 4:**

$$S_{T4} := \text{Strut}_3 \cdot \cos(\phi_3) \quad \boxed{S_{T4} = 1.054 \text{ kip}} \quad \text{Without concentrated prestressed load applied}$$

$$V_{s_{t4}} := \frac{6 \cdot A_{6b} \cdot f_y + f_{se} \cdot A_{ps} \cdot 38 \cdot \frac{6.125 \text{ in}}{30 \text{ in}}}{\frac{S_{T4}}{\text{kip}}} \quad \boxed{V_{s_{t4}} = 317.6 \text{ kip}} \quad \text{Shear capacity based on strut that turns into tie #4}$$

$$V_{s_{t4\_1}} := \frac{6 \cdot A_{6b} \cdot f_y + f_{se} \cdot A_{ps} \cdot 38 \cdot \frac{18.375 \text{ in}}{30 \text{ in}}}{\frac{S_{T4}}{\text{kip}}} \quad \boxed{V_{s_{t4\_1}} = 652.2 \text{ kip}} \quad \text{Shear capacity based on strut that turns into tie #4 at the edge of the extended nodal region.}$$



**Strut 5:**

$$\text{Strut}_5 := \frac{\text{Strut}_3 \cdot \cos(\phi_3) - \text{Tie}_1}{\cos(\phi_4)} \quad \boxed{\text{Strut}_5 = 0.57 \text{ kip}}$$

Strut Width                      Minimum beam width                      Strut Efficiency Factor

$$w_5 := 8 \cdot \text{in} \quad \boxed{b_5 := 15 \text{ in}} \quad \beta_s := 0.75$$

$$V_{s5} := \frac{0.85 \cdot \beta_s \cdot f_c \cdot b_5 \cdot w_5}{\text{Strut}_5} \quad \boxed{V_{s5} = 1341.5 \text{ kip}} \quad \text{Shear capacity based on strut 5}$$

kip

**Tie 3:**

$$\text{Tie}_3 := \text{Strut}_3 \cdot \sin(\phi_3) - \text{Strut}_5 \cdot \sin(\phi_4) \quad \boxed{\text{Tie}_3 = 0.409 \text{ kip}}$$

$$V_{t3} := \frac{(2 \cdot 6 \cdot A_{4b} + 4 \cdot A_{6b}) \cdot f_y}{\text{Tie}_3} \quad \boxed{V_{t3} = 610.6 \text{ kip}} \quad \text{Shear capacity based on tie 3}$$

kip

**Strut 6:**

$$\text{Strut}_6 := \frac{\text{Tie}_3}{\sin(\phi_5)} \quad \boxed{\text{Strut}_6 = 0.451 \text{ kip}}$$

Strut Width                      Minimum beam width                      Strut Efficiency Factor

$$w_6 := 15 \cdot \text{in} \quad \boxed{b_6 := 10 \text{ in}} \quad \beta_s := 0.75$$

$$V_{s6} := \frac{0.85 \cdot \beta_s \cdot f_c \cdot b_6 \cdot w_6}{\text{Strut}_6} \quad \boxed{V_{s6} = 2120.3 \text{ kip}} \quad \text{Shear capacity based on strut 6}$$

kip

**Strut 7:**

$$\text{Strut}_7 := S_{T4} + \text{Strut}_6 \cdot \cos(\phi_5) \quad \boxed{\text{Strut}_7 = 1.244 \text{ kip}} \quad \text{Without concentrated prestressed load applied}$$

Strut Width                      Minimum beam width                      Strut Efficiency Factor

$$w_7 := 10 \cdot \text{in} \quad \boxed{b_7 := 36 \text{ in}} \quad \beta_s := 0.75$$

$$V_{s7} := \frac{31 \cdot \text{kip} \cdot 38}{\text{Strut}_7} \quad \boxed{V_{s7} = 946.8 \text{ kip}} \quad \text{Shear capacity based on Strut 7, strands provide the original force on the section that needs to be overcome by the force on Strut 7 due to the applied load.}$$

kip

## Nodal Check (ACI Appendix A.5 pg. 392)

### **Check Singular Nodes:**

#### **Node 1:**

C-C-T node at bearing.

$$\beta_n := 0.80 \qquad f_{ce} := 0.85 \cdot \beta_n \cdot f_c$$

#### **Tie 1 Face:**

Node Width                      Minimum beam width

$$w_{t1} := 4.125\text{in} \qquad b_{t1} := 32\text{in}$$

Shear at node failure:

$$V_{t1\_n} := \frac{f_{ce} \cdot w_{t1} \cdot b_{t1}}{\text{Tie}_1} \qquad \boxed{V_{t1\_n} = 1282 \text{ kip}}$$

kip

#### **Strut 1 Face:**

Node Width                      Minimum beam width

$$w_{s1} := 9.5626\text{in} \qquad b_{s1} := 32\text{in}$$

Shear at node failure:

$$V_{s1\_n} := \frac{f_{ce} \cdot w_{s1} \cdot b_{s1}}{\text{Strut}_1} \qquad \boxed{V_{s1\_n} = 1705 \text{ kip}}$$

kip

#### **Bearing Face:**

Node Width                      Minimum beam width

$$w_{b1} := 9\text{in} \qquad b_{b1} := 32\text{in}$$

Shear at node failure:

$$V_{b1\_n} := f_{ce} \cdot w_{b1} \cdot b_{b1} \qquad \boxed{V_{b1\_n} = 1958 \text{ kip}}$$

#### **Node 3:**

C-T-T node at bearing.

$$\beta_n := 0.80 \qquad f_{ce} := 0.85 \cdot \beta_n \cdot f_c$$

**Tie 2 Face:**Node Width

$w_{t2} := 12.25\text{in}$

Minimum beam width

$b_{t2} := 36\text{in}$

Shear at node failure:

$$V_{t2\_n} := \frac{f_{ce} \cdot w_{t2} \cdot b_{t2}}{\frac{\text{Tie}_2}{\text{kip}}}$$

$V_{t2\_n} = 3502 \text{ kip}$

**Strut 3 Face:**Node Width

$w_{s3} := 15.5\text{in}$

Minimum beam width

$b_{s3} := 36\text{in}$

Shear at node failure:

$$V_{s3\_n} := \frac{f_{ce} \cdot w_{s3} \cdot b_{s3}}{\frac{\text{Strut}_3}{\text{kip}}}$$

$V_{s3\_n} = 2795 \text{ kip}$

**S/T4 Face:**Node Width

$w_{t4} := 10\text{in}$

Minimum beam width

$b_{t4} := 36\text{in}$

Shear at node failure:

$$V_{t4\_n} := \frac{f_{ce} \cdot w_{t4} \cdot b_{t4}}{\frac{\text{S\_T}_4}{\text{kip}}}$$

$V_{t4\_n} = 2323 \text{ kip}$

**Note:** Node under load is singular, but since it is a C-C-C node, previous experience and research indicates it will not control.

**Bearing Check (ACI 10.14 pg. 152)**

$A_1 := 32\text{in} \cdot 9\text{in}$

$A_1 = 288 \text{ in}^2$

*Bearing area*

$A_2 := 48\text{in} \cdot 16\text{in}$

$A_2 = 768 \text{ in}^2$

*Available area*

$$m := \begin{cases} \sqrt{\frac{A_2}{A_1}} & \text{if } \sqrt{\frac{A_2}{A_1}} \leq 2.0 \\ 2.0 & \text{otherwise} \end{cases} \quad m = 1.633$$

$P_n := 0.85f_c \cdot A_1 \cdot m$

$P_n = 3998 \text{ kip}$

Shear force achievable with provided bearing.

## C.7 DIRECT STRUT ACI CALCULATION: RF-3R-9(a)

### RF-3R-9(a) Direct Strut-and-Tie Model

#### Parameters

$$f'_c := 10\text{ksi} \quad f_y := 60\text{ksi} \quad f_{se} := 148.5\text{ksi} \quad A_{ps} := 0.153\text{in}^2$$

$$A_{4b} := 0.20\text{in}^2 \quad A_{5b} := 0.31\text{in}^2 \quad A_{6b} := 0.44\text{in}^2 \quad A_{7b} := 0.60\text{in}^2$$

#### Angles

$$\phi_1 := 53\text{deg} \quad \phi_2 := 13.2\text{deg} \quad \phi_3 := 45.9\text{deg}$$

### Strut and Tie Check (ACI Appendix A-3 & A-4 pg. 388)

Check if struts reinforced:

$$b_s := 8\text{in} \quad (\text{smallest expected strut width}) \quad s := 5\text{in} \quad (\text{spacing of stirrups})$$

$$\alpha_1 := 65\text{deg} \quad \alpha_2 := 25\text{deg} \quad \text{Maximum and minimum strut angles.}$$

$$0.003 \cdot b_s \cdot s \cdot \sin(\alpha_1) = 0.109 \cdot \text{in}^2 \quad 0.003 \cdot b_s \cdot s \cdot \sin(\alpha_2) = 0.051 \cdot \text{in}^2 \quad A_{prov} := 2 \cdot A_{4b}$$

$$A_{prov} = 0.4 \text{in}^2$$

$$\beta_s := 0.75 \quad \text{All struts have enough reinforcement with the vertical stirrups to be classified as reinforced struts.}$$

$$V := 1\text{kip}$$

#### **Strut 1:**

$$\text{Strut}_1 := \frac{V}{\sin(\phi_1)} \quad \text{Strut}_1 = 1.252 \cdot \text{kip}$$

Strut Width      Minimum beam width      Strut Efficiency Factor

$$w_1 := 9.5625 \cdot \text{in} \quad b_1 := 48\text{in} \quad \beta_s := 0.75$$

$$V_{s1} := \frac{0.85 \cdot \beta_s \cdot f'_c \cdot b_1 \cdot w_1}{\frac{\text{Strut}_1}{\text{kip}}} \quad V_{s1} = 2336.9 \cdot \text{kip} \quad \text{Shear capacity based on strut 1}$$

#### **Tie 1:**

$$\text{Tie}_1 := \frac{V}{\tan(\phi_1)} \quad \text{Tie}_1 = 0.754 \cdot \text{kip}$$

$$V_{t1} := \frac{12 \cdot A_{7b} \cdot f_y}{\frac{\text{Tie}_1}{\text{kip}}} \quad V_{t1} = 573.3 \cdot \text{kip} \quad \text{Shear capacity based on tie 1}$$

**Strut 2:**

$$\text{Strut}_2 := \frac{V}{\tan(\phi_1) \cos(\phi_2)} \quad \boxed{\text{Strut}_2 = 0.774 \cdot \text{kip}}$$

Strut Width                      Minimum beam width                      Strut Efficiency Factor

$$w_2 := 8 \cdot \text{in} \quad \boxed{b_2 := 54 \text{in}} \quad \beta_s := 0.75$$

$$V_{s2} := \frac{0.85 \cdot \beta_s \cdot f'_c \cdot b_2 \cdot w_2}{\text{Strut}_2} \quad \boxed{V_{s2} = 3558.1 \cdot \text{kip}} \quad \text{Shear capacity based on strut 2}$$

kip

**Tie 2:**

$$\text{Tie}_2 := V - V \cdot \frac{\tan(\phi_2)}{\tan(\phi_1)} \quad \boxed{\text{Tie}_2 = 0.823 \cdot \text{kip}}$$

$$V_{t2} := \frac{(2 \cdot 8 \cdot A_{6b} + 2 \cdot 2 \cdot A_{4b}) \cdot f_y}{\text{Tie}_2} \quad \boxed{V_{t2} = 571.4 \cdot \text{kip}} \quad \text{Shear capacity based on tie 2}$$

kip

**Strut 3:**

$$\text{Strut}_3 := \frac{V - V \cdot \frac{\tan(\phi_2)}{\tan(\phi_1)}}{\sin(\phi_3)} \quad \boxed{\text{Strut}_3 = 1.146 \cdot \text{kip}}$$

Strut Width                      Minimum beam width                      Strut Efficiency Factor

$$w_3 := 15 \cdot \text{in} \quad \boxed{b_3 := 36 \text{in}} \quad \beta_s := 0.75$$

$$V_{s3} := \frac{0.85 \cdot \beta_s \cdot f'_c \cdot b_3 \cdot w_3}{\text{Strut}_3} \quad \boxed{V_{s3} = 3002.9 \cdot \text{kip}} \quad \text{Shear capacity based on strut 3}$$

kip

**Strut/Tie 4:**

$$S_{T4} := \text{Strut}_3 \cdot \cos(\phi_3) \quad \boxed{S_{T4} = 0.798 \cdot \text{kip}} \quad \text{Without concentrated prestressed load applied}$$

$$V_{s_{t4}} := \frac{6 \cdot A_{6b} \cdot f_y + f_{se} \cdot A_{ps} \cdot 38 \cdot \frac{6.125 \text{in}}{30 \text{in}}}{S_{T4}} \quad \boxed{V_{s_{t4}} = 419.5 \cdot \text{kip}} \quad \text{Shear capacity based on strut that turns into tie #4}$$

kip

$$V_{s_{t4\_1}} := \frac{6 \cdot A_{6b} \cdot f_y + f_{se} \cdot A_{ps} \cdot 38 \cdot \frac{17 \text{in}}{30 \text{in}}}{S_{T4}} \quad \boxed{V_{s_{t4\_1}} = 811.8 \cdot \text{kip}} \quad \text{Shear capacity based on strut that turns into tie #4 at the edge of the extended nodal region.}$$

kip

## Nodal Check (ACI Appendix A.5 pg. 392)

### **Check Singular Nodes:**

#### **Node 1:**

C-C-T node at bearing.

$$\beta_n := 0.80 \qquad f_{ce} := 0.85 \cdot \beta_n \cdot f_c$$

#### ***Tie 1 Face:***

<u>Node Width</u>	<u>Minimum beam width</u>
$w_{t1} := 4.125\text{in}$	$b_{t1} := 32\text{in}$

Shear at node failure:

$$V_{t1\_n} := \frac{f_{ce} \cdot w_{t1} \cdot b_{t1}}{\frac{Tie_1}{\text{kip}}} \qquad \boxed{V_{t1\_n} = 1282 \text{ kip}}$$

#### ***Strut 1 Face:***

<u>Node Width</u>	<u>Minimum beam width</u>
$w_{s1} := 9.5626\text{in}$	$b_{s1} := 32\text{in}$

Shear at node failure:

$$V_{s1\_n} := \frac{f_{ce} \cdot w_{s1} \cdot b_{s1}}{\frac{\text{Strut}_1}{\text{kip}}} \qquad \boxed{V_{s1\_n} = 1705 \text{ kip}}$$

#### ***Bearing Face:***

<u>Node Width</u>	<u>Minimum beam width</u>
$w_{b1} := 9\text{in}$	$b_{b1} := 32\text{in}$

Shear at node failure:

$$V_{b1\_n} := f_{ce} \cdot w_{b1} \cdot b_{b1} \qquad \boxed{V_{b1\_n} = 1958 \text{ kip}}$$

#### **Node 3:**

C-T-T node at bearing.

$$\beta_n := 0.80 \qquad f_{ce} := 0.85 \cdot \beta_n \cdot f_c$$



**Tie 2 Face:**

Node Width

$$w_{t2} := 12.25\text{in}$$

Minimum beam width

$$b_{t2} := 36\text{in}$$

Shear at node failure:

$$V_{t2\_n} := \frac{f_{ce} \cdot w_{t2} \cdot b_{t2}}{\frac{Tie_2}{\text{kip}}}$$

$$V_{t2\_n} = 3502 \text{ kip}$$

**Strut 3 Face:**

Node Width

$$w_{s3} := 15.5\text{in}$$

Minimum beam width

$$b_{s3} := 36\text{in}$$

Shear at node failure:

$$V_{s3\_n} := \frac{f_{ce} \cdot w_{s3} \cdot b_{s3}}{\frac{\text{Strut}_3}{\text{kip}}}$$

$$V_{s3\_n} = 3182 \text{ kip}$$

**S/T4 Face:**

Node Width

$$w_{t4} := 10\text{in}$$

Minimum beam width

$$b_{t4} := 36\text{in}$$

Shear at node failure:

$$V_{t4\_n} := \frac{f_{ce} \cdot w_{t4} \cdot b_{t4}}{\frac{S\_T4}{\text{kip}}}$$

$$V_{t4\_n} = 2950 \text{ kip}$$

**Note:** Node under load is singular, but since it is a C-C-C node, previous experience and research indicates it will not control.

**Bearing Check (ACI 10.14 pg. 152)**

$$A_1 := 32\text{in} \cdot 9\text{in}$$

$$A_1 = 288 \text{ in}^2$$

*Bearing area*

$$A_2 := 48\text{in} \cdot 16\text{in}$$

$$A_2 = 768 \text{ in}^2$$

*Available area*

$$m := \begin{cases} \sqrt{\frac{A_2}{A_1}} & \text{if } \sqrt{\frac{A_2}{A_1}} \leq 2.0 \\ 2.0 & \text{otherwise} \end{cases} \quad m = 1.633$$

$$P_n := 0.85f_c \cdot A_1 \cdot m$$

$$P_n = 3998 \text{ kip}$$

Shear force achievable with provided bearing.

## C.8 DIRECT STRUT ACI CALCULATION: RF-3R-9(c)

### RF-3R-9(c) Direct Strut-and-Tie Model

#### Parameters

$$f_c := 10\text{ksi} \quad f_y := 60\text{ksi} \quad f_{se} := 148.5\text{ksi} \quad A_{ps} := 0.153\text{in}^2$$

$$A_{4b} := 0.20\text{in}^2 \quad A_{5b} := 0.31\text{in}^2 \quad A_{6b} := 0.44\text{in}^2 \quad A_{7b} := 0.60\text{in}^2$$

#### Angles

$$\phi_1 := 51\text{deg} \quad \phi_2 := 8.8\text{deg} \quad \phi_3 := 31.6\text{deg}$$

### Strut and Tie Check (ACI Appendix A-3 & A-4 pg. 388)

Check if struts reinforced:

$$b_s := 8\text{in} \quad (\text{smallest expected strut width}) \quad s := 5\text{in} \quad (\text{spacing of stirrups})$$

$$\alpha_1 := 65\text{deg} \quad \alpha_2 := 25\text{deg} \quad \text{Maximum and minimum strut angles.}$$

$$0.003 \cdot b_s \cdot s \cdot \sin(\alpha_1) = 0.109 \cdot \text{in}^2 \quad 0.003 \cdot b_s \cdot s \cdot \sin(\alpha_2) = 0.051 \cdot \text{in}^2 \quad A_{prov} := 2 \cdot A_{4b}$$

$$A_{prov} = 0.4 \text{in}^2$$

$\beta_s := 0.75$  All struts have enough reinforcement with the vertical stirrups to be classified as reinforced struts.

$$V := 1\text{kip}$$

#### **Strut 1:**

$$\text{Strut}_1 := \frac{V}{\sin(\phi_1)} \quad \boxed{\text{Strut}_1 = 1.287 \cdot \text{kip}}$$

<u>Strut Width</u>	<u>Minimum beam width</u>	<u>Strut Efficiency Factor</u>
$w_1 := 9.5625 \cdot \text{in}$	$\boxed{b_1 := 48\text{in}}$	$\beta_s := 0.75$

$$V_{s1} := \frac{0.85 \cdot \beta_s \cdot f_c \cdot b_1 \cdot w_1}{\frac{\text{Strut}_1}{\text{kip}}} \quad \boxed{V_{s1} = 2274 \cdot \text{kip}} \quad \text{Shear capacity based on strut 1}$$

#### **Tie 1:**

$$\text{Tie}_1 := \frac{V}{\tan(\phi_1)} \quad \boxed{\text{Tie}_1 = 0.81 \cdot \text{kip}}$$

$$V_{t1} := \frac{12 \cdot A_{7b} \cdot f_y}{\frac{\text{Tie}_1}{\text{kip}}} \quad \boxed{V_{t1} = 533.5 \cdot \text{kip}} \quad \text{Shear capacity based on tie 1}$$



**Strut 2:**

$$\text{Strut}_2 := \frac{V}{\tan(\phi_1) \cos(\phi_2)}$$

$$\text{Strut}_2 = 0.819 \cdot \text{kip}$$

Strut Width

$$w_2 := 8 \cdot \text{in}$$

Minimum beam width

$$b_2 := 54 \text{in}$$

Strut Efficiency Factor

$$\beta_s := 0.75$$

$$V_{s2} := \frac{0.85 \cdot \beta_s \cdot f'_c \cdot b_2 \cdot w_2}{\text{Strut}_2}$$

kip

$$V_{s2} = 3360.9 \cdot \text{kip}$$

*Shear capacity based on strut 2*

**Tie 2:**

$$\text{Tie}_2 := V - V \cdot \frac{\tan(\phi_2)}{\tan(\phi_1)}$$

$$\text{Tie}_2 = 0.875 \cdot \text{kip}$$

$$V_{t2} := \frac{(2 \cdot 8 \cdot A_{6b} + 2 \cdot 2 \cdot A_{4b}) \cdot f_y}{\text{Tie}_2}$$

kip

$$V_{t2} = 537.8 \cdot \text{kip}$$

*Shear capacity based on tie 2*

**Strut 3:**

$$\text{Strut}_3 := \frac{V - V \cdot \frac{\tan(\phi_2)}{\tan(\phi_1)}}{\sin(\phi_3)}$$

$$\text{Strut}_3 = 1.669 \cdot \text{kip}$$

Strut Width

$$w_3 := 15 \cdot \text{in}$$

Minimum beam width

$$b_3 := 36 \text{in}$$

Strut Efficiency Factor

$$\beta_s := 0.75$$

$$V_{s3} := \frac{0.85 \cdot \beta_s \cdot f'_c \cdot b_3 \cdot w_3}{\text{Strut}_3}$$

kip

$$V_{s3} = 2062.4 \cdot \text{kip}$$

*Shear capacity based on strut 3*

**Strut/Tie 4:**

$$S_{T4} := \text{Strut}_3 \cdot \cos(\phi_3)$$

$$S_{T4} = 1.422 \text{ kip}$$

Without concentrated prestressed load applied

$$V_{s_{t4}} := \frac{6 \cdot A_{6b} \cdot f_y + f_{se} \cdot A_{ps} \cdot 38 \cdot \frac{6.125 \text{ in}}{30 \text{ in}}}{\frac{S_{T4}}{\text{kip}}}$$

$$V_{s_{t4}} = 235.4 \text{ kip}$$

Shear capacity based on strut that turns into tie #4

$$V_{s_{t4\_1}} := \frac{6 \cdot A_{6b} \cdot f_y + f_{se} \cdot A_{ps} \cdot 38 \cdot \frac{20.375 \text{ in}}{30 \text{ in}}}{\frac{S_{T4}}{\text{kip}}}$$

$$V_{s_{t4\_1}} = 523.9 \text{ kip}$$

Shear capacity based on strut that turns into tie #4 at the edge of the extended nodal region.

**Nodal Check (ACI Appendix A.5 pg. 392)**

**Check Singular Nodes:**

**Node 1:**

C-C-T node at bearing.

$$\beta_n := 0.80$$

$$f_{ce} := 0.85 \cdot \beta_n \cdot f_c$$

**Tie 1 Face:**

Node Width

Minimum beam width

$$w_{t1} := 4.125 \text{ in}$$

$$b_{t1} := 32 \text{ in}$$

Shear at node failure:

$$V_{t1\_n} := \frac{f_{ce} \cdot w_{t1} \cdot b_{t1}}{\frac{\text{Tie}_1}{\text{kip}}}$$

$$V_{t1\_n} = 1108 \text{ kip}$$

**Strut 1 Face:**

Node Width

Minimum beam width

$$w_{s1} := 9.5626 \text{ in}$$

$$b_{s1} := 32 \text{ in}$$

Shear at node failure:

$$V_{s1\_n} := \frac{f_{ce} \cdot w_{s1} \cdot b_{s1}}{\frac{\text{Strut}_1}{\text{kip}}}$$

$$V_{s1\_n} = 1617 \text{ kip}$$

**Bearing Face:**

Node Width

$$w_{b1} := 9\text{in}$$

Minimum beam width

$$b_{b1} := 32\text{in}$$

Shear at node failure:

$$V_{b1\_n} := f_{ce} \cdot w_{b1} \cdot b_{b1}$$

$$V_{b1\_n} = 1958 \text{ kip}$$

**Node 3:**

C-T-T node at bearing.

$$\beta_n := 0.80$$

$$f_{ce} := 0.85 \cdot \beta_n \cdot f_c$$

**Tie 2 Face:**

Node Width

$$w_{t2} := 12.25\text{in}$$

Minimum beam width

$$b_{t2} := 36\text{in}$$

Shear at node failure:

$$V_{t2\_n} := \frac{f_{ce} \cdot w_{t2} \cdot b_{t2}}{\frac{\text{Tie}_2}{\text{kip}}}$$

$$V_{t2\_n} = 3429 \text{ kip}$$

**Strut 3 Face:**

Node Width

$$w_{s3} := 15.5\text{in}$$

Minimum beam width

$$b_{s3} := 36\text{in}$$

Shear at node failure:

$$V_{s3\_n} := \frac{f_{ce} \cdot w_{s3} \cdot b_{s3}}{\frac{\text{Strut}_3}{\text{kip}}}$$

$$V_{s3\_n} = 2273 \text{ kip}$$

**S/T4 Face:**

Node Width

$$w_{t4} := 10\text{in}$$

Minimum beam width

$$b_{t4} := 36\text{in}$$

Shear at node failure:

$$V_{t4\_n} := \frac{f_{ce} \cdot w_{t4} \cdot b_{t4}}{\frac{\text{S-T}_4}{\text{kip}}}$$

$$V_{t4\_n} = 1722 \text{ kip}$$

**Note:** Node under load is singular, but since it is a C-C-C node, previous experience and research indicates it will not control.

**Bearing Check (ACI 10.14 pg. 152)**

$$A_1 := 32\text{in} \cdot 9\text{in} \quad A_1 = 288 \text{ in}^2 \quad \text{Bearing area}$$

$$A_2 := 48\text{in} \cdot 16\text{in} \quad A_2 = 768 \text{ in}^2 \quad \text{Available area}$$

$$m := \begin{cases} \sqrt{\frac{A_2}{A_1}} & \text{if } \sqrt{\frac{A_2}{A_1}} \leq 2.0 \\ 2.0 & \text{otherwise} \end{cases} \quad m = 1.633$$

$$P_n := 0.85f'_c \cdot A_1 \cdot m \quad P_n = 3998 \text{ kip} \quad \text{Shear force achievable with provided bearing.}$$

## C.9 CUT ANALYSIS: RF-3R-9(c)

### Location of Compression Resultant

$$\text{CompRes} := 4.25\text{in} \quad (\text{Centroid of the top flange})$$

### Assumed Steel Properties

$$A_{4b} := 0.20\text{in}^2 \quad A_{5b} := 0.31\text{in}^2 \quad A_{6b} := 0.44\text{in}^2 \quad A_{7b} := 0.60\text{in}^2 \quad f_y := 60\text{ksi}$$

### Assumed Strand Properties

$$n_{\text{strand}} := 38 \quad (38 \text{ strands at cut}) \quad A_{ps} := 0.153\text{in}^2 \quad f_{se} := 148.5\text{ksi}$$

$$d_p := \frac{6 \cdot A_{ps} \text{in}^2 \cdot 52\text{in} + 6 \cdot A_{ps} \text{in}^2 \cdot 50\text{in} + 14 \cdot A_{ps} \text{in}^2 \cdot 48\text{in} + 12 \cdot A_{ps} \text{in}^2 \cdot 46\text{in}}{n_{\text{strand}} \cdot A_{ps} \text{in}^2} \quad d_p = 48.316\text{in}$$

### Stirr-up Locations (from AutoCAD)

$$\text{stirrup}_1 := 6.25\text{in} \quad \text{stirrup}_2 := \text{stirrup}_1 + 5\text{in} \quad \text{stirrup}_3 := \text{stirrup}_2 + 5\text{in}$$

$$\text{stirrup}_4 := \text{stirrup}_3 + 5\text{in} \quad \text{stirrup}_5 := \text{stirrup}_4 + 5\text{in} \quad \text{stirrup}_6 := \text{stirrup}_5 + 5\text{in}$$

$$\text{stirrup}_7 := \text{stirrup}_6 + 5\text{in} \quad \text{stirrup}_8 := \text{stirrup}_7 + 5\text{in} \quad \text{stirrup}_9 := \text{stirrup}_8 + 5\text{in}$$

$$\text{end}_{\text{void}} := \text{stirrup}_6$$

### Summation of Moments about Compression Resultant

$$M_{\text{cut}} := 2 \cdot A_{4b} \cdot f_y \cdot \left( \text{stirrup}_1 + \text{stirrup}_2 + \text{stirrup}_3 + \text{stirrup}_4 + \text{stirrup}_5 + \text{stirrup}_6 \dots \right) \dots \\ + 4 \cdot A_{6b} \cdot f_y \cdot \text{end}_{\text{void}} + \left( f_{se} \cdot A_{ps} \cdot 38 \cdot \frac{24.5\text{in}}{30\text{in}} + 6 \cdot A_{6b} \cdot f_y \right) \cdot (d_p + 4\text{in} - \text{CompRes})$$

$$M_{\text{cut}} = 4206\text{kip}\cdot\text{ft}$$

### Shear Force Resulting in Failure Moment

$$d_{\text{support}} := 81.25\text{in}$$

$$V_{\text{predict}} := \frac{M_{\text{cut}}}{d_{\text{support}}} \quad V_{\text{predict}} = 621.2\text{kip}$$

### Comparison to Measure Failure Shear

$$V_{\text{fail}} := 708\text{kip} \quad \frac{V_{\text{fail}}}{V_{\text{predict}}} = 1.14$$

## REFERENCES

- AASHTO LRFD Bridge Design Specifications* (4th ed.). (2007). Washington, D.C.: American Association of State Highway and Transportation Officials.
- ACI Committee 318. (2008). *Building Code Requirements for Structural Concrete (ACI 318-08) and Commentary*. Farmington Hills, MI: American Concrete Institute.
- Ahmed, T., Burley, E., & Rigden, S. (1998). The Static and Fatigue Strength of Reinforced Concrete Beams Affected by Alkali-Silica Reaction. *ACI Materials Journal* , 95 (4), 376-388.
- Bach, F., Thorsen, T. S., & Nielsen, M. P. (1993). Load-Carrying Capacity of Structural Members Subjected to Alkali-Silica Reactions. *Construction and Building Materials* , 7 (2), 109-115.
- Barton, D. L., Anderson, R. B., Bouadi, A., Jirsa, J. O., & Breen, J. E. (1991). *An Investigation of Strut-and-Tie Models for Dapped Beam Details*. The University of Texas at Austin. Austin, TX: Center for Transportation Research, Bureau of Engineering Research, The University of Texas.
- Bergmeister, K., Breen, J. E., Jirsa, J. O., & Kreger, M. E. (1993). *Detailing in Structural Concrete*. The University of Texas at Austin. Austin, TX: Center for Transportation Research, Bureau of Engineering, The University of Texas at Austin.
- Boenig, A., Funez, L., Klingner, R. E., & Fowler, T. J. (2001). *Bridges with Premature Concrete Deterioration: Field Observations and Large-Scale Testing*. The University of Texas at Austin. Austin, TX: Center for Transportation Research, Bureau of Engineering Research, The University of Texas.
- Chana, P. S., & Thompson, D. M. (1992). Laboratory Testing and Assessment of Structural Members Affected by Alkali Silica Reaction. *The 9th International Conference on Alkali-Aggregate Reaction in Concrete*, (pp. 156-166).
- Clayton, N., Currie, R. J., & Moss, R. M. (1990). Effects of alkali-silica reaction on the strength of prestressed concrete beams. *The Structural Engineer* , 68 (15), 287-292.
- Cook, W. D., & Mitchell, D. (1988). Studies of Disturbed Regions near Discontinuities in Reinforced Concrete Members. *ACI Structural Journal* , 85 (2), 206-216.

- Cope, R. J., & Slade, L. (1990). The Shear Capacity of Reinforced Concrete Members Subjected to Alkali-Silica Reaction. *Structural Engineering Review* , 2, 105-112.
- den Uijl, J. A., & Kaptijn, N. (2003). Shear Tests on Beams Cut from ASR-Affected Bridge Decks. *ACI SP-211-6* , 115-133.
- Diamond, S. (1996). Delayed Ettringite Formation - Processes and Problems. *Cement and Concrete Composites* , 18 (3), 205-215.
- Farny, J. A., & Kerkhoff, B. (2007). Diagnosis and Control of Alkali-Aggregate Reactions in Concrete. *Concrete Technology* , 1-11.
- Folliard, K. J., & Drimalas, T. (2008, March 18). Brief Summary of Evaluation of Houston Box Beams. Unpublished raw data.
- Folliard, K. J., Barborak, R., Drimalas, T., Du, L., Garber, S., Ideker, J., et al. (2006). *Preventing ASR/DEF in New Concrete: Final Report*. The University of Texas at Austin. Austin, TX: Center for Transportation Research at The University of Texas at Austin.
- Herzinger, R., & Elbadry, M. (2007). Alternative Reinforcing Details in Dapped Ends of Precast Concrete Bridge Girders: Experimental Investigation. *Transportation Research Record* , 111-121.
- Kapitan, J. G. (2006). *Structural Assessment of Bridge Piers with Damage similar to Alkali Silica Reaction and/or Delayed Ettringite Formation*. The University of Texas at Austin, Civil and Environmental Engineering. Austin: The University of Texas at Austin.
- Lin, I.-J., Hwang, S.-J., Lu, W.-Y., & Tsai, J.-T. (2003). Shear Strength of Reinforced Concrete Dapped-End Beams. *Structural Engineering and Mechanics* , 16 (3), 275-294.
- Mader, D. J. (1990). *Detailing Dapped Ends of Pretensioned Concrete Beams*. The University of Texas at Austin, Civil and Environmental Engineering. Austin, TX: The University of Texas at Austin.
- Mattock, A. H., & Chan, T. C. (1979). Design and Behavior of Dapped-End Beams. *PCI Journal* , 24 (6), 28-45.
- Mattock, A. H., & Theryo, T. S. (1986). Strength of Precast Prestressed Concrete Membranes with Dapped Ends. *Journal - Prestressed Concrete Institute* , 31 (5), 58-75.
- Menon, G., & Furlong, R. W. (1977). *Design of Reinforcement for Notched Ends of Prestressed Concrete Girders*. The University of Texas at Austin. Center for Transportation Research, Bureau of Engineering Research.

- Monette, L. J., Gardner, N. J., & Grattan-Bellew, P. E. (2002). Residual Strength of Reinforced Concrete Beams Damaged by Alkali-Silica Reaction—Examination of Damage Rating Index Method. *ACI Materials Journal* , 99 (1), 42-50.
- Precast/Prestressed Concrete Institute. (2004). *PCI Design Handbook* (6th Edition ed.). (L. D. Martin, & C. J. Perry, Eds.) Chicago, United States of America: Precast/Prestressed Concrete Institute.
- Sahu, S., & Thaulow, N. (2004). Delayed Ettringite Formation in Swedish Concrete Railroad Ties. *Cement and Concrete Research* , 34, 1675-1681.
- Swamy, R. N., & Al-Asali, M. M. (1989). Effect of Alkali-Silica Reaction on the Structural Behavior of Reinforced Concrete Beams. *ACI Structural Journal* , 86 (4), 451-459.
- Taylor, H. F., Famy, C., & Scrivener, K. L. (2001). Delayed Ettringite Formation. *Cement and Concrete Research* , 31, 683-693.
- Thomas, M., Folliard, K., Drimalas, T., & Ramlochan, T. (2008). Diagnosing Delayed Ettringite Formation in Concrete Structures. *Cement and Concrete Research* , 38, 841-847.
- Wang, Q., Guo, Z., & Hoogenboom, P. C. (2005). Experimental Investigation on the Shear Capacity of RC Dapped End Beams and Design Recommendations. *Structural Engineering and Mechanics* , 21 (2), 221-235.



## VITA

Bryan V. Bindrich was born in Madison, Wisconsin on January 24, 1984 to Doug and Dorie Bindrich. He is the first of two children with his brother Kurt joining the family on September 6, 1985. Growing up in a small farmhouse in rural Wisconsin, Bryan has always enjoyed the outdoors and has yet to find an unlikeable sport. He attended DeForest High School in DeForest, Wisconsin. Upon successful completion of his work in 2002, Bryan enrolled in the University of Wisconsin-Madison receiving a Bachelor of Science in Civil Engineering in May 2007. He pursued further education by attending graduate school at The University of Texas at Austin. Bryan graduated with a Master of Science in Engineering in May 2009 and looks to continue his contribution to the field of structural engineering at the professional level.

Permanent Address: 2812 Nueces Street, Apt. 201  
Austin, TX 78705

This thesis was typed by the author.